Annual Reports C

Dynamic Article Links

Cite this: *Annu. Rep. Prog. Chem., Sect. C: Phys. Chem.*, 2012, **108**, 222–277

www.rsc.org/annrepc

**REVIEW**

# Quantum-chemical embedding methods for treating local electronic excitations in complex chemical systems

**André Severo Pereira Gomes*[a] and Christoph R. Jacob*[b]**

**DOI: 10.1039/c2pc90007f**

Quantum chemistry has become an invaluable tool for studying the electronic excitation phenomena underlying many important chemical, biological, and technological processes. Here, we review quantum-chemical approaches for modeling such phenomena. In particular, embedding methods can be particularly useful for treating localized excitations in complex chemical systems. These split the total system into a number of interacting subsystems. The electronic excitations processes occurring in the subsystem of interest are then treated with high accuracy, while its environment is taken into account in a more approximate way. In this review, we use a formulation based on the formally exact frozen-density embedding theory as our starting point. This provides a common framework for discussing the different embedding approaches that are currently available. Moreover, it also forms the basis of emerging methods that allow for a seamless coupling of density-functional theory and wavefunction based approaches, both for ground and excited states. These provide new possibilities for studying electronic excitations in large systems with predictive quantum-chemical methods.

## 1 Introduction

Processes involving excited electronic states are crucial for many functions of biological or chemical systems. Examples include light absorption and energy transfer in photosynthetic proteins[1] or photovoltatic devices[2,3] as well as light emission from luminescent proteins[4] or from organic materials.[5] Over the past years, quantum chemistry has made significant progress in unraveling the underlying electronic processes (see, *e.g.*, ref. 4, 6). This includes the emergence of accurate and efficient computational methods for the treatment of excited states as well as the development of embedding and subsystem approaches that make an application of

---

[a] *Université de Lille 1, Laboratoire PhLAM, CNRS UMR 8532, Bat P5, 59655 Villeneuve d'Ascq Cedex, France. E-mail: andre.gomes@univ-lille1.fr*

[b] *Karlsruhe Institute of Technology (KIT), Center for Functional Nanostructures, Wolfgang-Gaede-Str. 1a, 76131 Karlsruhe, Germany. E-mail: christoph.jacob@kit.edu*

these quantum-chemical methods to complex systems possible (for reviews, see, *e.g.*, ref. 7–9). In particular, subsystem and embedding methods that allow for a seamless coupling of different quantum chemical methods have recently become available.[10–12] These open the way to a theoretical design of functional materials and chemical systems in the future.

A quantum-chemical description of electronic excitations requires methods that are capable of describing both ground and excited states with similar accuracy. Such methods have been developed extensively over the past decades (for reviews, see, *e.g.*, ref. 13–15). While time-dependent density-functional theory (TDDFT) offers a good cost–accuracy ratio and is applicable to rather large molecular systems with up to a few hundreds of atoms, it is also prone to unsystematic errors. On the other hand, wavefunction theory (WFT) based methods for excited states offer the potential for a systematic improvement, but their applicability is usually limited to rather small molecules. Thus, for isolated small molecules (*e.g.*, in gas-phase experiments), they can often provide very accurate predictions. Nevertheless, in difficult cases already for medium-sized molecules with only 10–20 atoms it can be impossible to obtain sufficiently accurate predictions (for an example, see ref. 16, and for a review highlighting some of the current challenges of quantum-chemical methods for excited states, see ref. 15).

It is therefore not surprising that the treatment of electronic excitations in even larger and more complex chemical systems presents a significant challenge for computational chemistry. Examples of such large systems are molecules in the condensed phase (*i.e.*, solvated molecules or molecular materials), biomolecules or biomolecular assemblies, molecular nanostructures (*e.g.*, metal organic frameworks or assemblies of molecular clusters), or complex solid-state system such as impurities in materials as well as molecules adsorbed on surfaces.

Such large systems present several challenges: First, the need to control the computational cost of quantum-chemical calculations, since these increase with the size of the system at a much faster rate than that of the availability of computer resources. This is partially addressed by the development of efficient (linear-scaling) algorithms and their implementation in modern program packages. These efforts are, however, offset by the need to account for dynamical effects, as is often mandatory for large systems. In particular for molecules in solution and for biological systems, it will be necessary to account for the structural flexibility by considering many different molecular structures. Second, even if calculations on rather large systems are possible, the choice of quantum-chemical methods is severely restricted. Often, approximate DFT calculations are the only available option and it is not possible to improve the description by applying more accurate wavefunction based methods. Finally, quantum-chemical calculations on large systems are also difficult to interpret. Usually, a very delocalized picture is obtained that makes it difficult to identify the important aspects.[17,18] In particular when local electronic excitation are of interest, these can be difficult to isolate among the many excited states of a large system. On the other hand, even delocalized excitation phenomena are best understood within a local picture.[8]

Already due to the increased computational cost, a full treatment of the complete system is in most cases out of reach for the calculation of excitation energies. However, many electronic excitations are local, *i.e.*, the change in the electronic structure upon excitation is mainly restricted to a comparably small part of the full system—for instance, a particular molecule in a complex environment, a particular chromophore in a bimolecular system, or an impurity in a solid. Under these circumstances, it is possible to apply additional simplifications and drastically reduce the total computational cost while retaining accuracy for the subsystem of interest. This is the goal of embedding methods, which restrict the explicit treatment to a small subsystem of interest while approximating that of its environment, effectively extending the applicability of accurate quantum chemical methods from small isolated molecules to complex chemical systems. At the same time, such a treatment simplifies the interpretation of the computational results considerably.

Our aim here is to highlight some of the currently available quantum chemical embedding approaches, with a particular focus on their application for describing local electronic excitations. The review is organized as follows: First, we give an overview of quantum-chemical methods for the treatment of excited states in section 2. Subsequently, embedding methods in quantum chemistry will be introduced. To this end, we outline an exact theoretical framework for quantum-chemical embedding methods, the frozen-density embedding (FDE) theory in section 3, before presenting an attempt of a classification and an overview of a variety of approximate embedding methods in section 4. Finally, we discuss two case studies for comparing some of these approaches in section 5.

## 2 Quantum chemistry for excited states

For predicting excitation energies, quantum-chemical methods that can treat both the ground-state and excited states are necessary. Here, we will provide an overview of the most important theoretical approaches. These can be divided into two groups that tackle the problem from two formally equivalent, but conceptually very different directions.

First, *time-independent approaches* take the stationary Schrödinger equation,

$$\hat{H}|\Psi_k\rangle = E_k|\Psi_k\rangle, \tag{1}$$

where $\hat{H}$ is the molecular Hamiltonian and $|\Psi_k\rangle$ is the many-electron wavefunction, as their starting point. The energy eigenvalues $E_k$ and their corresponding eigenfunctions $|\Psi_k\rangle$ are the energies and wavefunctions of the different electronic states. Thus, in a time-independent picture excitation energies can be calculated by solving the stationary Schrödinger equation (eqn (1)) for the ground state and the excited states of interest. This requires an explicit construction of the excited-state wavefunctions $|\Psi_k\rangle$.

On the other hand, *time-dependent approaches* start from a stationary ground-state wavefunction $|\Psi_0\rangle$ and consider the time evolution of this initial state after switching on a time-dependent external perturbation. Here, we will only consider an oscillating electric dipole perturbation with frequency $\omega$, *i.e.*,

$$\hat{V}_\omega(t) = (e^{\mathrm{i}\omega t} + e^{-\mathrm{i}\omega t})\sum_\beta \varepsilon_\beta(\omega)\hat{\mu}_\beta, \tag{2}$$

where $\hat{\mu}_\beta$ is the $\beta$-component ($\beta = x,y,z$) of the time-independent electric dipole operator and $\varepsilon_\beta(\omega)$ denotes the associated perturbation strength. The time evolution of the wavefunction could be obtained by solving the time-dependent Schrödinger equation

$$\mathrm{i}\hbar\frac{\partial}{\partial t}|\Psi(t)\rangle = [\hat{H} + \hat{V}_\omega(t)]|\Psi(t)\rangle. \tag{3}$$

With the time-dependent wavefunction $|\Psi(t)\rangle$, one can obtain molecular properties by investigating the time evolution of the expectation value of, for instance, a component of the dipole moment $\hat{\mu}_\alpha$, expressed as a series expansion,

$$\langle \hat{\mu}_\alpha \rangle(t) = \langle \hat{\mu}_\alpha \rangle + (e^{\mathrm{i}\omega t} + e^{-\mathrm{i}\omega t}) \sum_\beta \varepsilon_\beta(\omega) \langle\langle \hat{\mu}_\alpha; \hat{\mu}_\beta \rangle\rangle_\omega + \ldots \tag{4}$$

Here, $\langle \hat{\mu}_\alpha \rangle$ is the time-independent expectation value and $\langle\langle \hat{\mu}_\alpha;\hat{\mu}_\beta \rangle\rangle_\omega$ is the linear electric dipole–electric dipole response function describing the oscillations of the $\alpha$-component of the dipole moment in response to an oscillating electric dipole field in $\beta$-direction. To first order, only oscillations with frequency $\omega$ appear in this expansion. Terms involving higher-order response functions have been omitted here, and we refer the reader to the thorough derivations of higher-order response theory available in the literature.[19]

Within an exact treatment based on time-dependent perturbation theory (see, *e.g.*, ref. 20) the linear response function is given by the sum-over-states expression

$$\langle\langle \hat{\mu}_\alpha; \hat{\mu}_\beta \rangle\rangle_\omega = \sum_{n \neq 0} \left[ \frac{\langle 0|\hat{\mu}_\alpha|n\rangle\langle n|\hat{\mu}_\beta|0\rangle}{\omega - \omega_n} + \frac{\langle 0|\hat{\mu}_\beta|n\rangle\langle n|\hat{\mu}_\alpha|0\rangle}{\omega_n - \omega} \right] \tag{5}$$

where $\omega_n = E_n - E_0$ represents the excitation energy from the ground state to $n$-th excited state. It then becomes evident that the excitation energies occur at frequencies that correspond to the poles of the linear response function. Furthermore, the transition moments for these excitations can be obtained as the corresponding residues of the linear response function.

The sum-over-states expression for the linear response function would require the solution of the time-independent Schrödinger equation for *all* excited states. However, when combined with approximate parametrizations of the many-electron wave-function it becomes possible to determine the linear response function directly by solving a linear system of equations, thus avoiding the explicit calculation of excited state wavefunctions.[19,21] Such a response theory can, for instance, be obtained by using the quasienergy formalism, which will be outlined in section 2.2. Subsequently, excitation energies can be determined by identifying the poles of the linear response function.

While for an exact treatment, time-independent approaches (which construct a wavefunction for each excited state explicitly) and time-dependent approaches based on response theory (which avoid the calculation of excited state wavefunctions) are equivalent, this is usually not the case anymore for approximate quantum-chemical methods. Both time-independent and time-dependent approaches are widely used for the quantum chemical calculation of excitation energies, and some of the most important methods will be highlighted in the following.

## 2.1 Time-independent approaches

**2.1.1 Density-functional theory (DFT).** Instead of solving the stationary Schrödinger equation to determine a many-electron wavefunction $|\Psi_k\rangle$, DFT aims at calculating the corresponding electron density $\rho_k(\boldsymbol{r})$ directly. For the ground-state, the formal justification for replacing the wavefunction $|\Psi_0\rangle$ by the ground-state electron density $\rho_0(\boldsymbol{r})$ is given by the Hohenberg–Kohn theorem,[22] which establishes the existence of a density functional $E[\rho]$ for calculating the total electronic energy,

$$E[\rho] = F_{\mathrm{HK}}[\rho] + \int \rho(\boldsymbol{r}) v_{\mathrm{nuc}}(\boldsymbol{r}) \mathrm{d}^3 r, \tag{6}$$

where $F_{\mathrm{HK}}[\rho]$ is a system-independent functional (the so-called universal Hohenberg–Kohn functional) and where $v_{\mathrm{nuc}}(\boldsymbol{r}) = \sum_A \frac{Q_A}{|\boldsymbol{r}-\boldsymbol{R}_A|}$ is the Coulomb potential of the nuclei at positions $\boldsymbol{R}_A$ and with the charges $Q_A$. Furthermore, the Hohenberg–Kohn theorem provides a variational principle for calculating the ground-state energy $E_0$ and the corresponding ground-state electron density $\rho_0$ by minimizing this energy functional, *i.e.*, $E_0 = \min_\rho E[\rho]$.

In Kohn–Sham (KS) DFT,[23] the energy functional is decomposed as,

$$E[\rho] = T_s[\rho] + J[\rho] + E_{\mathrm{xc}}[\rho] + \int \rho(\boldsymbol{r}) v_{\mathrm{nuc}}(\boldsymbol{r}) \mathrm{d}^3 r, \tag{7}$$

where $T_s[\rho]$ is the kinetic-energy of a reference system of noninteracting electrons with density $\rho$, $J[\rho] = \frac{1}{2}\iint \frac{\rho(\boldsymbol{r})\rho(\boldsymbol{r}')}{|\boldsymbol{r}-\boldsymbol{r}'|}\mathrm{d}^3 r \mathrm{d}^3 r'$ is the classical Coulomb interaction of the electron density with itself, and the exchange–correlation functional $E_{\mathrm{xc}}[\rho]$ collects all the remaining energy terms. This energy functional is then minimized by introducing a wavefunction for the reference system of noninteracting electrons, which is given by a single Slater determinant $|\Phi_s\rangle$ built from the orbitals $\{\phi_i\}$. These Kohn–Sham orbitals can then be determined by solving the KS equations,

$$\left[-\frac{\Delta}{2} + v_{\mathrm{nuc}}(\boldsymbol{r}) + v_{\mathrm{Coul}}[\rho](\boldsymbol{r}) + v_{\mathrm{xc}}[\rho](\boldsymbol{r})\right]\phi_i(\boldsymbol{r}) = \varepsilon_i \phi_i(\boldsymbol{r}), \tag{8}$$

where $v_{\mathrm{Coul}}[\rho](\boldsymbol{r}) = \int \frac{\rho(\boldsymbol{r}')}{|\boldsymbol{r}-\boldsymbol{r}'|}\mathrm{d}^3 r'$ is the classical Coulomb potential of the electrons and $v_{\mathrm{xc}}[\rho](\boldsymbol{r}) = \frac{\delta E_{\mathrm{xc}}[\rho]}{\delta\rho(\boldsymbol{r})}$ is the exchange–correlation potential. Since these potentials both depend on the electron density, the KS equations have to be solved in self-consistent field (SCF) iterations. Even though KS-DFT provides a formally exact theory for calculating the ground-state density, the exact exchange–correlation functional is not know and approximate functionals have to be introduced. For overviews of the currently available approximate functionals, see, *e.g.*, ref. 24–26, and for a discussion of their limitations, see, *e.g.*, ref. 27 and 28.

Even though the Hohenberg–Kohn theorem was initially formulated only for the ground state, it can easily be extended to the lowest state in each spin or spacial symmetry.[29,30] However, in this case the Hohenberg–Kohn functional $F_{\mathrm{HK}}[\rho]$ is no longer universal, but becomes symmetry-specific. In practice, this symmetry-specific functional is unknown, and one usually resorts to impose the symmetry constraints on the noninteracting reference system, *i.e.*, the Slater determinant formed from the KS orbitals. Note, however, that in the exact theory neither the spin nor the spatial symmetry of the wavefunction of this reference system correspond to the one of the true wavefunction.[31]

Despite the lack of a formal justification,[32] excited states have been targeted in variational KS-DFT calculations by employing excited-state wavefunctions for the noninteracting reference system. In the simplest case, this corresponds to replacing an occupied KS orbital by an unoccupied one (*i.e.*, a non-Aufbau solution), but it might also be necessary to form linear combinations of different Slater determinants for specific states.[33] In particular, this ΔDFT approach has been applied to study multiplet energies in transition metal complexes with DFT.[34] This approach can be extended to a ΔSCF-DFT scheme, in which the orbitals of the excited Slater determinants constructed for the noninteracting reference system are re-optimized.[35] In this case, it has to be ensured that the SCF procedure does not collapse to the ground-state.[36]

For the calculation of excitation energies with DFT, the application of such ΔSCF-DFT calculations has been rather limited. Usually, time-dependent DFT (discussed in section 2.2.1) provides more accurate results and avoids the rather cumbersome optimization of the KS orbitals of excited Slater determinants. There is a revived interest in the use ΔSCF-DFT and related methods for overcoming some of the limitations of TDDFT, such as for the description of Rydberg states[37] or of large conjugated organic molecules.[38] An interesting related approach is the constricted variational DFT method by Ziegler and coworkers,[39,40] that is based on the determination of stationary points of the energy functional, subject to the condition that the density difference corresponds to an electronic excitation. Both ΔSCF-DFT and TDDFT emerge from this formulation.

**2.1.2 Configuration Interaction-based methods.** The starting point for most wavefunction based quantum chemical methods is the *Hartree–Fock (HF) approximation*, in which a single Slater determinant $|\Phi_{\mathrm{HF}}\rangle$ is used as ansatz for the ground-state wavefunction. Minimization of the energy expectation value then leads to the HF equations

$$\left[-\frac{\Delta}{2} + v_{\mathrm{nuc}}(\boldsymbol{r}) + v_{\mathrm{Coul}}[\rho](\boldsymbol{r}) + \hat{K}\right]\phi_i(\boldsymbol{r}) = \varepsilon_i\phi_i(\boldsymbol{r}), \tag{9}$$

for determining the orbitals in this determinant. These equations are very similar to the KS equations introduced above, but instead of the exchange–correlation potential the nonlocal exchange operator $\hat{K} = \sum_j \hat{k}[\phi_j]$ with

$$\hat{k}[\phi_j]\phi_i(\boldsymbol{r}) = \int \frac{\phi_j^*(\boldsymbol{r}')\phi_i(\boldsymbol{r}')}{|\boldsymbol{r}-\boldsymbol{r}'|}\mathrm{d}^3r'\phi_j(\boldsymbol{r}) \tag{10}$$

appears. One way of expressing the HF determinant, that will be particularly convenient later on, is an exponential parametrization,[41]

$$|\Phi_{\mathrm{HF}}\rangle = \exp(\hat{\kappa})|\Phi\rangle, \quad \hat{\kappa} = \sum_{p>q}[\kappa_{pq}\hat{a}_p^\dagger\hat{a}_q - \kappa_{pq}^*\hat{a}_q^\dagger\hat{a}_p], \tag{11}$$

where $|\Phi\rangle$ is a trial state (usually a single Slater determinant), and $\hat{a}_p^\dagger$ and $\hat{a}_q$ are the operators creating or annihilating an electron in orbital $p$ or $q$, respectively. The advantage of this parametrization is that it introduces only non-redundant parameters by ensuring the orthogonality of the HF orbitals. Therefore, the parameters $\kappa_{pq}$ can be determined from an unconstrained optimization of the HF energy.

Electron correlation can then be included by employing a more general ansatz for the wavefunction that also includes excited Slater determinants, *i.e.*, determinants in which one or more of the occupied HF orbitals are replaced by virtual ones. In *configuration interaction* (*CI*) methods,[42] the many-electron wavefunction $|\Psi_k\rangle$ for a given electron state $k$ is expanded in a basis of Slater determinants as

$$|\Psi_k\rangle = (1+\hat{C}_k)|\Phi_0\rangle, \quad |\Phi_0\rangle \equiv |\Phi_{\mathrm{HF}}\rangle \tag{12}$$

where the reference state $|\Phi_0\rangle$ is usually chosen as the HF determinant. The operator $\hat{C}_k$ is in turn expressed as

$$\hat{C}_k = \hat{C}_1^{(k)} + \hat{C}_2^{(k)} + \ldots = \sum_{\mu_1} C_{\mu_1}^{(k)}\hat{\tau}_{\mu_1} + \sum_{\mu_2} C_{\mu_2}^{(k)}\hat{\tau}_{\mu_2} + \ldots, \tag{13}$$

that is, in terms of the product between coefficients $C_\mu^{(k)}$ and excitations operators $\hat{\tau}_\mu$ of different ranks. Here, $\mu_1$ and $\mu_2$ represent single and double excitations from occupied to virtual orbitals, and the corresponding excitation operators are

$\hat{\tau}_{\mu_1} = \hat{a}_a^\dagger \hat{a}_i$ and $\hat{\tau}_{\mu_2} = \hat{a}_a^\dagger \hat{a}_i \hat{a}_b^\dagger \hat{a}_j$, where indices $i,j,k,\ldots$ refer to occupied orbitals whereas indices $a,b,c,\ldots$ label virtual orbitals. Note that the coefficients $C_\mu^{(k)}$ are different for each electronic state $k$.

The coefficients $C_\mu$ can then be determined using the variational principle, *i.e.*, by minimizing the energy with respect to these coefficients. This leads to the Hamiltonian matrix in the basis of the HF and excited determinants,

$$H_{ij} = \langle \Psi_i | \hat{H} | \Psi_j \rangle \tag{14}$$

from which the coefficients and energies for the ground and excited states can be obtained as eigenvectors and eigenvalues, respectively. When considering expansions up to the highest possible excitation rank one arrives at the full CI solution, which is exact within a given basis set. However, the size of the corresponding Hamiltonian matrix makes its use impractical for all but the smallest molecular systems. Therefore, one is often constraint to include not more than single and double excitations (CISD). A further truncation already after single excitations results in the CIS method. While it is far from accurate because it lacks a proper inclusion of electron correlation, it nevertheless remains one of the few wavefunction methods that can be used to investigate the spectra of relatively large systems.[43–45] This accuracy can be improved[46,47] by introducing double excitations in a perturbative fashion, resulting in the CIS(D) model.[48]

While in single-reference CI methods the HF determinant is used as reference state $|\Phi_0\rangle$, this is a poor choice in situations where there are other close-lying excited states. This is often the case in open-shell systems such as transition metal complexes. One is then better served by *multi-reference configuration interaction* (MR-CI) methods, which use a reference based on a multi-configurational (MC) wavefunction,

$$|\Phi_0\rangle \equiv |\Phi_{\mathrm{MC}}(\{\mathbf{C}'\})\rangle = \sum_\nu (1 + \hat{C}'_\nu)|\Phi_{\mathrm{HF}}\rangle, \tag{15}$$

which is a small CI expansion where excitations are allowed only from within a set of orbitals, the so-called active space. This is comprised of a relatively small number of occupied and virtual orbitals, which is indicated above by the use of use of $\hat{C}'_\nu$ instead of $\hat{C}_\nu$. There are different approaches for generating the determinants in eqn (15), the most widely used is the complete active space (CAS), where a full CI is performed within the active space.

A further improvement consists in taking the orbital coefficients $\kappa_{pq}$ as additional variational parameters,

$$|\Phi_0\rangle \equiv |\Phi_{\mathrm{CASSCF}}(\{\mathbf{C},\kappa\})\rangle = \sum_\nu (1 + \hat{C}'_\nu)|\Phi_\nu(\kappa_\nu)\rangle, \tag{16}$$

giving rise to the CASSCF[49] wavefunction. However, the number of configurations and thus the computational effort increases factorially with the size of the active space.[41] Thus, systems that would require large active spaces present a challenge in this respect. This is particularly the case for systems with severe quasi-degeneracies, such as (polynuclear) transition metal complexes or for early actinide compounds.[50] For alternative approaches that scale polynomically with the size of the active space and thus allow for the use of significantly larger active spaces, see ref. 51 and 52.

Irrespective of the construction of the reference wavefunction and even when the (MR)-CI expansion is truncated at the SD level, calculations on all but relatively small molecules remain computationally infeasible. This has motivated the development of specialized approximations where the size of the CI expansions is reduced by removing of certain classes of excitation on the basis of physical arguments. One such approach is the *difference-dedicated CI* (DDCI), where configurations that contribute in approximately the same way to both the ground and excited states (*e.g.*, determinants that are doubly excited with respect to inactive orbitals) are disregarded. This way, energy differences between the states can still be determined accurately, whereas total energies are in general rather inaccurate. In its different flavors,[53–55] DDCI has been extensively used for determining the different spin states in relatively large molecules containing one or more magnetic centers,[56–58] as well as the electronic spectra of transition metal complexes.[59,60]

Finally, it is also worth mentioning that—unlike full CI—all truncated CI methods (with the exception of CIS) are not size-extensive. Thus, upon extending the size of the system a spurious decrease in the correlation energy occurs. As a result, excitation energies are not size-intensive, *i.e.*, they can spuriously change as the size of the system is increased (*e.g.*, when studying the effect of the solvation shell on the spectrum of a solute molecule), which may even change the results qualitatively. This can be approximately corrected by using suitable correction schemes,[61] but a more rigorous way for achieving size-extensivity of the correlation energy and size-intensivity of excitation energies is provided by coupled-cluster methods, that will be discussed in the following section.

**2.1.3 Single-reference coupled cluster methods.** In the coupled cluster approach,[41,62] the ground-state many-electron wavefunction is obtained by the so-called exponential parametrization, acting upon the HF determinant

$$|\Psi_0\rangle = \exp(\hat{T})|\Phi_{\mathrm{HF}}\rangle \tag{17}$$

where the operator $\hat{T}$ is of the same form as the excitation operator $\hat{C}_k$ in CI methods, but different labels are now used for the expansion coefficients to distinguish these different methods,

$$\hat{T} = \hat{T}_1 + \hat{T}_2 + \ldots = \sum_{\mu_1} t_{\mu_1}\hat{\tau}_{\mu_1} + \sum_{\mu_2} t_{\mu_2}\hat{\tau}_{\mu_2} + \ldots. \tag{18}$$

As with CI methods, this expansion is usually truncated, for instance after double excitations (resulting in the CCSD approximation). However, the exponential parametrization now generates higher excitation levels even when $\hat{T}$ is truncated, because terms such as $\hat{T}_1^2$, $\hat{T}_1\hat{T}_2$, and $\hat{T}_2^2$ now occur, which correspond to certain double, triple, and quadruple excitations, respectively. By construction, the exponential parametrization of the wavefunction ensures that the resulting energies will be size-extensive.

Since a variational determination of the coupled cluster amplitudes $t_\mu$ is not feasible, projection techniques are used instead. To this end, the Schrödinger equation is left-multiplied by $\langle\mu_i|\exp(-\hat{T})$, resulting in the ground-state energy

$$E_0 = \langle\Phi_{\mathrm{HF}}|\hat{H}\exp(\hat{T})|\Phi_{\mathrm{HF}}\rangle \tag{19}$$

and the amplitudes equations

$$\Omega_{\mu_i} = \langle\mu_i|\exp(-\hat{T})\hat{H}\exp(\hat{T})|\Phi_{\mathrm{HF}}\rangle = 0 \tag{20}$$

where $\langle\mu_i| = \langle\Phi_{\mathrm{HF}}|\hat{\tau}^{\dagger}_{\mu_i}$ with $\mu_i$ running over all possible excited determinants of excitation rank $i$. The amplitudes will have the general form

$$t_{\mu_1} = \frac{\langle\mu_1|\hat{A}|\Phi_{\mathrm{HF}}\rangle}{\Delta\varepsilon_{\mu_1}} = \frac{\langle{}^{a}_{i}|\hat{A}|\Phi_{\mathrm{HF}}\rangle}{\varepsilon_i - \varepsilon_a} \tag{21}$$

$$t_{\mu_2} = \frac{\langle\mu_2|\hat{B}|\Phi_{\mathrm{HF}}\rangle}{\Delta\varepsilon_{\mu_2}} = \frac{\langle{}^{ab}_{ij}|\hat{B}|\Phi_{\mathrm{HF}}\rangle}{\varepsilon_i + \varepsilon_j - \varepsilon_a - \varepsilon_b} \tag{22}$$

where $\hat{A}$ and $\hat{B}$ are operators involving the product of $\hat{H}$ and $\hat{T}$ operators. As the expressions for the former depend on the truncation level, we refer to the literature for concrete examples.[41,62]

Because of the projective nature of the coupled cluster method, it is not possible to invoke a variational principle in order to obtain excited states. Therefore, to construct excited state wavefunctions one would need to employ different reference states. This could, for instance, be an open-shell determinant corresponding to a single excitation with respect to $|\Phi_{\mathrm{HF}}\rangle$. This approach has several disadvantages. First, the above coupled cluster equations would have to be solved for each excited state, which can become computationally rather demanding. Second, different electronic states will no longer be orthogonal, which complicates the calculation of transition moments. Finally, excited states that are not dominated by a single determinant cannot be easily described, as they would require a multi-reference coupled cluster method.

An alternative that remedies part of these difficulties is the *equation-of-motion coupled cluster* method for excitation energies (EOM-EE), where one introduces the parametrization

$$|\Psi_k\rangle = \hat{C}_k \exp(\hat{T})|\Phi_{\mathrm{HF}}\rangle \tag{23}$$

$$\langle\bar{\Psi}_l| = \langle\Phi_{\mathrm{HF}}|(1 + \hat{\bar{C}}_l \exp(-\hat{T})). \tag{24}$$

Thus, instead of the HF determinant the coupled cluster wavefunction is used as reference state of a CI-like expansion. In this EOM-EE parametrization, the bra and ket states $|\Psi_k\rangle$ and $\langle\bar{\Psi}_l|$ are neither Hermitian conjugate nor orthogonal among themselves, but rather biorthogonal, *i.e.*, $\langle\bar{\Psi}_l|\Psi_k\rangle = \delta_{kl}$. This parametrization allows for a Hamiltonian matrix

$$H_{ij} = \langle\bar{\Psi}_i|\hat{H}|\Psi_j\rangle = \bar{\mathbf{C}}_i^T \mathbf{H} \mathbf{C}_j \tag{25}$$

to be formed, which can then be diagonalized to obtain the excitation energies. From the definitions of $|\Psi_k\rangle$ and $\langle\bar{\Psi}_l|$ the matrix **H** is obtained as

$$\mathbf{H} = \begin{pmatrix} E_0 & \boldsymbol{\eta}^T \\ \mathbf{0} & \mathrm{A} + E_0\mathbf{I} \end{pmatrix}, \tag{26}$$

where $E_0$ is the ground-state coupled cluster energy, $\eta_\nu$ is the vector

$$\eta_\nu = \langle\Phi_{\mathrm{HF}}|[\hat{H},\hat{\tau}_\nu]\exp(\hat{T})|\Phi_{\mathrm{HF}}\rangle, \tag{27}$$

and **A** is the so-called coupled cluster Jacobian with the elements

$$\mathrm{A}_{\mu\nu} = \langle\mu|\exp(-\hat{T})[\hat{H},\hat{\tau}_\nu]\exp(\hat{T})|\Phi_{\mathrm{HF}}\rangle. \tag{28}$$

By rewriting the above equations in terms of the energy difference with respect to the coupled-cluster ground-state energy,[41,62] one can identify the eigenvalues of the matrix **A** in eqn (26) with the excitation energies for the system.

These excitation energies are size-intensive,[63] thus presenting a significant advantage over CI approaches. The CI-like parametrization for the excited-states makes the calculation of transition moments and other expectation values rather simple, even though both left and right eigenvectors need to be calculated because **A** is not Hermitian. However, these transition moments are not size-intensive[64] and therefore in general not reliable for large systems.

**2.1.4 Multi-reference coupled cluster methods.** The coupled cluster-based methods discussed above present a significant improvements over CI-based methods, in particular because excitation energies are size-intensive. However, they are based on a single determinant reference for the ground state. As such, they might not be applicable in more complicated cases where already the ground state requires a multi-reference treatment. This limitation can be remedied by employing multi-reference coupled-cluster approaches[65] such as the Hilbert-space (HSCC) and Fock-space (FSCC) coupled cluster or other, more approximate multi-reference methods.[66] In the following we shall focus on the Fock-space approach, because it provides a direct route to excited states and has been applied in a number of applications in actinide and heavy-element chemistry.[67–74]

All multi-reference methods define a reference (or model) space $P$, consisting of a set of determinants $\{|\varphi_i\rangle\}$. Usually, this is achieved by defining an active space, and all determinants contributing to a full CI expansion within this active space are considered. In MRCI methods this is usually the active space obtained from a CASSCF calculation, whereas in multi-reference coupled-cluster methods the HF orbitals are used directly without reoptimization. Of course, it is important that this model space contains all relevant configurations for the states that are of interest.[62] All other possible contributions to the exact wavefunctions that are not contained in the model space $P$ are within its orthogonal complement $Q$.

This model space then serves as the starting point for obtaining a set $\{|\Psi_k\rangle\}$ of exact solutions of the Schrödinger equation with the same dimension as $P$. The correspondence between wavefunctions in the model space $\{|\varphi_k\rangle\}$ and the exact wavefunctions $\{|\Psi_k\rangle\}$ is then established through a projection operator $\hat{P} = \sum_i |\varphi_i\rangle\langle\varphi_i|$ so that

$$|\varphi_k\rangle = \hat{P}|\Psi_k\rangle. \tag{29}$$

In addition, one defines the wave operator $\hat{\Omega}$ that establishes the reverse mapping and generate the exact wavefunction from one belonging to the model space,

$$|\Psi_k\rangle = \hat{\Omega}|\varphi_k\rangle. \tag{30}$$

Using these definitions, one can now change from the problem of solving the exact Schrödinger equation, $\hat{H}|\Psi_m\rangle = E_m|\Psi_m\rangle$, to that of solving a Schrödinger equation for the model space

$$\hat{H}_{\text{eff}}|\varphi_m\rangle = \Omega^{-1}\hat{H}\hat{\Omega}|\varphi_m\rangle = E_m|\varphi_m\rangle, \tag{31}$$

where the exact Hamiltonian $\hat{H}$ is now replaced by an effective Hamiltonian $\hat{H}_{\text{eff}}$ which has the same eigenvalues. The wave operator $\hat{\Omega}$ and, consequently, the effective Hamiltonian $\hat{H}_{\text{eff}}$ can be defined *via* the solution of the so-called Bloch equation. For details, we refer to ref. 75.

Once $\hat{\Omega}$ is obtained, $\hat{H}_{\text{eff}}$ in eqn (31) can be constructed and its matrix representation can be diagonalized to obtain the energies $\{E_m\}$. In multi-reference coupled cluster, an exponential parametrization is used as ansatz for the wave operator $\hat{\Omega}$,

$$\hat{\Omega} = \exp(\hat{S}) \tag{32}$$

where the operator $\hat{S}$ contains operators exciting electrons from the $P$ to the $Q$ spaces, multiplied with the corresponding amplitudes. The form of $\hat{S}$ will depend on the details of the approach. In the case of FSCC, it is constructed by considering operators defined for different sectors of Fock-space, where each sector comprises a model space which differs from the reference situation by the addition or removal of electrons, starting from a the original closed-shell determinant $|\Phi_0\rangle$. Each of these sector is identified by the tuple $(n,m)$, where $n$ represents the number of holes and $m$ the number of electrons created on $|\Phi_0\rangle$. Thus, $\hat{S}$ is expressed as

$$\hat{S} = \hat{S}^{(0,0)} + \hat{S}^{(1,0)} + \hat{S}^{(0,1)} + \hat{S}^{(1,1)} + \ldots \tag{33}$$

and similar decompositions are used for the projection operators $\hat{P}$ and $\hat{Q}$. Using this decomposition, the amplitudes can be determined in a hierarchical fashion for the different sectors. For instance, in order to obtain the contributions from the $(a,b)$ sector to $\hat{S}$, one must first solve all $(m,n)$ sectors for which $m < a$, $n < b$.[75,76] For a given sector, one obtains amplitude equations of the form

$$\langle \chi_j^{(m,n)} | \hat{H}\hat{\Omega} - \hat{\Omega}\hat{H}_{\text{eff}}^{(m,n)} | \varphi_i^{(m,n)} \rangle = 0 \tag{34}$$

where $\{\chi_j^{(m,n)}\}$ are the determinants belonging to the complement space for the $(m,n)$ sector. For the (0,0) sector this is equivalent to the single-reference amplitude equations in eqn (20).

However, in their original formulation FSCC methods are plagued by the so-called intruder state problem.[77] This occurs during the iterative solution of eqn (34). When certain low-lying states belonging to $Q^{(m,n)}$ turn out to have energies close to (or even lower than) the higher-lying states from $P^{(m,n)}$ in some amplitudes equations (which are similar to those in eqn (21) and (22)) might have very small energy denominators and prevent the solution of the linear system. The larger the $P^{(m,n)}$ space, the more serious this problem becomes, as accidental degeneracies with $Q$ states become increasingly likely. To alleviate this difficulty, approaches based on an intermediate Hamiltonian formulation (IHFSCC) have been introduced.[78–82] These divide the $P$ space as $P = P_m + P_i$ and $P_m$ now serves as the basis for projecting the lower exact solutions, whereas for $P_i$ this requirement is relaxed. This provides enough flexibility so that when $Q$ states interact strongly with the higher-lying $P_i$ states, the corresponding amplitude equations can be approximated to assure convergence. The IHFSCC approach has become the *de facto* standard for treating (small) molecules containing heavy elements.[67,68,71,74,83,84]

For situations where the reference is a closed-shell determinant it is instructive to compare the EOM-EE and Fock-space approaches. Starting from the definitions in eqn (32), we can write the wavefunction for state $k$ as

$$|\Psi_k^{(\text{FS})}\rangle = \hat{\Omega}^{\text{FS}}|\Phi_0\rangle = \exp(\hat{S})|\Phi_0\rangle = \exp(\hat{S} - \hat{T})\exp(\hat{T})|\Phi_0\rangle. \tag{35}$$

Comparing eqn (35) and (24), one sees that unlike EOM-EE, Fock-space coupled cluster departs from the linear parametrization for the excited states. The exponential parametrization ensures that only connected terms are taken into account, making the excited state energies different in both cases. The differences in electronic spectra calculated with FSCC for the (1,1) sector and by EOM-EE have recently been shown[71,85–87] to be non-negligible for absolute excitation energies, with the latter being in general higher. However, relative excited state energies are in general very similar.

**2.1.5 Multireference perturbation theory-based methods.** Given that coupled cluster methods can be computationally expensive, in particular for higher excitation levels such as CCSDT, other approaches have been devised that attempt to combine a reasonable accuracy in the description of electron correlation and flexibility to obtain excited states even when the reference wavefunction present a significant multi-configurational character. The perhaps most popular of such approaches is the CASPT2 method of Roos and coworkers[88,89] where one combines a CASSCF wavefunction with second-order perturbation theory.

Being based on perturbation theory, one now starts from a partitioning of the Hamiltonian into a zeroth-order contribution $\hat{H}_0$ and a perturbing part $\hat{V}$,

$$\hat{H} = \hat{H}_0 + \hat{V} \tag{36}$$

where $\hat{H}_0$ is a Fock-like operator that has the CASSCF wavefunctions $|\varphi_m\rangle$ as eigenvectors, *i.e.*,

$$\hat{H}_0|\varphi_m\rangle = E_{0,m}|\varphi_m\rangle. \tag{37}$$

As in the multi-reference coupled cluster methods above, in the multistate CASPT2 method[89] one partitions Hilbert space into different subspaces. First, the model space $P_0$ contains a subset $\{|\varphi_i\rangle\}$ of the CASSCF wavefunctions as reference states. Second, the subspace $P'$ orthogonal to $P_0$ contains the remaining $\{|\varphi_j\rangle\}$ CASSCF wavefunctions. Finally, the orthogonal complement $Q$ is made up of all other determinants not contained within the CASSCF active space. Furthermore, one defines a wave operator $\hat{\Omega}^{\mathrm{PT2}}$ that provide the mapping between the model space and the exact solutions. Instead of the exponential parametrization in coupled cluster methods, $\hat{\Omega}^{\mathrm{PT2}}$ is now expressed as a linear expansion in the orders of perturbation, and only the terms up to first order are retained,

$$\hat{\Omega}^{\mathrm{PT2}} = 1 + \hat{\Omega}^{(1)} \tag{38}$$

In multistate CASPT2,[90] $\hat{\Omega}^{\mathrm{PT2}}$ can be expressed as a linear combination of state-specific[90,91] wave operators,

$$\hat{\Omega}^{(1)} = \sum_i \hat{\Omega}_i^{(1)} |\varphi_i\rangle\langle\varphi_i|, \tag{39}$$

where the index runs over all the functions in the model space $P_0$.

Using such a formalism, one arrives at the equations for the individual states

$$\hat{\Omega}^{(1)}|\varphi_i\rangle = \hat{R}_i\hat{V}|\varphi_i\rangle = \sum_k \frac{|k\rangle\langle k|\hat{V}|\varphi_i\rangle}{(E_0^i - F^k)}, \tag{40}$$

where $k$ runs over the states belonging to the $Q$ subspace and where the actual form of the denominator involves orbital energy differences, whereas $F^k$ is a generalized Fock operator.

The main weakness of CASPT2 is its susceptibility to intruder states, that is, states that belong to $Q$ and are thus outside of active spaces, but that have energies close to $E_0^i$. These will makes the expression for $\hat{R}_i$ go to infinity, causing the perturbation expansion to diverge. Instead of adopting the intermediate Hamiltonian technique as done in the coupled cluster case, Roos and coworkers[92–94] as well as others[95] devised practical solutions based on the modification of such denominators by the application of a global level shift parameter that modifies the Hamiltonian in such a way that any effects due to the quasidegeneracy of $E_0^i$ and $F^k$ can be avoided. This approach has been found to work very well in practice for the so-called "weak" intruder states that do not interact too strongly with the reference. For more strongly interacting states other solutions must be sought (*e.g.*, including them into the active space), otherwise one should employ alternative formulations such as the NEVPT2 approach[96] that avoid intruder states by construction.

The performance of CASPT2 relative to methods such as MRCI, EOM-EE or IHFSCC has been evaluated for a number of cases, for instance in heavy-element chemistry.[71,73,74,84,97,98] In general, CASPT2 yields excitation energies rather close to those obtained with methods that are formally more accurate at a fraction of the computational cost. However, their relative position and the corresponding symmetry classification are often less reliable, which can be attributed to the relatively low accuracy in which dynamical correlation is taken into account. In spite of that, CASPT2 remains one of the few methods (along with MRCI approaches discussed earlier) that can accurately describe both static and dynamic correlation effects for large molecular complexes containing centers with a number of half-filled *d* or *f* shells such as those containing (bi)metallic centers.[57,99,100] It is also routinely employed to study the spectra and photochemistry of other complexes of transition metals and heavy elements.[72,101–105]

## 2.2 Time-dependent approaches based on response theory

Instead of explicitly calculating the wavefunctions of the different excited states, approaches based on response theory set out to calculated the linear response function $\langle\langle\hat{\mu}_\alpha;\hat{\mu}_\beta\rangle\rangle_\omega$ (see eqn (5)). A common theoretical framework for achieving this with different methods of quantum chemistry is provided by the quasienergy formalism pioneered by Christiansen and coworkers.[19,106] It defines a quasienergy as the time-dependent generalization of the energy,

$$Q(t) = \left\langle \tilde{\Psi}_0(t) \middle| \hat{H} + \hat{V}_\omega(t) - \mathrm{i}\frac{d}{dt} \middle| \tilde{\Psi}_0(t) \right\rangle \tag{41}$$

with

$$|\tilde{\Psi}_0(t)\rangle = e^{-\mathrm{i}E_0 t}|\Psi_0(t)\rangle, \tag{42}$$

as well as its time average over one period of the perturbation $T = 2\pi/\omega$

$$\{Q(t)\}_T = \frac{1}{T}\int_{-T/2}^{T/2} Q(t)dt. \tag{43}$$

With these definitions, the (time-dependent) wavefunction $|\tilde{\Psi}_0(t)\rangle$ can be determined by making the time-averaged quasienergy stationary with respect to variations in the wavefunction,

$$\delta\{Q(t)\}_T = 0. \tag{44}$$

Response functions can then be determined as derivatives of the time-averaged quasi-energy with respect to the perturbation strengths. In particular, the electric dipole–electric dipole linear response function is given by

$$\langle\langle\hat{\mu}_\alpha;\hat{\mu}_\beta\rangle\rangle_\omega = \frac{d^2\{Q(t)\}_T}{d\varepsilon_\alpha(\omega)d\varepsilon_\beta(\omega)}. \tag{45}$$

Note that this is analogous to the time-independent case, where the wavefunction is determined by making the expectation value of the energy stationary, and where the corresponding static properties (*e.g.*, the polarizability) can be determined as derivatives of the energy. The quasienergy formalism allows one to employ the same techniques also for frequency-dependent problems.

In any quantum chemical method, a parametrization of the wavefunction is introduced, *i.e.*, the wavefunction depends on a set of parameters $\boldsymbol{\lambda}$. In so-called variational methods these parameters are in the time-independent case determined by minimizing the energy expectation value. In the time-dependent case, the corresponding parameters can be determined by minimizing the time-averaged quasienergy $\{Q(t,\boldsymbol{\lambda})\}_T$. However, a number of important quantum-chemical methods, such as coupled cluster theory, are not variational, *i.e.*, the wavefunction parameters $\boldsymbol{\lambda}$ are determined from other conditions. In this case, one can replace $Q(t,\boldsymbol{\lambda})$ by the Lagrangian

$$L(t,\boldsymbol{\lambda},\bar{\boldsymbol{\lambda}}) = Q(t,\boldsymbol{\lambda}) + \bar{\boldsymbol{\lambda}}\boldsymbol{g}(\boldsymbol{\lambda}). \tag{46}$$

The new set of parameters $\bar{\boldsymbol{\lambda}}$ are the Lagrange multipliers and $\boldsymbol{g}(\boldsymbol{\lambda}) = 0$ is a set of auxiliary time-dependent equations. Both the parameters $\boldsymbol{\lambda}$ and the Lagrange multipliers $\bar{\boldsymbol{\lambda}}$ can then be treated as variational parameters.

The parameters and possibly also the multipliers can then be determined using variational perturbation theory by expanding the quasienergy Lagrangian in orders of the perturbation strengths and taking the time average,

$$\begin{aligned}\{L(t,\boldsymbol{\lambda},\bar{\boldsymbol{\lambda}})\}_T &= L^{(0)} + \sum_{\alpha} \varepsilon_\alpha(\omega) L_\alpha^{(1)}(\omega) \\ &\quad + \sum_{\alpha\beta} \varepsilon_\alpha(\omega)\varepsilon_\beta(\omega) L_{\alpha\beta}^{(2)}(\omega) + \ldots,\end{aligned} \tag{47}$$

where the linear response function can be identified as

$$\langle\langle \hat{\mu}_\alpha; \hat{\mu}_\beta \rangle\rangle_\omega = \frac{\mathrm{d}^2\{L(t,\boldsymbol{\lambda},\bar{\boldsymbol{\lambda}})\}_T}{\mathrm{d}\varepsilon_\alpha(\omega)\mathrm{d}\varepsilon_\beta(\omega)} = L_{\alpha\beta}^{(2)}(\omega). \tag{48}$$

Similarly, the wavefunction parameters $\boldsymbol{\lambda}$ and multipliers $\bar{\boldsymbol{\lambda}}$ can be expanded as

$$\boldsymbol{\lambda}(t) = \boldsymbol{\lambda}^{(0)} + (e^{\mathrm{i}\omega t} + e^{-\mathrm{i}\omega t}) \sum_\alpha \varepsilon_\alpha(\omega) \boldsymbol{\lambda}_\alpha^{(1)}(\omega) + \ldots \tag{49}$$

$$\bar{\boldsymbol{\lambda}}(t) = \bar{\boldsymbol{\lambda}}^{(0)} + (e^{\mathrm{i}\omega t} + e^{-\mathrm{i}\omega t}) \sum_\alpha \varepsilon_\alpha(\omega) \bar{\boldsymbol{\lambda}}_\alpha^{(1)}(\omega) + \ldots, \tag{50}$$

where we will use $\boldsymbol{\lambda}^{(1)}(\omega)$ and $\bar{\boldsymbol{\lambda}}^{(1)}(\omega)$ to refer to the first order terms in these expansions. These can then be determined from the variational conditions

$$\frac{\mathrm{d}\{L(t,\boldsymbol{\lambda},\bar{\boldsymbol{\lambda}})\}_T}{\mathrm{d}\boldsymbol{\lambda}} = \frac{\mathrm{d}\{L(t,\boldsymbol{\lambda},\bar{\boldsymbol{\lambda}})\}_T}{\mathrm{d}\bar{\boldsymbol{\lambda}}} = 0 \tag{51}$$

at each perturbation order.

Taking the second derivative of $\{L(\mathrm{t},\boldsymbol{\lambda},\bar{\boldsymbol{\lambda}})\}_T$ with respect to the perturbation strengths $\varepsilon_\alpha(\omega)$ and $\varepsilon_\beta(\omega)$ while taking the implicit dependence of $\boldsymbol{\lambda}$ and $\bar{\boldsymbol{\lambda}}$ on the perturbation strengths into account *via* the chain rule leads to[19]

$$\begin{aligned}\langle\langle \hat{\mu}_\alpha; \hat{\mu}_\beta \rangle\rangle_\omega &= L_{\alpha\beta}^{(2)}(\omega) \\ &= \begin{pmatrix} \boldsymbol{\lambda}_\alpha \\ \bar{\boldsymbol{\lambda}}_\alpha \end{pmatrix}^T \begin{pmatrix} \boldsymbol{F} & \boldsymbol{A} \\ \boldsymbol{A}^T & \boldsymbol{J} \end{pmatrix} \begin{pmatrix} \boldsymbol{\lambda}_\beta \\ \bar{\boldsymbol{\lambda}}_\beta \end{pmatrix} + \begin{pmatrix} \boldsymbol{\eta}_\alpha \\ \boldsymbol{\xi}_\alpha \end{pmatrix}^T \begin{pmatrix} \boldsymbol{\lambda}_\beta \\ \bar{\boldsymbol{\lambda}}_\beta \end{pmatrix} + \begin{pmatrix} \boldsymbol{\lambda}_\alpha \\ \bar{\boldsymbol{\lambda}}_\alpha \end{pmatrix}^T \begin{pmatrix} \boldsymbol{\eta}_\beta \\ \boldsymbol{\xi}_\beta \end{pmatrix}\end{aligned} \tag{52}$$

where we introduced $\boldsymbol{\lambda}_{\alpha/\beta} = \boldsymbol{\lambda}_{\alpha/\beta}{}^{(1)}$ and $\bar{\boldsymbol{\lambda}}_{\alpha/\beta} = \bar{\boldsymbol{\lambda}}_{\alpha/\beta}{}^{(1)}$ to simplify the notation and define the abbreviations for the partial derivatives with respect to the parameters and multipliers

$$\mathbf{F} = \frac{\partial^2\{L^{(2)}\}_T}{\partial\boldsymbol{\lambda}^{(1)}(\omega)\partial\boldsymbol{\lambda}^{(1)}(\omega)} \quad \mathbf{A} = \frac{\partial^2\{L^{(2)}\}_T}{\partial\boldsymbol{\lambda}^{(1)}(\omega)\partial\bar{\boldsymbol{\lambda}}^{(1)}(\omega)} \quad \mathbf{J} = \frac{\partial^2\{L^{(2)}\}_T}{\partial\bar{\boldsymbol{\lambda}}^{(1)}(\omega)\partial\bar{\boldsymbol{\lambda}}^{(1)}(\omega)} \tag{53}$$

and for the mixed partial derivatives with respect to parameters or multipliers and perturbation strength

$$\boldsymbol{\eta}_{\alpha/\beta} = \frac{\partial\{L^{(2)}\}_T}{\partial\boldsymbol{\lambda}^{(1)}(\omega)\partial\varepsilon_{\alpha/\beta}(\omega)} \quad \boldsymbol{\xi}_{\alpha/\beta} = \frac{\partial\{L^{(2)}\}_T}{\partial\bar{\boldsymbol{\lambda}}^{(1)}(\omega)\partial\varepsilon_{\alpha/\beta}(\omega)}. \tag{54}$$

Note that all these partial derivatives depend on the perturbation frequency $\omega$.

The first-order parameters $\boldsymbol{\lambda}_{\alpha/\beta}$ and multipliers $\bar{\boldsymbol{\lambda}}_{\alpha,\beta}$ can be determined from the variational conditions of eqn (51). They only appear in the second-order term

$L_{\alpha\beta}{}^{(2)}(\omega)$ and setting the derivative of eqn (52) with respect to $\boldsymbol{\lambda}_\alpha$ and $\bar{\boldsymbol{\lambda}}_\alpha$ to zero leads to the linear equations

$$\begin{pmatrix} \boldsymbol{\lambda}_\beta \\ \bar{\boldsymbol{\lambda}}_\beta \end{pmatrix} = -\begin{pmatrix} \boldsymbol{F} & \boldsymbol{A} \\ \boldsymbol{A}^T & \boldsymbol{J} \end{pmatrix}^{-1} \begin{pmatrix} \boldsymbol{\eta}_\beta \\ \boldsymbol{\xi}_\beta \end{pmatrix}. \tag{55}$$

Substituting this back into eqn (52) yields the linear response function

$$\langle\langle \hat{\mu}_\alpha; \hat{\mu}_\beta \rangle\rangle_\omega = -\begin{pmatrix} \boldsymbol{\eta}_\alpha \\ \boldsymbol{\xi}_\alpha \end{pmatrix}^T \begin{pmatrix} \boldsymbol{F} & \boldsymbol{A} \\ \boldsymbol{A}^T & \boldsymbol{J} \end{pmatrix}^{-1} \begin{pmatrix} \boldsymbol{\eta}_\beta \\ \boldsymbol{\xi}_\beta \end{pmatrix}, \tag{56}$$

which has poles for frequencies that lead to zero eigenvalues of the matrix whose inverse appears in the above equation. This provides a route to the calculation of excitation energies within response theory, whereas the corresponding oscillator strengths can be calculated as the residues corresponding to these poles of the linear response function.

**2.2.1 Time-dependent DFT (TDDFT).** The theoretical foundation for the time-dependent generalization of DFT was introduced by Runge and Gross,[107] and the subsequently introduced TDDFT response theory[108] forms the basis for its application for the calculation of excited states. In TDDFT, the time-dependent density is obtained from the KS wavefunction of a reference system of noninteracting electrons, *i.e.*, a single Slater determinant $|\tilde{\Phi}_s(t)\rangle$, where the KS orbitals $\tilde{\phi}_i(\boldsymbol{r},t)$ now become time-dependent. This gives rise to the time-dependent density $\rho(\boldsymbol{r},t) = \sum_i |\tilde{\phi}_i(\boldsymbol{r},t)|^2$. Within the adiabatic approximation any explicit time or history dependence of the exchange-correlation contribution is neglected, and one arrives at the time-averaged quasienergy functional[109,110]

$$\begin{aligned} \{Q[\rho](t)\}_T &= \{E[\rho](t)\}_T + \{\langle\tilde{\Phi}_s|\hat{V}_\omega(t)|\tilde{\Phi}_s\rangle\}_T \\ &\quad - \left\{\langle\tilde{\Phi}_s|\mathrm{i}\frac{\partial}{\partial t}|\tilde{\Phi}_s\rangle\right\}_T, \end{aligned} \tag{57}$$

where $E[\rho]$ is the energy functional of eqn (7) evaluated for the time-dependent density $\rho(\boldsymbol{r},t)$, the second term accounts for the time-dependent perturbation (eqn (2)), and the last term arises from the time derivative in the definition of the quasienergy (eqn (41)).

In order to obtain expressions for the response equations and the linear response function one introduces a parametrization of the time-dependent KS determinant $|\tilde{\Phi}_s\rangle$. This can be achieved by using an exponential parametrization acting upon the ground-state Kohn-Sham determinant $|\Phi_s\rangle$ (*cf.* eqn (11))

$$|\tilde{\Phi}_s\rangle = \exp(\hat{\kappa}(t))|\Phi_s\rangle, \quad \hat{\kappa}(t) = \sum_{p>q} [\kappa_{pq}(t)\hat{a}_p^\dagger\hat{a}_q - \kappa_{pq}^*(t)\hat{a}_q^\dagger\hat{a}_p], \tag{58}$$

*i.e.*, the time dependence is contained in the operator $\hat{\kappa}(t)$. This parametrization automatically ensures the orthogonality of the time-dependent KS orbitals without introducing additional Lagrange multipliers. Using this parametrization, the linear response function can be determined by differentiating the time-averaged quasienergy with respect to the parameters $\kappa_{pq}(t)$.

Because these parameters can be determined variationally, no additional Lagrange multipliers are needed and the linear response function is given by

$$\langle\langle \hat{\mu}_\alpha;\hat{\mu}_\beta \rangle\rangle_\omega = -\boldsymbol{\eta}_\alpha \mathbf{F}(\omega)^{-1}\boldsymbol{\eta}_\beta \tag{59}$$

where for the **F** matrix one obtains

$$\mathbf{F}(\omega) = \frac{\partial^2 \{Q^{(2)}\}_T}{\partial \boldsymbol{\kappa}^{(1)} \partial \boldsymbol{\kappa}^{(1)}} = \boldsymbol{E}^{[2]} - \omega \boldsymbol{S}^{[2]} \tag{60}$$

where $\mathbf{S}^{[2]}$ is a diagonal matrix arising from the last term in eqn (57) and $\mathbf{E}^{[2]}$, is the electronic Hessian which has the form

$$\mathbf{E}^{[2]} = \begin{pmatrix} \mathbf{A} & \mathbf{B} \\ \mathbf{B}^* & \mathbf{A}^* \end{pmatrix}. \tag{61}$$

The subblocks of this matrix are given by

$$A_{ia,jb} = \delta_{ij}\delta_{ab}(\varepsilon_a - \varepsilon_i) + 2(ia|bj) + (ia|f_{\mathrm{xc}}|bj), \tag{62}$$

$$B_{ia,jb} = 2(ia|jb) + (ia|f_{\mathrm{xc}}|jb), \tag{63}$$

where $\varepsilon_p$ are the KS orbital energies, $(pq|rs)$ are two-electron integrals in the Mulliken (charge cloud) notation and

$$(ia|f_{\mathrm{xc}}|jb) = \iint \phi_i(\boldsymbol{r})\phi_a(\boldsymbol{r}) \left[\frac{\delta^2 E_{\mathrm{xc}}[\rho]}{\delta\rho(\boldsymbol{r})\delta\rho(\boldsymbol{r}')}\right] \phi_j(\boldsymbol{r}')\phi_b(\boldsymbol{r}')\mathrm{d}^3r\mathrm{d}^3r' \tag{64}$$

are the integrals over the exchange-correlation kernel. Thus, excitation energies can be calculated by determining the eigenvalues of $\mathbf{E}^{[2]}$. Since the size of this matrix is generally rather large, iterative diagonalization procedures which only require the calculation of matrix–vector products are usually employed (see *e.g.* the discussion in ref. 111).

TDDFT has been widely used for studying excited states in medium to large molecules.[112–114] Its main advantage is its excellent cost–accuracy ratio. For a broad range of chemical applications, TDDFT is capable of providing results which are qualitatively correct, and often come close to the accuracy of more sophisticated wavefunction-based methods such as CASPT2. This has been demonstrated in a number of recent benchmarking studies on light[115–121] and heavy-element containing[73] molecules. However, the accuracy often depends on the proper choice of the exchange–correlation functional and kernel, and choosing these appropriately for a particular application is based on experience and often requires careful comparison with more accurate wavefunction based calculations.

However, with the currently available approximations, TDDFT also has some severe shortcomings.[122] First, with standard non-hybrid exchange–correlation functionals, it does not provide a correct description of Rydberg states. This is caused by the wrong asymptotic form of the exchange–correlation potential.[123] This problem can be addressed by constructing approximations for the exchange–correlation potential that enforce the correct asymptotic behavior, for instance by using orbital-dependent model potentials.[124] Alternatively, range-separated hybrid functionals can be used that also result in asymptotically correct exchange–correlation potentials.[28] Second, charge-transfer excitations are not described correctly. For detailed discussions of this problem and possible solutions, we refer to ref. 125–127. Finally, within the adiabatic approximation TDDFT does not include double excitations. This could in principle be addressed by using a frequency-dependent exchange–correlation kernel,[128,129] but such approximations are not suitable for general applications yet.

**2.2.2 Linear-response coupled cluster.** While conventional coupled-cluster theory does not provide a direct route to excited states, it can still be used as starting point for a response theory. Starting from the exponential parametrization of the (time-dependent) wavefunction,

$$|\hat{\Psi}\rangle = \exp(\hat{T}(t))|\Phi_{\mathrm{HF}}\rangle, \tag{65}$$

and performing a projection of the time-dependent Schrödinger onto the ground-state reference $\langle\Phi_0|$ as well as onto the set of excited determinants $\langle\mu_i|$ one arrives at the time-dependent analogs of eqn (19) and (20)

$$Q(\mathbf{t};t) = \langle\Phi_{\mathrm{HF}}|(\hat{H} + \hat{V}_{\omega}(t))\exp(\hat{T}(t))|\Phi_{\mathrm{HF}}\rangle \tag{66}$$

$$0 = \Omega_{\mu_i}(\mathbf{t};t) = \left\langle \mu_i \middle| \exp(-\hat{T}(t))\left(\hat{H} + \hat{V}_{\omega}(t) - \mathrm{i}\frac{\partial}{\partial t}\right)\exp(\hat{T}(t)) \middle| \Phi_{\mathrm{HF}} \right\rangle \tag{67}$$

for the coupled cluster quasienergy and time-dependent amplitude equations, respectively.

As in the time-independent case, the coupled-cluster wavefunction is not determined variationally. Therefore, the coupled-cluster Lagrangian[19,106]

$$L_{CC}(\mathbf{t},\bar{\mathbf{t}};t) = Q(\mathbf{t};t) + \sum_{\mu}\bar{t}_{\mu}\Omega_{\mu}(\mathbf{t};t), \tag{68}$$

is used as starting point for a response theory, where the multipliers $\bar{\mathbf{t}}$ have been introduced and the amplitude equations $\Omega_{\mu}(\mathbf{t};t)$ serve as constraints. The linear response function can then be determined by taking the derivative of the time-averaged Lagrangian $\{L_{\mathrm{CC}}(\mathbf{t},\bar{\mathbf{t}};t)\}_T$, yielding the linear response function (*cf.* eqn (56))

$$\langle\langle\hat{\mu}_{\alpha};\hat{\mu}_{\beta}\rangle\rangle_{\omega} = -\begin{pmatrix}\boldsymbol{\eta}_{\alpha}\\ \boldsymbol{\xi}_{\alpha}\end{pmatrix}^{T}\begin{pmatrix}\boldsymbol{F} & \boldsymbol{A}\\ \boldsymbol{A}^{T} & \mathbf{0}\end{pmatrix}^{-1}\begin{pmatrix}\boldsymbol{\eta}_{\beta}\\ \boldsymbol{\xi}_{\beta}\end{pmatrix}, \tag{69}$$

where the matrix $\boldsymbol{J}$ is zero because the multipliers $\bar{\boldsymbol{\lambda}}$ only appear linearly in the Lagrangian. This response function can be rewritten as

$$\langle\langle\hat{\mu}_{\alpha};\hat{\mu}_{\beta}\rangle\rangle_{\omega} = -\begin{pmatrix}\boldsymbol{\eta}_{\alpha}\\ \boldsymbol{\xi}_{\alpha}\end{pmatrix}^{T}\begin{pmatrix}\mathbf{0} & -(\boldsymbol{A}^{T})^{-1}\\ -\boldsymbol{A}^{-1} & \boldsymbol{A}^{-1}\boldsymbol{F}(\boldsymbol{A}^{T})^{-1}\end{pmatrix}\begin{pmatrix}\boldsymbol{\eta}_{\beta}\\ \boldsymbol{\xi}_{\beta}\end{pmatrix}, \tag{70}$$

which reveals that the poles of the response function correspond to zero eigenvalues of the matrix $\boldsymbol{A}$, which is given by

$$\frac{\partial^2\{L_{CC}^{(2)}(\mathbf{t},\bar{\mathbf{t}})\}_T}{\partial t_{\nu}^{(1)}\partial\bar{t}_{\mu}^{(1)}} = A_{\mu\nu} - \omega\delta_{\mu\nu} \tag{71}$$

where $A_{\mu\nu}$ are the elements of the Jacobian introduced in eqn (28). Therefore, excitation energies can be obtained as eigenvalues of this matrix. For details and for the form of the matrix elements for the other quantities ($\mathbf{F}$, $\boldsymbol{\xi}^{Y}$,...), appearing in coupled-cluster response theory we refer to the original literature.[19,106] The approach outlined above is applicable to the different levels of the coupled cluster hierarchy,[130] starting with CCS (equivalent to CIS for excitation energies) and proceeding to CCSD, CCSDT and so on.

While feasible for small molecules, the relatively large computational cost of calculating and diagonalizing the CCSD Jacobian have motivated the development of more approximate coupled cluster methods based on perturbative approaches that yield energies correct to second order or higher. The first of these is the CC2 method,[131] where the main idea is to retain the singles equation $\Omega_{\mu_1}$ as in CCSD but to approximate the doubles equation $\Omega_{\mu_2}$. This results in a Jacobian in which the doubles–doubles block is diagonal, thus resulting in significant computational gains.

To make these linear response coupled-cluster methods, in particular CC2, applicable to truly large molecular systems, there has been significant work in recent years to combine it with efficient computational techniques.[132,133]

## 3 Embedding methods: basic ideas and exact theory

All quantum-chemical methods for excited states discussed in the previous section show a rather steep increase of the computational effort with the size of the system. This is particularly the case for wavefunction based methods where there are well-defined hierarchies that allow for a systematic improvement of the calculation. Thus, their applicability is limited to comparably small molecules and a treatment of electronic excitations in complex chemical systems remains a challenge. However, if only local excitations are of interest, additional simplifications can be introduced.

The simplest possibility for exploiting this locality is the truncation of the full system to a smaller model. Such a model contains only the part of the system where the local excitations of interest take place and of its environment. For the case of a chromophore molecule in solution the definition of such cluster models is rather straightforward: In the simplest case, one starts from an isolated chromophore, which is then progressively surrounded by solvent molecules up to some limit *e.g.* to include a complete solvation shell. Similar constructions can be used for chromophores in protein environments by only including specific amino acid residues that are close to the chromophore. Also for treating impurities in solids truncated cluster models can be set up by including only atoms within a certain distance from the impurity. Even though such a truncation of the full system may be a rather crude approximation, the results obtained with such cluster models will eventually converge towards a full calculation if the size of the model system is systematically enlarged. However, this convergence can be rather slow and, therefore, cluster models that provide sufficiently accurate results will often be rather large and contain hundreds or thousands of atoms. Thus, a full quantum-chemical treatment of sufficiently large truncated models is rarely possible with accurate quantum-chemical methods.

Embedding methods follow an intermediate strategy between a full quantum-chemical treatment and the use of small truncated model systems: They still restrict the accurate treatment to a small subsystem of interest, but instead of neglecting the environment of this model system, it is included in a more approximate manner. As with truncated model systems, the results obtained with such embedding schemes will eventually converge towards those of a full treatment when enlarging the size of the explicitly treated subsystem. However, since the environment is always included, this convergence should be much faster, which makes it possible to restrict the size of the active subsystem considerably if only local excitations or other local spectroscopic properties are of interest.

Formally, such embedding approaches can be formulated as an exact theory as outlined in the following subsection. From this exact embedding theory one always obtains the same results as with a full quantum-chemical treatment, independent of the chosen size of the active subsystem. However, such a treatment is not suitable for practical applications since its computational cost would be comparable to (or even larger than) the one of a full quantum-chemical treatment. Therefore, approximations have to be applied for the description of the environment. The quality of these approximations determines how fast the results of embedding calculations converge with the size of the explicitly treated subsystem. More accurate embedding methodologies will allow for the use of a smaller active subsystem, which in turn makes it possible to apply more sophisticated and more accurate quantum-chemical methods for the description of the local excitations of interest. It should also be noted that embedding approaches also simplify the interpretation of the computational results significantly, since information from the parts of the system not treated explicitly will, in effect, be filtered away by construction.

### 3.1 Frozen-density embedding theory

Embedding approaches start from a partitioning of the total system into a subsystem of interest (subsystem I in the following) and its environment (subsystem II). The frozen-density embedding (FDE) theory formulated by Wesolowski and Warshel[134]—following earlier work of Senatore and Subbaswamy[135,136] and of Cortona[137]—provides a formally exact theoretical framework for introducing such a partitioning. It is based on the formally exact DFT (*i.e.*, considering exact density functionals) and uses the electron density of the total system $\rho_{\mathrm{tot}}(\boldsymbol{r})$ as its starting point. This total density is partitioned into the electron densities of the active subsystem, $\rho_{\mathrm{I}}(\boldsymbol{r})$, and of the environment, $\rho_{\mathrm{II}}(\boldsymbol{r})$, *i.e.*,

$$\rho_{\mathrm{tot}}(\boldsymbol{r}) = \rho_{\mathrm{I}}(\boldsymbol{r}) + \rho_{\mathrm{II}}(\boldsymbol{r}). \tag{72}$$

These subsystem densities are allowed to overlap. In the following, we will always assume that the subsystem densities $\rho_{\mathrm{I}}(\boldsymbol{r})$ and $\rho_{\mathrm{II}}(\boldsymbol{r})$ integrate to an integer number of electrons. However, the theory can be generalized to subsystems with fractional electron numbers.[138] In addition to the electron density, the nuclear charges are also partitioned. These divisions of the density and the nuclei define the two subsystems I and II. The environment density $\rho_{\mathrm{II}}$ could be further partitioned into an arbitrary number of subsystems[137,139,140] as

$$\rho_{\mathrm{II}}(\boldsymbol{r}) = \sum_n \rho_{\mathrm{II}}^{(n)} \tag{73}$$

This is particularly useful for formulating subsystem approaches, in which a large system is partitioned into many smaller subsystems, that are then treated on an equal footing. For a recent review of such fragment-based methods in quantum chemistry, see ref. 141. As our focus here will be on methods that single out a specific subsystem of interest, the discussion in the following will be restricted to two subsystems, *i.e.*, the densities of all but one subsystem will be collected into a single environment density $\rho_{\mathrm{II}}$.

**3.1.1 Interaction energy.** Using this partitioning into subsystems, the DFT total energy can be expressed as a functional of the two subsystem densities $\rho_{\mathrm{I}}$ and $\rho_{\mathrm{II}}$,

$$\begin{aligned}E_{\mathrm{tot}} &= E[\rho_{\mathrm{I}},\rho_{\mathrm{II}}] = E_{\mathrm{NN}} + \int (\rho_{\mathrm{I}}(\boldsymbol{r}) + \rho_{\mathrm{II}}(\boldsymbol{r}))(v_{\mathrm{I}}^{\mathrm{nuc}}(\boldsymbol{r}) + v_{\mathrm{II}}^{\mathrm{nuc}}(\boldsymbol{r}))\mathrm{d}^3r \\ &\quad + \frac{1}{2}\int \frac{(\rho_{\mathrm{I}}(\boldsymbol{r}) + \rho_{\mathrm{II}}(\boldsymbol{r}))(\rho_{\mathrm{I}}(\boldsymbol{r}') + \rho_{\mathrm{II}}(\boldsymbol{r}'))}{|\boldsymbol{r}-\boldsymbol{r}'|}\mathrm{d}^3r\mathrm{d}^3r' \\ &\quad + E_{\mathrm{xc}}[\rho_{\mathrm{I}}] + E_{\mathrm{xc}}[\rho_{\mathrm{II}}] + E_{\mathrm{xc}}^{\mathrm{nadd}}[\rho_{\mathrm{I}},\rho_{\mathrm{II}}] \\ &\quad + T_s[\rho_{\mathrm{I}}] + T_s[\rho_{\mathrm{II}}] + T_s^{\mathrm{nadd}}[\rho_{\mathrm{I}},\rho_{\mathrm{II}}],\end{aligned} \tag{74}$$

where $E_{\mathrm{NN}}$ is the nuclear repulsion energy, $v_{\mathrm{I}}{}^{\mathrm{nuc}}$ and $v_{\mathrm{II}}{}^{\mathrm{nuc}}$ are the electrostatic potentials of the nuclei in subsystems I and II, respectively, $E_{xc}[\rho]$ is the exchange–correlation energy functional, and $T_s[\rho]$ is the kinetic energy of a reference system of noninteracting electrons with density $\rho$. The nonadditive exchange–correlation and kinetic energies are defined as

$$E_{\mathrm{xc}}^{\mathrm{nadd}}[\rho_{\mathrm{I}},\rho_{\mathrm{II}}] = E_{\mathrm{xc}}[\rho_{\mathrm{I}} + \rho_{\mathrm{II}}] - E_{\mathrm{xc}}[\rho_{\mathrm{I}}] - E_{\mathrm{xc}}[\rho_{\mathrm{II}}] \tag{75}$$

and

$$T_s^{\mathrm{nadd}}[\rho_{\mathrm{I}},\rho_{\mathrm{II}}] = T_s[\rho_{\mathrm{I}} + \rho_{\mathrm{II}}] - T_s[\rho_{\mathrm{I}}] - T_s[\rho_{\mathrm{II}}], \tag{76}$$

respectively.

The total energy given in eqn (74) can be partitioned as,

$$E_{\mathrm{tot}} = E_{\mathrm{I}} + E_{\mathrm{II}} + E_{\mathrm{int}}, \tag{77}$$

into the energies of the two individual subsystems ($n$ = I,II)

$$\begin{aligned} E_{\mathrm{n}} &= E[\rho_{\mathrm{n}}] = E_{\mathrm{NN}}^{(n)} + \int \rho_n(\boldsymbol{r}) v_{\mathrm{nuc}}^{(n)}(\boldsymbol{r}) \mathrm{d}^3 r \\ &\quad + \frac{1}{2} \int \frac{\rho_n(\boldsymbol{r}) \rho_n(\boldsymbol{r}')}{|\boldsymbol{r} - \boldsymbol{r}'|} \mathrm{d}^3 r \mathrm{d}^3 r' + E_{\mathrm{xc}}[\rho_{\mathrm{n}}] + T_s[\rho_{\mathrm{n}}], \end{aligned} \tag{78}$$

and the interaction energy

$$\begin{aligned} E_{\mathrm{int}} &= E_{\mathrm{int}}[\rho_{\mathrm{I}}, \rho_{\mathrm{II}}] = E_{\mathrm{NN}}^{(\mathrm{int})} + \int \rho_{\mathrm{I}}(\boldsymbol{r}) v_{\mathrm{nuc}}^{\mathrm{II}}(\boldsymbol{r}) \mathrm{d}^3 r \\ &\quad + \int \rho_{\mathrm{II}}(\boldsymbol{r}) v_{\mathrm{nuc}}^{\mathrm{I}}(\boldsymbol{r}) \mathrm{d}^3 r + \int \frac{\rho_{\mathrm{I}}(\boldsymbol{r}) \rho_{\mathrm{II}}(\boldsymbol{r}')}{|\boldsymbol{r} - \boldsymbol{r}'|} \mathrm{d}^3 r \mathrm{d}^3 r' \\ &\quad + E_{\mathrm{xc}}^{\mathrm{nadd}}[\rho_{\mathrm{I}}, \rho_{\mathrm{II}}] + T_s^{\mathrm{nadd}}[\rho_{\mathrm{I}}, \rho_{\mathrm{II}}], \end{aligned} \tag{79}$$

where the nuclear repulsion energy is partitioned into the repulsion among nuclei in the same subsystem $E_{\mathrm{NN}}^{(n)}$ and between those in different subsystems $E_{\mathrm{NN}}^{(\mathrm{int})}$.

Eqn (79) provides an exact expression for the interaction energy between two subsystems with fixed electron densities $\rho_{\mathrm{I}}$ and $\rho_{\mathrm{II}}$. The first four terms add up to the classical electrostatic interaction energy between the nuclei and electron densities of the two subsystems. In addition, the nonadditive exchange–correlation energy $E_{\mathrm{xc}}^{\mathrm{nadd}}[\rho_{\mathrm{I}},\rho_{\mathrm{II}}]$ and the nonadditive kinetic energy $T_s^{\mathrm{nadd}}[\rho_{\mathrm{I}},\rho_{\mathrm{II}}]$ account for the non-classical contributions to the interaction energy. While the classical terms can be calculated directly for any two subsystems once the nuclear charges and positions as well as the subsystem electron densities are known, the evaluation of the non-classical contributions requires the knowledge of the exchange–correlation and kinetic-energy functionals, $E_{\mathrm{xc}}[\rho]$ and $T_s[\rho]$. Even though these are not know, eqn (79) provides a useful starting point for the development of embedding methods. We note that its applicability is not limited to DFT calculations since an electron density can always be defined within any theoretical framework and then used to evaluate an interaction energy within FDE theory.

**3.1.2 Embedding potential.** So far, the electron densities of the two subsystems were kept fixed. However, the total electron density of two *interacting* subsystems will not be equal to the sum of the densities of the *isolated* subsystems. Therefore, the subsystem electron densities change when the two subsystems interact and the presence of an environment, $\rho_{\mathrm{II}}(\boldsymbol{r})$, modifies the electron density of the active subsystem, $\rho_{\mathrm{I}}(\boldsymbol{r})$. To account for this, the environment has to be included in the quantum-chemical description of the active subsystem. This is possible both for a description of the active subsystem with KS-DFT and for a wavefunction based treatment.

For the case of a KS-DFT description, the density of the active subsystem I can be obtained from the KS orbitals $\{\phi_i^{\mathrm{I}}\}$ as $\rho_{\mathrm{I}}(\boldsymbol{r}) = \sum_i |\phi_i^{\mathrm{I}}(\boldsymbol{r})|^2$. Note that in this case the noninteracting kinetic energy $T_s[\rho_\mathrm{I}]$ can also be calculated directly from the KS orbitals. For a given frozen electron density $\rho_\mathrm{II}(\boldsymbol{r})$ in subsystem II, the KS orbitals (and the electron density) of the active subsystem I can then be determined by minimizing the total energy given in eqn (74) with respect to $\rho_\mathrm{I}$, while keeping $\rho_\mathrm{II}$ frozen. Performing this minimization under the constraint that the number of electrons $N_\mathrm{I}$ in subsystem I is conserved leads to a set of equations for the KS orbitals of subsystem I,

$$\left[-\frac{\nabla^2}{2} + v_\mathrm{KS}[\rho_\mathrm{I}](\boldsymbol{r}) + v^\mathrm{I}_\mathrm{emb}[\rho_\mathrm{I}, \rho_\mathrm{II}](\boldsymbol{r})\right]\phi^\mathrm{I}_i(\boldsymbol{r}) = \varepsilon^\mathrm{I}_i \phi^\mathrm{I}_i(\boldsymbol{r}), \tag{80}$$

where $v_\mathrm{KS}[\rho_\mathrm{I}](\boldsymbol{r})$ is the KS effective potential of the isolated subsystem I containing the usual terms of the nuclear potential, the Coulomb potential of the electrons, and the exchange–correlation potential,

$$v_\mathrm{KS}[\rho_\mathrm{I}](\boldsymbol{r}) = \frac{\delta E[\rho_\mathrm{I}]}{\delta \rho_\mathrm{I}(\boldsymbol{r})} = v^\mathrm{I}_\mathrm{nuc}(\boldsymbol{r}) + \int \frac{\rho_\mathrm{I}(\boldsymbol{r}')}{|\boldsymbol{r}-\boldsymbol{r}'|}\mathrm{d}^3r' + \frac{\delta E_\mathrm{xc}[\rho_\mathrm{I}]}{\delta \rho_\mathrm{I}(\boldsymbol{r})}, \tag{81}$$

and the effective embedding potential $v^\mathrm{I}_\mathrm{emb}[\rho_\mathrm{I},\rho_\mathrm{II}](\boldsymbol{r})$ describes the interaction of subsystem I with the frozen density and nuclei of subsystem II,

$$\begin{aligned} v^\mathrm{I}_\mathrm{emb}[\rho_\mathrm{I}, \rho_\mathrm{II}](\boldsymbol{r}) \;=\; & \frac{\delta E_\mathrm{int}[\rho_\mathrm{I}, \rho_\mathrm{II}]}{\delta \rho_\mathrm{I}(\boldsymbol{r})} = v^\mathrm{II}_\mathrm{nuc}(\boldsymbol{r}) + \int \frac{\rho_\mathrm{II}(\boldsymbol{r}')}{|\boldsymbol{r}-\boldsymbol{r}'|}\mathrm{d}^3r' \\ & + \left.\frac{\delta E_\mathrm{xc}[\rho]}{\delta \rho(\boldsymbol{r})}\right|_{\rho_\mathrm{tot}} - \left.\frac{\delta E_\mathrm{xc}[\rho]}{\delta \rho(\boldsymbol{r})}\right|_{\rho_\mathrm{I}} \\ & + \left.\frac{\delta T_s[\rho]}{\delta \rho(\boldsymbol{r})}\right|_{\rho_\mathrm{tot}} - \left.\frac{\delta T_s[\rho]}{\delta \rho(\boldsymbol{r})}\right|_{\rho_\mathrm{I}}. \end{aligned} \tag{82}$$

This embedding potential accounts for the presence of the frozen environment when determining the electron density of the active subsystem with KS-DFT. Note that the embedding potential is a local potential that depends only on the electron densities of the two subsystems.

The first two terms of the embedding potential of eqn (82) describe the classical electrostatic potential of the nuclei and of the electrons in the frozen environment. In addition, the embedding potential also contains an exchange–correlation component and a kinetic-energy component. These account for the non-classical contributions, such as the Pauli (exchange) repulsion of the electrons in the frozen subsystem and chemical bonding (*i.e.*, orbital interactions) between the subsystems. While the electrostatic part of the embedding potential can be evaluated directly for given subsystem densities, this is not possible for the exchange–correlation and kinetic energy parts, as these require the knowledge of the corresponding exact functionals.

The same embedding potential can also be derived for the case that a wavefunction based description is used for the active subsystem.[142,143] In this case a wavefunction $\Psi_\mathrm{I}(\boldsymbol{r}_1, s_1, \boldsymbol{r}_2, s_2, \ldots)$ is used to represent the electron density $\rho_\mathrm{I}(\boldsymbol{r})$ of subsystem I. By using that

$$E_\mathrm{I} = E[\rho_\mathrm{I}] = E^\mathrm{(I)}_\mathrm{NN} + \langle \Psi_\mathrm{I}|\hat{T} + \hat{V}^\mathrm{I}_\mathrm{nuc} + \hat{V}_\mathrm{ee}|\Psi_\mathrm{I}\rangle, \tag{83}$$

where $\hat{T}$, $\hat{V}^\mathrm{I}_\mathrm{nuc}$, and $\hat{V}_\mathrm{ee}$ are the operators of the kinetic energy, the electron–nuclear attraction energy, and of the electron–electron interaction, respectively, the total energy of eqn (74) and (77) can be rewritten as

$$E_\mathrm{tot} = E[\Psi_\mathrm{I},\rho_\mathrm{II}] = E^\mathrm{(I)}_\mathrm{NN} + \langle \Psi_\mathrm{I}|\hat{T} + \hat{V}^\mathrm{I}_\mathrm{nuc} + \hat{V}_\mathrm{ee}|\Psi_\mathrm{I}\rangle + E_\mathrm{int}[\rho_\mathrm{I},\rho_\mathrm{II}] + E_\mathrm{II}, \tag{84}$$

where $E_{\mathrm{int}}[\rho_{\mathrm{I}},\rho_{\mathrm{II}}]$ and $E_{\mathrm{II}} = E[\rho_{\mathrm{II}}]$ are the interaction energy and the energy of subsystem II as defined in eqn (78) and (79), respectively.

The wavefunction describing subsystem I in the presence of the frozen density $\rho_{\mathrm{II}}(\boldsymbol{r})$ can then be obtained by minimizing this total energy functional with respect to $\Psi_{\mathrm{I}}$ while keeping the electron density $\rho_{\mathrm{II}}$ of the environment frozen, under the constraint that the number of electron $N_{\mathrm{I}}$ in subsystem I is conserved. This leads to the condition,

$$\begin{aligned} 0 &= (\hat{T} + \hat{V}^{\mathrm{I}}_{\mathrm{nuc}} + \hat{V}_{\mathrm{ee}})\Psi_{\mathrm{I}} + \int \frac{\delta E_{\mathrm{int}}[\rho_{\mathrm{I}},\rho_{\mathrm{II}}]}{\delta \rho_{\mathrm{I}}(\boldsymbol{r}')} \frac{\delta \rho_{\mathrm{I}}(\boldsymbol{r}')}{\delta \Psi_{\mathrm{I}}} \mathrm{d}^3 r' - \lambda \Psi_{\mathrm{I}} \\ &= [\hat{T} + \hat{V}^{\mathrm{I}}_{\mathrm{nuc}} + \hat{V}_{\mathrm{ee}} + \hat{V}^{\mathrm{I}}_{\mathrm{emb}}[\rho_{\mathrm{I}},\rho_{\mathrm{II}}]]\Psi_{\mathrm{I}} - \lambda \Psi_{\mathrm{I}}, \end{aligned} \tag{85}$$

with the embedding operator

$$\hat{V}^{\mathrm{I}}_{\mathrm{emb}}[\rho_{\mathrm{I}},\rho_{\mathrm{II}}] = \sum_i v^{\mathrm{I}}_{\mathrm{emb}}[\rho_{\mathrm{I}},\rho_{\mathrm{II}}](\boldsymbol{r}_i), \tag{86}$$

that is, the wavefunction of subsystem I in the presence of the frozen density $\rho_{\mathrm{II}}(\boldsymbol{r})$ can be determined by solving an eigenvalue equation, in which the embedding potential of eqn (82) enters as an additional one-electron operator. However, the eigenvalue $\lambda$ in this embedded Schrödinger equation does not correspond to an energy. Instead, the energy has to be evaluated using eqn (84) once the embedded wavefunction $\Psi_{\mathrm{I}}$ has been determined.

For solving this embedded Schrödinger equation, the common approximations of wavefunction based quantum chemistry can be applied. Note that the derivation given here differs from the one in ref. 143, where an approximate wavefunction of subsystem I was introduced before performing the energy minimization. In this case, the embedding potential contains an additional term correcting for the difference between the approximate and the exact wavefunctions. However, it can be argued that a correction for deficiencies of an employed wavefunction approximation should not be contained in the embedding potential.[70,144] Therefore, the derivation given here avoids this correction by introducing an approximate wavefunction only at a later stage.

**3.1.3 Polarization of the environment.** In an exact embedding calculation using a frozen environment density $\rho_{\mathrm{II}}$ the electron density $\rho_{\mathrm{I}}$ of the active subsystem should be determined such that the total electron density $\rho_{\mathrm{tot}} = \rho_{\mathrm{I}} + \rho_{\mathrm{II}}$ is identical to the one obtained from a calculation of the full system. This can be achieved by minimizing the total energy with respect to the density (or wavefunction) of the active subsystem, and leads to the local embedding potential derived above.

However, such an agreement with the results of a full calculation is only possible if the frozen density fulfills certain conditions.[145,146] In particular, the frozen density $\rho_{\mathrm{II}}$ has to be smaller than or equal to the correct total density $\rho_{\mathrm{tot}}$ at every point in space, *i.e.*, $\rho_{\mathrm{II}}(\boldsymbol{r}) \leq \rho_{\mathrm{tot}}(\boldsymbol{r})$. Otherwise, the complementary density of the active system would have to be negative, which is not possible. In addition, this complementary density $\rho_{\mathrm{tot}} - \rho_{\mathrm{II}}$ has to be noninteracting $v_s$-representable in the case of a KS-DFT description for the active system or interacting $v$-representable in the case of a wavefunction based treatment.

In particular the first condition is usually not fulfilled for most approximate frozen densities. Usually, these will be too small in some regions and too large in others. Consequently, the application of the embedding potential of eqn (82) does not lead to the exact total density with such choices for $\rho_{\mathrm{II}}$. This problem can be alleviated by switching from an embedding method to a subsystem approach in which both the densities of subsystem I and II are determined. That is, the densities of both subsystems are determined separately, but in each case the (frozen) density of the other subsystem is taken into account. When using KS-DFT, this can be formulated as a set of coupled equations for the KS orbitals of the two subsystems,

$$\left[-\frac{\nabla^2}{2} + v_{\mathrm{KS}}[\rho_{\mathrm{I}}](\boldsymbol{r}) + v_{\mathrm{emb}}^{\mathrm{I}}[\rho_{\mathrm{I}}, \rho_{\mathrm{II}}](\boldsymbol{r})\right]\phi_i^{\mathrm{I}}(\boldsymbol{r}) = \varepsilon_i^{\mathrm{I}}\phi_i^{\mathrm{I}}(\boldsymbol{r}) \tag{87}$$

$$\left[-\frac{\nabla^2}{2} + v_{\mathrm{KS}}[\rho_{\mathrm{II}}](\boldsymbol{r}) + v_{\mathrm{emb}}^{\mathrm{II}}[\rho_{\mathrm{I}}, \rho_{\mathrm{II}}](\boldsymbol{r})\right]\phi_i^{\mathrm{II}}(\boldsymbol{r}) = \varepsilon_i^{\mathrm{II}}\phi_i^{\mathrm{II}}(\boldsymbol{r}) \tag{88}$$

Note that because of the different roles of the active and frozen densities in eqn (82), the embedding potentials in these two equations differ.

The simplest strategy for solving these coupled equations for the two subsystems is through so-called freeze-and-thaw iterations.[147] First the density of subsystem I is determined in the presence of an approximate frozen density for subsystem II. Subsequently, the roles of the two subsystems are interchanged and the density calculated for subsystem I in the previous step is now frozen, whereas an updated density is determined for subsystem II. This is repeated iteratively until convergence is reached. Alternatively, the two sets of equations (eqn (87) and (88)) can be solved simultaneously.[139] Note that the resulting partitioning into subsystems is not unique, because density can be moved between the two subsystems without changing the total electron density. However, a unique partitioning can be obtained when requiring that both subsystems share the same embedding potential, *i.e.*, that $v_{\mathrm{emb}}^{\mathrm{I}}[\rho_{\mathrm{I}},\rho_{\mathrm{II}}] = v_{\mathrm{emb}}^{\mathrm{II}}[\rho_{\mathrm{I}},\rho_{\mathrm{II}}]$.[11,138]

When focussing on one subsystem of interest, such an iterative subsystem scheme can be considered as an embedding scheme that not only accounts for the effect of the environment on the active subsystem but also includes the polarization of the environment caused by the active subsystem. Thus, such a polarizable embedding goes beyond a scheme in which a fixed frozen density is employed for the environment. Consequently, it will always converge to the same density as a full treatment, irrespective of the initial choice of $\rho_{\mathrm{II}}$ if no further approximations are introduced.

**3.1.4 Excitation energies and response properties.** When treating excited states within FDE theory, one has to distinguish between the two available theoretical approaches: time-independent (state-specific) methods and response theory. The conceptually simpler theory is obtained in the case of time-independent methods in which a wavefunction is calculated explicitly for each excited state of interest. In this case, the embedding theory outlined above can be applied directly, with the only difference that the wavefunction and electron density of the active subsystem are different for each excited state. Thus, the embedding potential is different for each excited state, and for each excited state the environment density has to be determined iteratively (*e.g.*, in freeze-and-thaw iterations). The theoretical justification for such a state-specific treatment of excited states is given in ref. 148.

In a formalism based on response theory,[149–152] the (time-dependent) electron densities $\rho_{\mathrm{I}}(\boldsymbol{r},t)$ and $\rho_{\mathrm{II}}(\boldsymbol{r},t)$ of the two subsystems are in a KS-DFT framework represented by two separate Slater determinants $|\tilde{\Phi}_{\mathrm{I}}\rangle$ and $|\tilde{\Phi}_{\mathrm{II}}\rangle$, respectively. Consequently, the total time-averaged quasi-energy can be expressed as

$$\{\mathrm{Q}(t)\}_T = \{Q[\rho_\mathrm{I}](t)\}_T + \{Q[\rho_\mathrm{II}](t)\}_T + \{E_\mathrm{int}[\rho_\mathrm{I},\rho_\mathrm{II}](t)\}_T, \tag{89}$$

where the first two terms are the time-averaged quasi-energies of the two subsystems according to eqn (57), and the third term is the time-average of the interaction energy given in eqn (79). Subsequently, an exponential parametrization with the parameters $\boldsymbol{\kappa}_\mathrm{I}$ and $\boldsymbol{\kappa}_\mathrm{II}$ can be introduced for both subsystems (*cf.* eqn (58)), *i.e.*, the total time-dependent density is expressed as

$$\rho(\boldsymbol{r},t) = \rho_\mathrm{I}(\boldsymbol{r},\boldsymbol{\kappa}_\mathrm{I}) + \rho_\mathrm{II}(\boldsymbol{r},\boldsymbol{\kappa}_\mathrm{II}). \tag{90}$$

With this parametrization, the matrix $\boldsymbol{F}$, which determines the poles of the response function, assumes a block structure,

$$\boldsymbol{F} = \frac{\partial^2\{Q^{(2)}\}_T}{\partial\boldsymbol{\kappa}^{(1)}\partial\boldsymbol{\kappa}^{(1)}} = \begin{pmatrix} \boldsymbol{F}_\mathrm{I,I} & \boldsymbol{F}_\mathrm{II,I} \\ \boldsymbol{F}_\mathrm{I,II} & \boldsymbol{F}_\mathrm{II,II} \end{pmatrix} \text{ with } \boldsymbol{F}_\mathrm{n,m} = \frac{\partial^2\{Q^{(2)}\}_T}{\partial\boldsymbol{\kappa}_n^{(1)}\partial\boldsymbol{\kappa}_m^{(1)}}. \tag{91}$$

By separating the contributions arising from the different terms in eqn (89), this matrix can be decomposed into

$$\boldsymbol{F} = \begin{pmatrix} \boldsymbol{F}_\mathrm{I,I} & \boldsymbol{F}_\mathrm{II,I} \\ \boldsymbol{F}_\mathrm{I,II} & \boldsymbol{F}_\mathrm{II,II} \end{pmatrix} = \begin{pmatrix} \boldsymbol{F}_\mathrm{I} & 0 \\ 0 & \boldsymbol{F}_\mathrm{II} \end{pmatrix} + \begin{pmatrix} \boldsymbol{F}_\mathrm{int}^\mathrm{I} & \boldsymbol{F}_\mathrm{int}^\mathrm{II,I} \\ \boldsymbol{F}_\mathrm{int}^\mathrm{I,II} & \boldsymbol{F}_\mathrm{int}^\mathrm{II} \end{pmatrix}, \tag{92}$$

where $\boldsymbol{F}_\mathrm{I}$ and $\boldsymbol{F}_\mathrm{II}$ arise from the differentiation of the quasi-energies of the isolated subsystems (as in eqn (60)) while the second contribution originates from the differentiation of the interaction energy. This interaction contribution contains blocks $\boldsymbol{F}_\mathrm{int}^\mathrm{I}$ and $\boldsymbol{F}_\mathrm{int}^\mathrm{II}$, which modify the diagonal of $\boldsymbol{F}$ and can therefore be regarded as modifying the isolated subsystem $\boldsymbol{F}_\mathrm{I}$ and $\boldsymbol{F}_\mathrm{II}$ matrices,

$$\begin{aligned} \boldsymbol{F}_\mathrm{int}^\mathrm{(n)} &= \frac{\partial^2\{E_\mathrm{int}^{(2)}[\rho_\mathrm{I},\rho_\mathrm{II}]\}_T}{\partial\boldsymbol{\kappa}_n^{(1)}\partial\boldsymbol{\kappa}_n^{(1)}} \\ &= \iint w_\mathrm{emb}^{nn}(\boldsymbol{r},\boldsymbol{r}')\frac{\partial\rho_n^{(1)}(\boldsymbol{r})}{\partial\boldsymbol{\kappa}_n^{(1)}}\frac{\partial\rho_n^{(1)}(\boldsymbol{r}')}{\partial\boldsymbol{\kappa}_n^{(1)}}\mathrm{d}^3r\mathrm{d}^3r' + \int v_\mathrm{emb}^n(\boldsymbol{r})\frac{\partial^2\rho_n^{(2)}(\boldsymbol{r})}{\partial\boldsymbol{\kappa}_n^{(1)}\partial\boldsymbol{\kappa}_n^{(1)}}\mathrm{d}^3r \end{aligned} \tag{93}$$

with the embedding kernel

$$\begin{aligned} w_\mathrm{emb}^{nn}(\boldsymbol{r},\boldsymbol{r}') &= \frac{\delta^2 E_\mathrm{int}[\rho_\mathrm{I},\rho_\mathrm{II}]}{\delta\rho_n(\boldsymbol{r})\delta\rho_n(\boldsymbol{r}')} = \left.\frac{\delta^2 E_\mathrm{xc}[\rho]}{\delta\rho(\boldsymbol{r})\delta\rho(\boldsymbol{r}')}\right|_{\rho_\mathrm{tot}} - \left.\frac{\delta^2 E_\mathrm{xc}[\rho]}{\delta\rho(\boldsymbol{r})\delta\rho(\boldsymbol{r}')}\right|_{\rho_n} \\ &\quad + \left.\frac{\delta^2 T_s[\rho]}{\delta\rho(\mathbf{r})\delta\rho(\mathbf{r}')}\right|_{\rho_\mathrm{tot}} - \left.\frac{\delta^2 T_s[\rho]}{\delta\rho(\mathbf{r})\delta\rho(\mathbf{r}')}\right|_{\rho_n}. \end{aligned} \tag{94}$$

These lead to additional embedding contributions to the subsystem $\boldsymbol{A}$ and $\boldsymbol{B}$ matrices (*cf.* eqn (62)–(63))

$$A_{ia,jb}^{nn} = \delta_{ij}\delta_{ab}(\varepsilon_a^n - \varepsilon_i^n) + 2(ia|bj) + (ia|f_\mathrm{xc}|bj) + (ia|w_\mathrm{emb}^{nn}|bj), \tag{95}$$

$$B_{ia,jb}^{nn} = 2(ia|jb) + (ia|f_\mathrm{xc}|jb) + (ia|w_\mathrm{emb}^{nn}|jb), \tag{96}$$

where all orbital indices refer to the considered subsystem and the contributions arising from the second term in eqn (93) have been included in the orbital energies (*i.e.*, it is assumed that the orbitals are obtained from eqn (80)).

Second, the off-diagonal blocks introduce a coupling between the subsystems, which is given by

$$\boldsymbol{F}_\mathrm{int}^\mathrm{I,II} = \frac{\partial^2\{E_\mathrm{int}^{(2)}[\rho_\mathrm{I},\rho_\mathrm{II}]\}_T}{\partial\boldsymbol{\kappa}_\mathrm{I}^{(1)}\partial\boldsymbol{\kappa}_\mathrm{II}^{(1)}} = \iint w_\mathrm{emb}^\mathrm{I,II}(\boldsymbol{r},\boldsymbol{r}')\frac{\partial\rho_\mathrm{I}^{(1)}(\boldsymbol{r})}{\partial\boldsymbol{\kappa}_\mathrm{I}^{(1)}}\frac{\partial\rho_\mathrm{II}^{(1)}(\boldsymbol{r}')}{\partial\boldsymbol{\kappa}_\mathrm{II}^{(1)}}\mathrm{d}^3r\mathrm{d}^3r' \tag{97}$$

with the embedding kernel

$$w_{\mathrm{emb}}^{\mathrm{I,II}}(\boldsymbol{r},\boldsymbol{r}') = \left.\frac{\delta^2 E_{\mathrm{xc}}[\rho]}{\delta\rho(\boldsymbol{r})\delta\rho(\boldsymbol{r}')}\right|_{\rho_{\mathrm{tot}}} + \left.\frac{\delta^2 T_s[\rho]}{\delta\rho(\boldsymbol{r})\delta\rho(\boldsymbol{r}')}\right|_{\rho_{\mathrm{tot}}} + \frac{1}{|\boldsymbol{r}-\boldsymbol{r}'|}. \tag{98}$$

These give rise to $\boldsymbol{A}$ and $\boldsymbol{B}$ matrices corresponding to coupling between subsystems, with elements

$$A^{\mathrm{I,II}}_{i_{\mathrm{I}}a_{\mathrm{I}},j_{\mathrm{II}}b_{\mathrm{II}}} = (i_{\mathrm{I}}a_{\mathrm{I}}|w^{\mathrm{I,II}}_{\mathrm{emb}}|b_{\mathrm{II}}j_{\mathrm{II}}), \tag{99}$$

$$B^{\mathrm{I,II}}_{i_{\mathrm{I}}a_{\mathrm{I}},j_{\mathrm{II}}b_{\mathrm{II}}} = (i_{\mathrm{I}}a_{\mathrm{I}}|w^{\mathrm{I,II}}_{\mathrm{emb}}|j_{\mathrm{II}}b_{\mathrm{II}}), \tag{100}$$

where the subscripts indicate that orbital indices refer to the different subsystems.

In should be noted that the subsystem response theory discussed above in the framework of TDDFT can also be generalized to a wavefunction based description of the active subsystem. In this case, the DFT quasi-energy of subsystem I in eqn (89) is replaced by the quasi-energy Lagrangian of a wavefunction based method, *i.e.*,

$$\{L(t)\}_T = \{L[\rho_{\mathrm{I}}](t)\}_T + \{Q[\rho_{\mathrm{II}}](t)\}_T + \{E_{\mathrm{int}}[\rho_{\mathrm{I}},\rho_{\mathrm{II}}](t)\}_T, \tag{101}$$

and an appropriate parametrization of the wavefunction of subsystem I is introduced. This translates to a parametrization of the total time-dependent density

$$\rho(\boldsymbol{r},t) = \rho_{\mathrm{I}}(\boldsymbol{r},\boldsymbol{\lambda}_{\mathrm{I}},\bar{\boldsymbol{\lambda}}_{\mathrm{I}}) + \rho_{\mathrm{II}}(\boldsymbol{r},\boldsymbol{\kappa}_{\mathrm{II}}) \tag{102}$$

in which the density of subsystem I depends on the parameters $\boldsymbol{\lambda}_{\mathrm{I}}$ and possibly the multipliers $\bar{\boldsymbol{\lambda}}_{\mathrm{I}}$. Embedding contributions to the isolated subsystem matrices $\boldsymbol{F}_{\mathrm{I}}$, $\boldsymbol{A}_{\mathrm{I}}$, and $\boldsymbol{J}_{\mathrm{I}}$ as appearing in the response function (eqn (56)) can then be derived by differentiating the interaction energy with respect to the parameters and multipliers. As in the TDDFT case, these will introduce both embedding contributions entering into the subsystem response and embedding contributions that couple the two subsystems. In general, linear-response function in eqn (56) will now involve the matrix[152]

$$\begin{pmatrix} \boldsymbol{F}_{\mathrm{I,I}} & \boldsymbol{A}_{\mathrm{I,I}} & \boldsymbol{A}_{\mathrm{II,I}} \\ \boldsymbol{A}^T_{\mathrm{I,I}} & \boldsymbol{J}_{\mathrm{I,I}} & \boldsymbol{F}_{\mathrm{II,I}} \\ \boldsymbol{F}_{\mathrm{I,II}} & \boldsymbol{A}_{\mathrm{I,II}} & \boldsymbol{F}_{\mathrm{II,II}} \end{pmatrix} = \begin{pmatrix} \boldsymbol{F}_{\mathrm{I}} & \boldsymbol{A}_{\mathrm{I}} & 0 \\ \boldsymbol{A}^T_{\mathrm{I}} & \boldsymbol{J}_{\mathrm{I}} & 0 \\ 0 & 0 & \boldsymbol{F}_{\mathrm{II}} \end{pmatrix} + \begin{pmatrix} \boldsymbol{F}^{\mathrm{I}}_{\mathrm{int}} & \boldsymbol{F}^{\mathrm{I}}_{\mathrm{int}} & \boldsymbol{F}^{\mathrm{II,I}}_{\mathrm{int}} \\ (\boldsymbol{A}^{\mathrm{I}}_{\mathrm{int}})^T & \boldsymbol{J}^{\mathrm{I}}_{\mathrm{int}} & \boldsymbol{A}^{\mathrm{II,I}}_{\mathrm{int}} \\ \boldsymbol{F}^{\mathrm{I,II}}_{\mathrm{int}} & \boldsymbol{A}^{\mathrm{I,II}}_{\mathrm{int}} & \boldsymbol{F}^{\mathrm{II}}_{\mathrm{int}} \end{pmatrix}, \tag{103}$$

due to the presence of additional coupling blocks. Note that because of the nonlinear dependence of the interaction energy on the multipliers (via the density $\rho_{\mathrm{I}}$) the matrix $\boldsymbol{J}_{\mathrm{I,I}}$ will in general not be zero anymore, even if the isolated subsystem contribution $\boldsymbol{J}_{\mathrm{I}}$ is. For further discussion and explicit equations, we refer to ref. 152.

## 4 Approximate embedding methods

While the FDE theory presented in the previous section provides an exact theoretical framework for embedding methods in quantum chemistry, it is not directly suitable for numerical applications. In particular, it requires the knowledge of the exact nonadditive kinetic-energy functional, which is not easily available in practice. Therefore, numerous approximate embedding schemes have been developed instead. For discussing these in the following section, it is useful to establish a classification scheme for such methods.

One scheme for classifying approximate embedding methods has been proposed by Bakowies and Thiel (BT)[153] and follows the steps taken above for presenting the FDE theory.

- **Mechanical coupling**: The simplest way to setup an embedding scheme is to treat each subsystem individually and introduce the coupling only through the total energy. To this end, an interaction energy between the subsystems is calculated according to eqn (79) or some approximation to it. With such a simple scheme only the geometrical structure of the active subsystem is altered. All electronic properties, in particular the electron density, are identical to those obtained when treating the subsystem of interest in isolation.
- **Electronic coupling**: Embedding schemes that include the effect of the environment in the quantum-chemical treatment of the active subsystem in some way form the next category. This can be achieved by including the embedding potential of eqn (82) both in a KS-DFT or in a wavefunction based treatment of the subsystem of interest. In practice, this embedding potential is usually approximated. With such a coupling through an embedding potential, the electronic properties of the subsystem of interest can be affected by its environment.
- **Polarizable embedding**: In the simplest case of embedding schemes with electronic coupling, the (approximate) embedding potential is determined solely by the geometric structure of the environment. For instance, the frozen electron density calculated for the isolated environment (*i.e.*, in the absence of the subsystem of interest) can be used in eqn (82). More advanced schemes can be set up by including the polarization of the environment due to the presence of the active subsystem. This leads to schemes where the embedding potential has to be determined iteratively.
- **Embedding including environment response:** When treating electronic excitation energies or other response properties, a fourth category—not contained in the original BT classification—can be introduced. In this case one can distinguish whether or not the response of the environment to the electronic excitation is included. With state-specific methods, this can be achieved by iteratively updating the environment density for each excited state instead of employing one common frozen environment density for all excited states. Within response theory, the response of the environment can be included through the additional subsystem and coupling contributions to the response matrices discussed in the previous section. Several different strategies can be introduced to approximate these contributions. First, the coupling contributions can be neglected and only those modifying the subsystem response are retained. Second, the coupling contributions can be included in an approximate fashion. Finally, it is also possible to fold the contributions of the environment as well as the coupling in an approximate fashion into the response matrices of the active subsystem. While this will not account for coupling between individual excitation energies, it does allow for an efficient inclusion of the polarization of the environment density.

Among those groups, different methods can be classified according to the approximations that are introduced for calculating the interaction energy and the embedding potential. First, in continuum solvation models the discrete molecular structure of the environment is neglected and replaced by a dielectric continuum. Next, a large variety of embedding methods uses a discrete description for the environment and models the electrostatic part of the environment using point charges or localized multipole moments. Such a purely electrostatic description can be augmented with additional terms accounting for non-classical interactions. As a further step, there are embedding methods that retain a full electron density for the environment using the embedding potential of eqn (82), but employing an approximate electron density for the environment and introduce approximations for the nonadditive kinetic-energy functional. Finally, embedding methods that do not

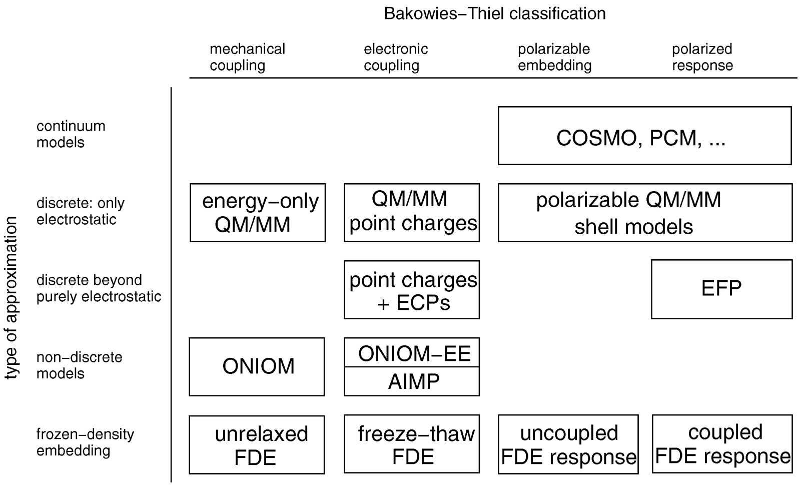

**Fig. 1** Overview of some of the available approximate embedding scheme. On the horizontal axis are the categories of the extended Bakowies–Thiel classification, while the vertical axis sorts different approaches according to the models employed for the environment.

introduce such approximations have also been proposed for embedding accurate wavefunction theory calculations into an environment treated with DFT.

In the following, we will discuss these different approximations. We note, however, that a classification in terms of sophistication does not imply an equivalence in terms of accuracy. Often, seemingly simple schemes have been parametrized so that they provide rather accurate results. At all levels of approximations, embedding methods can operate in the different categories in the BT classification scheme. This is sketched in the two-dimensional overview in Fig. 1. In all cases further distinctions can be made according to the methods used for describing the active subsystems. However, in most cases this does not affect the embedding methodology significantly, so we will only make this distinction in a few cases.

## 4.1 Continuum models

The simplest possible way to account for environment effects in quantum-chemical calculations are continuum models. These neglect the specific molecular structure of the environment and replace it by a continuum characterized by its dielectric constant $\varepsilon^{(\text{env})}$. The subsystem of interest is then placed in a cavity inside this dielectric continuum. The nuclear charges and the electron density of the active subsystem induce charges on the surface of this cavity (apparent surface charges), and the electrostatic potential of these surface charges is included in the quantum-chemical treatment of the active subsystem as an embedding potential.

Commonly, the cavity surface is discretized, and a distribution of point charges $q_s$ at positions $\boldsymbol{r}_s$ on the cavity surface is used to approximate the apparent surface charges. The resulting embedding potential is then given by

$$\tilde{v}_{\text{emb}}^{(\text{continuum})}[\rho_{\text{I}}](\boldsymbol{r}) = \sum_s \frac{q_s[\varepsilon^{(\text{env})}, \rho_{\text{I}}]}{|\boldsymbol{r} - \boldsymbol{r}_s|}. \tag{104}$$

Here and in the following, a tilde is used to denote approximate quantities. Numerous variants of such continuum models have been developed that differ in the definition of the cavity and in the equation used for calculating the apparent surface charges. For details, we refer to the dedicated reviews on this subject.[154–160] Of widespread use are the polarizable continuum model (PCM),[156] which also exists in several variants, and the conductor-like screening model (COSMO).[161]

Continuum models are particularly suited for modeling solvent effects. They model not the effect of a specific molecular structure of the solvent environment but rather an implicit average over the different solvent configurations. Therefore, they provide an efficient way of including the dynamics of the solvent without considering many different molecular structures explicitly. Instead of providing an interaction energy according to eqn (79) for a specific structure, they try to approximate the free energy of the solvated molecule and the free solvation energy.

While for the dielectric constant $\varepsilon^{(\text{env})}$ one commonly uses the experimentally determined one for a specific solvent, the size and shape of the cavity are parametrized to reproduce free energies. Usually, this requires a solvent-specific parametrization. Thus, the embedding potential used in continuum models is not just an approximation to the electrostatic part of eqn (82), but implicitly also includes non-electrostatic contributions as well as the aforementioned dynamical averaging. Since by construction the embedding potential depends on the density of the active subsystem, continuum models can be categorized as polarizable embedding methods in the BT classification.

Continuum models can be easily combined with a variety of quantum-chemical methods, given the simplicity of the embedding potential in eqn (104). However, for determining the surface apparent charges $q_s$ the electron density of the active subsystem is required. While this is directly available in HF and DFT calculations, its calculation can be more involved with wavefunction based correlation methods and a fully self-consistent determination of the surface charges can become computationally rather demanding. Therefore, approximate schemes for the combination of continuum models with, *e.g.*, perturbation theory[162] or coupled cluster theory[163] have been devised.

For the calculation of excitation energies, continuum models allow for a rather straightforward inclusion of the response of the environment (for a review, see ref. 164). With state-specific methods, this is achieved by determining a different set of surface charges for each excited state of interest, *i.e.*, the difference in the electron density of the active subsystem induce a change $\Delta q_s$ in the surface charges. Such a fully self-consistent state-specific treatment is, for instance, possible for including solvent effects in CASSCF calculations.[165,166] Similarly, when employing response theory for the calculation of excitation energies, the response of the environment can be included by accounting for the response of the surface charges by an embedding kernel, which in the case of TDDFT has the form

$$(ia|\tilde{w}_{\text{emb}}^{(\text{continuum})}|jb) = \sum_s \Delta q_s[\phi_j\phi_b] \int \frac{\phi_i(\boldsymbol{r})\phi_a(\boldsymbol{r})}{|\boldsymbol{r}-\boldsymbol{r}_s|}\mathrm{d}^3r. \tag{105}$$

It describes the interaction of the surface charge $\Delta q_s[\phi_j\phi_b]$ induced by the charge distrubution $\phi_j\phi_b$ with the charge distribution $\phi_i\phi_a$. Similar response contributions can be derived in the case of wavefunction based response theory, in particular for linear response coupled cluster methods.[167–170] Note that in all these approaches, the off-diagonal environment contributions to the response matrices, corresponding to the coupling terms in eqn (92) or (103), are folded into with the environment contributions to the response matrices of the active subsystem. When combined with linear-response coupled-cluster methods, one further commonly invokes the approximation[167,171] of disregarding $\boldsymbol{J}_{\mathrm{I,I}}$ (*i.e.*, the coupling between amplitudes and multipliers).

A detail that is worth discussing is the meaning of the response of the surface charges $\Delta q_s$ when treating excited states. Because the continuum model implicitly accounts for the dynamics of the solvent environment, the environment response not only accounts for the response of the electron density of the environment, but also includes the structural relaxation of the solvent after the electronic excitation. This is usually referred to as equilibrium solvation. However, it is possible to decompose the environment response into a fast contribution $\Delta q_s^{(\mathrm{fast})}$ (corresponding to the response of the solvent electrons) and a slow contribution $\Delta q_s^{(\mathrm{slow})}$ (corresponding to the response of the nuclei in the environment). By separating these two contributions and including only the fast one in the quantum-chemical calculation it is possible to access vertical excitation energies (for details, see, *e.g.* ref. 164).

The simplicity of continuum models has made them the method of choice for obtaining a first estimate of solvent effects on excitation energies.[159,164] However, the neglect of the explicit structure of the environment is at the same time the biggest disadvantage of continuum models, in particular if specific solvent–solute interactions such as hydrogen bonding are present. In this case, usually several solvent molecules have to be included explicitly in the active subsystem.[172–174] For the same reason, continuum models are less successful for describing the effect of structured environments, such as in proteins or solid-state systems, even though they are often still used to model the bulk contribution of the outer shells of the such environments.

### 4.2 Discrete approximations: electrostatic embedding

A next step beyond continuum models are discrete approximations, in which molecular structures are considered and determine the interaction energy and the embedding potential. In contrast to continuum models, these discrete models will make an explicit treatment of the dynamics of the environment necessary. In particular for describing solvent effects or biomolecular environments, this usually requires calculations for a large number of different molecular structures of the environment in combination with a suitable averaging.

The simplest discrete approximation to the interaction energy and the embedding potential can be obtained by using a classical molecular mechanics (MM) model. The combination of the quantum mechanical (QM) treatment of the subsystem of interest with a MM description of the environment and its interaction with the active subsystem leads to so-called QM/MM methods. Such QM/MM models are common both for describing solvent effects and biomolecular structures as well as for the treatment of solid state systems and surfaces. These were first pioneered by Warshel and Levitt,[175] and have been further developed by numerous researchers in the past decades. Several excellent recent reviews are available on QM/MM methods, mostly with a focus on their use for biological systems.[176–180] Therefore, we will only highlight the most important ideas in the following and put a special focus on the application of QM/MM methods for studying excited states.

**4.2.1 Interaction energy in QM/MM.** Instead of using a quantum mechanical description, MM methods approximate the total energy through a classical force field. Commonly, such a force field energy expression has the form

$$
\begin{aligned}
\tilde{E}_{\mathrm{MM}} &= \sum_{\text{bonds}} k_d(d-d_0) + \sum_{\text{angles}} k_\theta(\theta-\theta_0) + \sum_{\text{dihedrals}} k_\phi(1+\cos(n\phi+\delta)) \\
&\quad + {\sum_{AB}}' \frac{q_A q_B}{R_{AB}} + {\sum_{AB}}' \varepsilon_{AB}\left[\left(\frac{\sigma_{AB}}{R_{AB}}\right)^{12} - \left(\frac{\sigma_{AB}}{R_{AB}}\right)^{6}\right].
\end{aligned}
\tag{106}
$$

where the three terms on the first line describe the bonding interactions in terms of bond lengths $d$, angles $\theta$, and dihedral angles $\phi$ between specific atoms. Those on the second line are nonbonding electrostatic and van der Waals interactions between all pairs of atoms (where the primed sum indicates that pairs of atoms directly connected by bonds are usually excluded). The distance between atoms $A$ and $B$ is denoted as $R_{AB} = |\boldsymbol{R}_A - \boldsymbol{R}_B|$, and $q_A$ denote partial charges assigned to each atom, whereas $\varepsilon_{AB}$ and $\sigma_{AB}$ denote Lennard–Jones parameters for the atom pair $A$,$B$.

QM/MM methods replace the energy of the environment $E_{\mathrm{II}}$ and the interaction energy $E_{\mathrm{int}}$ in eqn (77) by the corresponding energy from a classical force field, while a full quantum-chemical description is only retained for the energy of the active subsystem $E_{\mathrm{I}}$. This is possible because the total MM energy of eqn (106) can usually be partitioned according to eqn (77) in a straightforward way. If there are no covalent bonds between the active subsystem and its environment, this leads to an interaction energy of the form

$$
\tilde{E}_{\mathrm{int}}^{(\mathrm{QM/MM})} = \sum_{A}^{\text{subs.I}} \sum_{B}^{\text{subs.II}} \frac{q_A q_B}{r_{AB}} + \varepsilon_{AB}\left[\left(\frac{\sigma_{AB}}{R_{AB}}\right)^{12} - \left(\frac{\sigma_{AB}}{R_{AB}}\right)^{6}\right], \tag{107}
$$

where each sum only runs over atoms in one of the subsystems. This interaction energy contains an electrostatic part $\tilde{E}_{\mathrm{int,elstat}}^{(\mathrm{QM/MM})}$ as well as a van-der-Waals contribution. If covalent bonds connecting the active subsystem and the environment are present, the partitioning is slightly more involved and requires the introduction of linking atoms into the active subsystem. Several strategies are available and are discussed in detail in, *e.g.*, ref. 180. In general, the interaction energy will then also contain certain bonding terms as well as a correction for the additional linking atoms in the active subsystem to avoid double counting.

Instead of evaluating the electrostatic part of the interaction energy completely at the molecular mechanics level, the true charge density of the active subsystem can also be used instead of molecular mechanics charges for this subsystem, *i.e.*,

$$
\tilde{E}_{\mathrm{int,elstat}}^{(\mathrm{QM/MM})} = \sum_{A}^{\text{subs.I}} \sum_{B}^{\text{subs.II}} \frac{Q_A q_B}{R_{AB}} + \sum_{B}^{\text{subs.II}} \int \frac{\rho_{\mathrm{I}}(\boldsymbol{r}) q_B}{|\boldsymbol{r} - \boldsymbol{R}_B|} \mathrm{d}^3 r, \tag{108}
$$

where $Q_A$ are the charges of the nuclei in the active subsystem. This provides a more accurate description and offers the additional advantage that no MM charges are needed for the active subsystem. The van der Waals and (if applicable) bonding contributions to the interaction energy are, however, always evaluated using appropriate MM parameters.

**4.2.2 Electrostatic embedding in QM/MM.** QM/MM schemes including only an interaction energy while treating the active subsystem in a QM calculation without an additional embedding potential correspond to the mechanical coupling category in the BT classification. Except for a change in the ground-state geometry, the electron density of the active subsystem and molecular properties are not affected by the presence of an environment. Therefore, it is common to introduce an electronic coupling by including an embedding potential in the QM calculation of the active subsystem, that in the simplest case only consists of an electrostatic part,

$$\tilde{v}_{\mathrm{emb}}^{(\mathrm{QM/MM})}(\boldsymbol{r}) = \sum_{B}^{\mathrm{subs.II}} \frac{q_B}{|\boldsymbol{r} - \boldsymbol{R}_B|} \tag{109}$$

*i.e.*, the electrostatic potential of the atomic charges $q_B$ is included as an additional potential in the QM calculation. This additional embedding potential will modify the electron density as well as molecular properties of the active subsystem. Usually, the molecular mechanics partial charges from a standard force field are used for constructing the electrostatic embedding potential. However, it should be noted that these charges have usually not been optimized to give a faithful representation of the electrostatic potential, but emerge from other criteria during the parametrization of classical force fields. Nevertheless their use is widespread, mainly because they are easily available.[180] On the other hand, it is important to point out that these partial charges are often parametrized in such a way that they implicitly include some of the non-classical contributions to the interaction energy and the embedding potential.

QM/MM calculations employing an electrostatic embedding potential are in many cases the method of choice for describing local excitations in protein environments. Two widely studied examples are rhodopsins, where the protein environment plays an important role in tuning the absorption energy of the retinal chromophore,[181–185] and green fluorescent protein.[186–189] For these photoactive proteins, a large variety of quantum-chemical methods, ranging from TDDFT to CI and quantum Monte–Carlo calculations, have been employed in combination with an electrostatic embedding potential. While some of these studies have employed only a single static structure for the protein environment, others have included an explicit averaging over different protein conformations by sampling a number of snapshots from molecular dynamics simulations.

Note that the electrostatic embedding potential in such QM/MM calculations is independent of the electron density of the active subsystem. Therefore, no additional response contributions appear in the calculation of excitation energies, *i.e.*, the response of the environment is not included, and the presence of the environment only enters *via* a shift of the orbital energies. However, for the treatment of excitations in photoactive proteins an adequate quantum-chemical description of the isolated chromophore is already challenging.[16,181] Moreover, it has been pointed out that already the environment effect obtained with a fixed electrostatic embedding potential sensitively depends on the correct description of the transition dipole moments, which again is often difficult to achieve.[181] Thus, polarizable embedding approaches (discussed in section 4.2) have so far not been extended to photoactive proteins.

**4.2.3 Point-charge embedding for solid-state systems.** An analogous embedding potential is also commonly used for modeling local properties in ionic crystals, for instance for describing the adsorption of molecules on surfaces or for studying locally excited states in impurities. In such studies, one considers a cluster model of the subsystem of interest, and its embedding into the environment is described by point charges at the positions of the surrounding ions. For reviews of such approaches, see, *e.g.* ref. 178, 190 and 191. In particular, we want to highlight ref. 192, in which a systematic classification of the different possible strategies is provided. Here, we only want to highlight some important approaches and point out the main differences to QM/MM embedding methods employed for solvent effects or protein environments.

The most obvious difference is that the environment has a periodic structure and an infinite summation over the environment charges is in principle required, *i.e.*, the point-charge embedding potential now has the form

$$\tilde{v}_{\mathrm{emb}}^{(\mathrm{QM/MM})}(\boldsymbol{r}) = \sum_{\boldsymbol{k}\neq 0} \sum_{B}^{\text{unit cell}} \frac{q_B}{|\boldsymbol{r} - (\boldsymbol{R}_B + \boldsymbol{k})|}, \tag{110}$$

where $\boldsymbol{k}$ is the lattice vector and the second sum only runs over the ions in one unit cell. Different possibilities exist for taking this infinite sum into account. The simplest would be to truncate this series, but in the form given above its convergence is rather slow.[193] More severely, the infinite series is not absolutely convergent, *i.e.*, the sum depends on the order in which the summation is performed. This problem can be alleviated by explicitly removing dipole and quadrupole moments, either with Evjen's original method[194] or with its extensions.[195,196]

A different approach to the infinite series in eqn (110) is Ewald summation,[197] where the series is split into a short-range part that is summed in real space and a long-range part for which the summation is performed in reciprocal space, both of which converge quickly. The resulting potential can then be fitted to a finite array of point charges, from which the embedding potential is constructed.[193,198–200] Alternatively, an approach that uses the potential resulting from the Ewald summation directly in a quantum-chemical calculation has been developed by Burow *et al.* based on the periodic fast multipole method.[201]

Such periodic point-charge environments have been combined with a variety of quantum-chemical methods for studying local excitations in solid-state systems. Examples include the description of color centers in bulk ZnO with CASSCF calculations,[202] of local excitations at the $Cr_2O_3$(0001) surface with CASSCF and CI-based methods,[203] and of surface and bulk excitations in KBr with TDDFT and with EOM-CC methods.[204] These studies always employ a fixed embedding potential, *i.e.*, the response of the environment is not included.

In all applications of point-charge embedded cluster models, several options exist for defining these charges. The simplest is to use the formal charges corresponding to the oxidation states of the respective ions, another possibility is the use of partial charges, which could be derived from full quantum-chemical calculations using different schemes. For an overview and a discussion, we refer to ref. 192. If homogenous periodic systems (*i.e.*, bulk structures) are considered, the environment charges can be updated iteratively to correspond to those obtained for the embedded cluster. This is done, for instance, in the embedded ion methods and its extensions[192,205] and a similar scheme can be employed in QM/MM embedding calculations for molecular crystals.[206,207] Such schemes implicitly account for ground-state polarization of the environment by the embedded cluster.

For studying impurities in ionic crystals, this polarization is more difficult to include and has to be modeled explicitly. The use of atomic polarizabilities at the site of the ions in the environment (see below) is less common in studies of solid-state systems. Instead, shell models[208] are often employed,[209–211] in which one augments the ionic charges with a shell of the opposite charge connected to the ion by a harmonic spring. This shell can then "move" in response to the electric fields generated by the embedded cluster to account for the polarization of the environment.

### 4.2.4 Polarizable embedding in QM/MM.

In the QM/MM methods discussed so far, the partial charges assigned to the atoms in the environment are fixed, and the resulting embedding potential is thus independent of the electron density of the active subsystem. A logical next step is to go from such a fixed embedding potential to a polarizable embedding scheme in the BT classification. In QM/MM this can be achieved by using polarizable models for describing the environment. This was proposed already in the early paper of Warshel and Levitt that first introduced QM/MM approaches.[175]

One possibility of setting up such a polarizable QM/MM scheme is the discrete reaction field (DRF) model,[212] in which an embedding potential of the form

$$\tilde{v}_{\mathrm{emb}}^{(\mathrm{DRF})}[\rho_{\mathrm{I}}](\boldsymbol{r}) = \sum_{B}^{\mathrm{subs.II}} \frac{q_B}{|\boldsymbol{r}-\boldsymbol{R}_B|} + \sum_{B}^{\mathrm{subs.II}} \frac{\boldsymbol{\mu}_B^{\mathrm{ind}}[\rho_{\mathrm{I}}]\cdot(\boldsymbol{r}-\boldsymbol{R}_B)}{|\boldsymbol{r}-\boldsymbol{R}_B|^3} \tag{111}$$

is used, *i.e.*, the electrostatic potential generated by induced dipoles $\boldsymbol{\mu}_B^{\mathrm{ind}}$ at the positions $\boldsymbol{R}_B$ of the nuclei in the environment is added to the standard electrostatic QM/MM embedding potential of eqn (109). These induced dipoles are calculated as

$$\boldsymbol{\mu}_B^{\mathrm{ind}}[\rho_{\mathrm{I}}] = \boldsymbol{\alpha}_B\left(\boldsymbol{F}[\rho_{\mathrm{I}}](\boldsymbol{R}_B) + \sum_{C\neq B}^{\mathrm{subs.II}} \boldsymbol{T}_{BC}^{(2)}\cdot\boldsymbol{\mu}_C^{\mathrm{ind}}\right), \tag{112}$$

where $\boldsymbol{T}_{BC}^{(2)} = \frac{\mathrm{d}^2}{\mathrm{d}\boldsymbol{R}_B \mathrm{d}\boldsymbol{R}_C}\frac{1}{|\boldsymbol{R}_B-\boldsymbol{R}_C|}$ is the dipole interaction tensor and $\boldsymbol{F}$ is the electric field generated by the charge density of the active subsystem and all atomic partial charges of the environment,

$$\begin{aligned}\boldsymbol{F}[\rho_{\mathrm{I}}](\boldsymbol{R}_B) \;=\; & \sum_{A}^{\mathrm{subs.I}} Q_A \frac{\boldsymbol{R}_B-\boldsymbol{R}_A}{|\boldsymbol{R}_B-\boldsymbol{R}_A|^3} + \int \rho_{\mathrm{I}}(\boldsymbol{r})\frac{\boldsymbol{R}_B-\boldsymbol{r}}{|\boldsymbol{R}_B-\boldsymbol{r}|^3}\mathrm{d}^3r \\ & + \sum_{C\neq B}^{\mathrm{subs.II}} q_C \frac{\boldsymbol{R}_B-\boldsymbol{R}_C}{|\boldsymbol{R}_B-\boldsymbol{R}_C|^3}\end{aligned} \tag{113}$$

Thus, *via* this electric field, that in turn determines the induced dipoles, the embedding potential becomes dependent on $\rho_{\mathrm{I}}$. In addition, the induced dipoles depend on all other induced dipoles *via* eqn (112) and, therefore, have to be determined self-consistently. To avoid artifacts at small distances resulting in an over polarization, the dipole–dipole interaction is commonly smeared out,[213] *i.e.*, a damped version of the interaction tensor $\boldsymbol{T}^{(2)}$ is used.[214]

For the calculation of excitation energies, such a polarizable embedding potential can be applied within response theory. In this case, the dependence of the embedding potential on the density of the active subsystem leads to additional embedding contributions to the response matrices. In the case of TDDFT, this results in the embedding kernel[215]

$$(ia|\tilde{w}_{\mathrm{emb}}^{(\mathrm{DRF})}|jb) = \sum_{B}^{\mathrm{subs.II}} \delta\boldsymbol{\mu}_B^{\mathrm{ind}}[\phi_j\phi_b]\int \phi_i(\boldsymbol{r})\phi_a(\boldsymbol{r})\frac{\boldsymbol{r}-\boldsymbol{R}_B}{|\boldsymbol{r}-\boldsymbol{R}_B|^3}\mathrm{d}^3r, \tag{114}$$

where $\delta\boldsymbol{\mu}_B^{\mathrm{ind}}[\phi_j\phi_b]$ is the linear response of the induced dipole $\boldsymbol{\mu}_{\mathrm{B}}$ to the density change $\phi_j\phi_b$. Note that as for continuum models, the off-diagonal environment contributions to the response matrices in eqn (92) or (103) are not included explicitly, but are instead folded into the response matrices of the active subsystem.

Such polarizable QM/MM embedding potentials have been combined with (TD-)DFT[214–216] as well as with linear-response coupled cluster methods[171,217,218]—where, as for the continuum models, the approximation of neglecting $\boldsymbol{J}_{\mathrm{I,I}}$ is used. The latter have been applied in numerous studies of solvent effects on excitation energies.[219–221] Note that QM/MM approaches for the description of solvent effects always require an explicit averaging over a large number of snapshots from molecular dynamics simulations.

A slightly improved formalism and implementation, both for TDDFT and for coupled cluster, have been presented recently by Kongsted and coworkers.[222–224] The main difference of this polarizable embedding scheme is the use of not only partial charges, but also of dipole, quadrupole, and possibly higher multipole moments in the static part of the electrostatic embedding potential, whereas the polarizable part is still modeled with induced dipole moments. However, both for the static and for the polarizable part solvent models have been parametrized that in addition to those at the positions of nuclei include partial charges, dipoles, *etc.* also at additional locations. Such polarizable QM/MM schemes can be further combined with continuum models to account for outer solvation shells.[225]

### 4.3 Discrete approximations: beyond purely electrostatic embedding

The approximate embedding potentials discussed above only contain an electrostatic component. Depending on their parametrization, these can implicitly also account for some of the non-electrostatic contributions in the exact local embedding potential (eqn (82)). However, the absence of these explicit non-electrostatic contributions can pose a severe problem. This becomes particularly obvious in point-charge embedding methods modeling an ionic crystal environment, as discussed in section 4.2. If the basis set employed for the active subsystem is sufficiently flexible, positive charges in the environment can act as artificial nuclei and orbitals spuriously localize at these centers.[226] This problem is particularly severe if formal charges are employed.

A simple way of fixing such problems is the introduction of pseudopotentials modeling the core electrons at these centers.[227–229] Such effective core pseudopotentials are widely used in quantum chemistry and are readily available for most atoms. Note that these pseudopotentials contain nonlocal projection operators and do therefore not emerge in the FDE theory outlined above, but are derived within a different theoretical framework. However, their use for describing environment effects can only be considered a pragmatic solution, as such effective core pseudopotentials are derived in a very different context. For a discussion of the pseudopotential approximation in quantum chemistry, see ref. 230. A more rigorous way of deriving nonlocal embedding potentials is provided by the *ab initio* model potential (AIMP) method, which will be discussed below.

**4.3.1 Effective fragment potential method.** Another approach that also includes non-classical contributions to the interaction energy and to the embedding potentials is the effective fragment potential (EFP) scheme of Gordon and coworkers. It can be considered as an extension of the polarizable QM/MM models described in section 4.2. In its original form (EFP-1)[231,232] it was developed as a specific model for describing water and employs the interaction energy,

$$\tilde{E}_{\mathrm{int}}^{(\mathrm{EFP\text{-}1})} = E_{\mathrm{Coul}} + E_{\mathrm{pol}} + E_{\mathrm{rep}}, \tag{115}$$

and the embedding potential

$$\tilde{v}_{\text{emb}}^{(\text{EFP-1})}[\rho_{\text{I}}](\boldsymbol{r}) = v_{\text{Coul}}(\boldsymbol{r}) + v_{\text{pol}}[\rho_{\text{I}}](\boldsymbol{r}) + v_{\text{rep}}(\boldsymbol{r}), \tag{116}$$

The Coulomb contributions are modeled by partial charges and multipole moments (up to octupoles) located at the nuclei and bond midpoints, whereas the polarization is included *via* induced dipoles, as discussed earlier. The required parameters are extracted from quantum-chemical calculations using a well-defined scheme. The additional terms describe the non-classical repulsion contributions. For the potential, it is modeled by Gaussian functions centered at the nuclei and the center of mass,

$$v_{\text{rep}}(\boldsymbol{r}) = \sum_{B}^{\text{subs.1}} \sum_{i=1}^{2} \beta_{i,B} e^{-\alpha_{i,B}(\boldsymbol{r}-\boldsymbol{R}_B)^2}, \tag{117}$$

where the parameters $\beta_{i,B}$ and $\alpha_{i,B}$ are fitted to HF calculations of dimers. The EFP-1 model has been applied to describe the effect of water solvation on excitation energies, both using CI-based methods[233] and within TDDFT.[234] In the former case, only the ground-state polarization of the environment is included, whereas for TDDFT the response of the environment can be included as described above.

Subsequently, the EFP scheme has been refined and extended to arbitrary solvents.[232,235,236] In this EFP-2 method, the interaction energy is modeled as

$$\tilde{E}_{\text{int}}^{(\text{EFP-2})} = E_{\text{Coul}} + E_{\text{pol}} + E_{\text{exrep}} + E_{\text{disp}} + E_{\text{ct}}, \tag{118}$$

while the same EFP-1 form is kept for the embedding potential. The Coulomb and polarization contributions are described with distributed multipoles and induced dipoles as in the EFP-1 scheme, but an additional damping is introduced to avoid inaccuracies at short distances. For details on the calculation of the additional energy terms accounting for exchange-repulsion, dispersion, and charge-transfer terms, we refer to the original literature[232,236] as well as the reviews of Gordon and coworkers.[141,235] Commonly, the repulsion terms are neglected in the EFP-2 embedding potential, but they can be obtained in a similar fashion as for the energy.[237] A very appealing feature of the EFP-2 scheme is that it provides a clear prescription for extracting the interaction energy as well as the embedding potential from quantum-chemical calculations. Therefore, no empirical parameters and no dedicated fitting procedures have to be employed, thus providing an "*ab initio* route" to polarizable QM/MM embedding calculations.

## 4.4 Beyond a discrete representation of the environment

**4.4.1 ONIOM family of methods.** While the embedding methods discussed so far use a discrete approximation to the environment, usually in terms of partial charges and possibly additional potentials centered at the nuclei, the ONIOM method aims at retaining a full quantum chemical description of the environment.[238–240] It employs the interaction energy

$$\tilde{E}_{\text{int}}^{(\text{ONIOM})} = E_{\text{tot}}^{\text{low}} - (E_{\text{I}}^{\text{low}} + E_{\text{II}}^{\text{low}}), \tag{119}$$

which leads to the total energy expression

$$\tilde{E}_{\text{tot}}^{(\text{ONIOM})} = E_{\text{I}}^{\text{high}} + E_{\text{tot}}^{\text{low}} - E_{\text{I}}^{\text{low}}, \tag{120}$$

where the superscript "high" denotes energies calculated with an accurate quantum-chemical method, whereas the superscript "low" indicates energies calculated with a more approximate method. This could, for instance, be an accurate wavefunction based method combined with DFT as more approximate method. Thus, the ONIOM scheme allows for the combination of different quantum chemical methods. However, in its original formulation, the energies $E_{\mathrm{I}}^{\mathrm{high}}$ and $E_{\mathrm{tot}}^{\mathrm{low}}$ are calculated for the isolated active subsystem, *i.e.*, only mechanical coupling is included.

This has been extended to include an electrostatic embedding potential as in eqn (109), where the partial charges are extracted from the quantum-chemical calculation performed for the environment with a more approximate quantum-chemical method.[241,242] Recently, a ONIOM electrostatic embedding scheme has been devised that uses the full electrostatic embedding potential,[243] *i.e.*,

$$\tilde{v}_{\mathrm{emb}}^{(\mathrm{elstat})}[\rho_{\mathrm{II}}](\boldsymbol{r}) = \sum_{B} \frac{Q_B}{|\boldsymbol{r} - \boldsymbol{R}_B|} + \int \frac{\rho_{\mathrm{II}}(\boldsymbol{r}')}{|\boldsymbol{r} - \boldsymbol{r}'|} \mathrm{d}^3 r \qquad (121)$$

Such an embedding potential is also commonly used in the fragment molecular orbital (FMO) method[244] and in the related electrostatically embedded many-body method.[245] However, it has been pointed out that such a purely electrostatic embedding potential can lead to spurious results. In particular if large basis sets are used, an artificial localization of electron density of the active subsystem at nuclei of the environment can occur.[246–248] Thus, the nonclassical repulsive parts of the full FDE embedding potential should also be included, at least in an approximate fashion.

**4.4.2** ***Ab initio* model potentials.** One possibility to account for these non-classical contributions to the embedding potential is provided by the *ab initio* model potential (AIMP) method.[249–251] Instead of using a local embedding potential as the FDE theory outlined above, it uses a non-local embedding potential which is derived by partitioning the HF wavefunction into an anti-symmetrized product of Slater determinants.[252] Thus, the environment is explicitly represented by orbitals $\{\phi_j^{\mathrm{II}}\}$, and one arrives at a non-local embedding potential of the form

$$\hat{v}_{\mathrm{emb}}^{(\mathrm{AIMP})}[\{\phi_j^{\mathrm{II}}\}] = \tilde{v}_{\mathrm{emb}}^{(\mathrm{elstat})}[\rho_{\mathrm{II}}](\boldsymbol{r}) + \sum_{j} \hat{k}[\phi_j^{\mathrm{II}}] + \sum_{j} B_j |\phi_j^{\mathrm{II}}\rangle\langle\phi_j^{\mathrm{II}}|, \qquad (122)$$

where $\tilde{v}_{\mathrm{emb}}^{(\mathrm{elstat})}[\rho_{\mathrm{II}}](\boldsymbol{r})$ is the full electrostatic embedding potential, the second term accounts for the exchange interaction with the environment orbitals, and the last terms is a projection operator that ensures the orthogonality of the orbitals of the active subsystem to those of the environment. The constants $B_j$ are usually chosen as $B_j = -2\varepsilon_j^{\mathrm{II}}$, but other choices are also possible.[251]

The AIMP method has been used extensively in studies of electronic excitations in solid-state systems using a variety of wavefunction based quantum chemical methods, for instance for studying transition metal[253] or lanthanide and actinide centers[254–256] in ionic crystals. In this case, the environment can be described by an array at atomic ions. Thus, the environment orbitals can be pre-calculated and the resulting embedding potentials can be stored and reused. It must be noted that for ionic solids, an AIMP description of the first shells of the environment usually has to be combined with a further point-charge embedding to account for the long-range electrostatic interactions.[257] To account for the polarization of the environment, the AIMP method can be combined with shell-models,[249,258] where the electrostatic part of the embedding potential is modified.

**4.4.3 Orbital space partitioning.** At this point it is also worth mentioning that a number of embedding methods for combining wavefunction based correlation methods with a HF or DFT description of the environment exist that are based on a partitioning of the orbital space.[259–262] These start with a full HF or DFT calculation an a periodic solid or a rather large cluster and then perform a transformation to localized orbitals. A number of these orbitals are then selected to describe the active subsystem, and are used as starting point for a wavefunction based treatment. Such an approach forms, for instance, the basis of the incremental method for calculating electron correlation in extended systems with wavefunction based methods (for a review, see, *e.g.*, ref. 263).

### 4.5 Frozen-density embedding with approximate kinetic-energy functionals

The frozen-density embedding (FDE) scheme aims at providing a full description of environment effects by approximating the exact embedding potential of eqn (82). However, for the exchange–correlation functional $E_{\mathrm{xc}}[\rho]$ and for the nonadditive kinetic-energy functional $T_s^{\mathrm{nadd}}[\rho_{\mathrm{I}},\rho_{\mathrm{II}}]$ (eqn (76)) and its functional derivative

$$v_T[\rho_{\mathrm{I}},\rho_{\mathrm{II}}](\boldsymbol{r}) = \frac{\delta T_s^{\mathrm{nadd}}[\rho_{\mathrm{I}},\rho_{\mathrm{II}}]}{\delta\rho_{\mathrm{I}}(\boldsymbol{r})} = \left.\frac{\delta T_s[\rho]}{\delta\rho(\boldsymbol{r})}\right|_{\rho_{\mathrm{tot}}} - \left.\frac{\delta T_s[\rho]}{\delta\rho(\boldsymbol{r})}\right|_{\rho_{\mathrm{I}}} \qquad (123)$$

one now has to introduce approximations. Thus, in the interaction energy given in eqn (79) and in the embedding potential the contributions of the kinetic energy and of the exchange–correlation energy are approximated. The idea to use an approximate kinetic-energy functional to evaluate the interaction energy between two fixed electron densities dates back to the work of Kim and Gordon.[264,265] Later, it was extended to electron densities determined using the above embedding potential, both in subsystem approaches[135–137] and in embedding schemes.[134]

If both the active subsystem and its environment are described with DFT using an approximate exchange–correlation functional that depends only locally on the electron density (*i.e.*, LDA or GGA functionals), the exchange–correlation contribution can be treated consistently. With hybrid functionals or with orbital-dependent exchange–correlation potentials, a local functional has to be used for the nonadditive exchange–correlation contributions, which constitutes an additional approximation.[266,267]

**4.5.1 Approximation to $T_s^{\mathrm{nadd}}[\rho_{\mathrm{I}},\rho_{\mathrm{II}}]$ and $v_T[\rho_{\mathrm{I}},\rho_{\mathrm{II}}]$.** With a local exchange–correlation functional, differences between a full DFT calculation and an embedding treatment in which the densities of both subsystems are optimized are due to the approximations applied for the kinetic energy, provided that the full supermolecular basis set expansion is used for both subsystems.[147,268] Thus, comparing the electron densities from such calculations offers a way for assessing the quality of approximations for $v_T[\rho_{\mathrm{I}},\rho_{\mathrm{II}}]$, whereas a comparison of the total energies also probes the quality of $T_s^{\mathrm{nadd}}[\rho_{\mathrm{I}},\rho_{\mathrm{II}}]$. These strategies have been used to develop and tests approximations both for the kinetic-energy component of the embedding potentials and to the nonadditive kinetic energy. Here, we will only give a brief overview of the most widely used approximations and highlight some more recent developments. Dedicated reviews on kinetic-energy functionals in general[269,270] and in the context of the FDE scheme[145] are available in the literature (for more recent overviews, see, *e.g.*, the introductions of ref. 146, 271–273).

The simplest class of approximations applies an approximate kinetic energy functional in eqn (76) as well as for the functional derivative in eqn (123). These are referred to as *decomposable approximations*. Early studies employed the well-known

Thomas–Fermi functional, but following a series of tests for hydrogen-bonded systems,[274,275] Wesolowski proposed the use of generalized-gradient approximation (GGA) kinetic-energy functionals within the FDE scheme. In particular, he recommended[275] the use of the PW91k functional of Lembarki and Chermette,[276] which has been used almost exclusively in applications of the FDE scheme in the past decades. More recently, new GGA kinetic-energy functionals have also been proposed for the use in decomposable approximations to the kinetic-energy component of the FDE interaction energy and embedding potential.[273]

Several studies have assessed the quality of the available decomposable approximations. Generally, these provide a good accuracy of the electron densities and molecular properties as long as the interaction between the subsystems in dominated by weak, non-covalent interactions such as hydrogen bonding. This has, for instance, been demonstrated by comparing the electron densities obtained in FDE calculations to those of a full treatment.[277,278] For interaction energies, the PW91k approximation provides a typical accuracy of *ca.* 1–2 kcal/mol in hydrogen bonded complexes.[272]

Even though successful for weak interactions between the subsystems, several shortcomings of the available decomposable approximations based on GGA functionals have been pointed out. In the limit of infinitely separated subsystems the potential shows a wrong form at the frozen subsystem, which affect the resulting orbital energies and can lead to spuriously low excitation energies.[279] This shortcoming can partly be addressed with so-called *non-decomposable approximations*,[271,279] in which the non-additive kinetic energy or the potential $v_T[\rho_{\mathrm{I}},\rho_{\mathrm{II}}]$ are approximated directly. Even more severe is the failure of all presently available approximations for subsystems connected by covalent bonds,[278] even if these covalent bonds are very weak.[280] These problems have so far not been addressed satisfactorily, but recent work provides some possible directions for future improvements.[146] Alternatively, the insufficiencies of the currently available approximations can be circumvented by using a more general partitioning that introduces capping groups.[281]

**4.5.2 DFT-in-DFT embedding.** Initial applications of the FDE embedding potential in combination with approximate kinetic-energy functionals focussed on ionic crystals.[136,137] This early work aimed at a subsystem formulation of DFT, and treats all subsystems—in this case the individual ions—on the same footing, *i.e.*, the density of all subsystems are optimized iteratively in freeze-and-thaw iterations. In the scheme of Cortona, only spherical ions are considered and the embedding potential is spherically averaged.[282–284] Mehl and coworkers extended this scheme to general, non-spherical fragments.[285–287] Wesolowski and Warshel pioneered the use of the approximate FDE embedding potential in applications that focus on a specific subsystem of interest, while its environment is kept frozen.[134] Their initial applications concerned the solvation of lithium ions in water as well as the solvation free energies of water and methane. In these applications, an additional approximations was introduced: Instead of obtaining the electron density $\rho_{\mathrm{II}}$ of the environment from a full DFT calculation (or from a fully self-consistent subsystem DFT calculation), it was approximated as the sum of the densities of isolated solvent molecules. Such approximate ways of constructing the environment density are key to efficient DFT-in-DFT FDE calculations.

The applications discussed so far focussed on ground-state properties. Excited states can be treated in such DFT-in-DFT embedding calculations either with a state-specific approach or within response theory. A state-specific approach is realized if excited states of the active subsystem are described using a $\Delta$DFT or

ΔSCF-DFT approach (see section 2.1.1). This was applied by Wesolowski and coworkers to study crystal field splittings for impurities in ionic crystals,[288–290] using the ground-state embedding potential also for the excited states.

As outlined in section 3.1.4, the FDE theory can also be extended to a description of excited states within response theory, in particular with TDDFT. In applications of such an approach, one usually—in addition to the use of approximations to the kinetic-energy contribution to the embedding kernel—introduces approximations for the treatment of the embedding contributions to the response equations (eqn (92)). The simplest approximation is to neglect the off-diagonal coupling blocks $\boldsymbol{F}_{\text{int}}^{\text{I,II}}$ and $\boldsymbol{F}_{\text{int}}^{\text{II,I}}$ arising from the embedding contribution.[291] This leads to a decoupling of the response equations of the two subsystems, and the energies of local excitations of the active subsystem can be determined by considering only the matrix $\boldsymbol{F}_{\text{I,I}} = \boldsymbol{F}_{\text{I}} + \boldsymbol{F}_{\text{int}}^{\text{I,I}}$, where the additional embedding contribution is determined by the embedding kernel given in eqn (94). This approximation corresponds to a neglect of the response of the environment.

Such a scheme can be employed for the calculation of solvent effects on local excitation energies by combining it with approximate construction of the solvent electron density.[292] Because the TDDFT response calculation is limited to the active subsystem describing the solute molecule this results in an efficient treatment and allows for the inclusion of large frozen solvent shells as well as an averaging over a sufficient number of solvent structures. The simplest approximation for the solvent density is to use the sum of the densities of isolated water molecules. Such a description can be further refined by updating the density of a few solvent molecules close to the active subsystem in freeze-and-thaw iterations.[140,293] Similar schemes can be used to treat local excitations in protein environments.[294,295]

With a fixed frozen density, such FDE calculations correspond to electronic embedding in the BT classification. Accounting for the ground-state polarization of the environment leads to a polarizable embedding scheme, but within the approximation discussed so far the polarized response of the environment density is not included. A discussion of these different contributions and a comparison to a polarizable QM/MM description can be found in ref. 296.

A computational strategy for an efficient treatment of the full embedding contributions to the response matrices has been devised by Neugebauer.[150,151] In his subsystem TDDFT scheme, off-diagonal coupling contributions to the response matrices are not neglected. Instead, the excitation energies of the individual subsystems are determined first, and in a second step the coupling contributions are included only for those excitations that are of interest. This allows for an efficient treatment of both the polarization of the environment[151,297] and of couplings between local excitations.[150] Neugebauer and coworkers have employed their scheme in several studies of photosynthetic systems, in particular light harvesting complexes.[294,298] Recent reviews on the calculation of excitation energies with subsystem TDDFT and on the related applications are available.[6,8,9]

### 4.5.3 WFT-in-DFT embedding.

The application of the FDE embedding potential in combination with approximations for the kinetic-energy functional for embedding a wavefunction based description of the active subsystem in an environment described by DFT (WFT-in-DFT embedding) was pioneered by Carter and coworkers.[142,299] Their work focussed on the description of molecules absorbed on metallic surfaces. Their pilot application concerned the description of ground-state properties of CO on a Cu(111) surface and used a scheme in which the density of the active subsystem is obtained with CI or CASSCF and is updated iteratively, while the total density is obtained from a periodic DFT calculation and is kept fixed. Subsequently, this scheme was extended to the treatment of excited states within these state-specific methods for the active subsystem to describe the local excitations of CO on a Pt(111) surface.[300,301]

The limitations of these scheme where addressed in later work, in which the constraint that the total density is kept fixed was relaxed.[302,303] Instead, the environment density is chosen as $\rho_{\mathrm{II}} = \rho_{\mathrm{tot}} - \rho_{\mathrm{I}}^{\mathrm{bare}}$, where the total density is obtained from a periodic DFT calculation and $\rho_{\mathrm{I}}^{\mathrm{bare}}$ is the density of the isolated subsystem I. This environment density is then kept frozen, *i.e.*, the polarization of the environment is only included through the periodic DFT description, but not updated according to the wavefunction based calculation. This scheme has been applied in a number of studies of ground state properties[304–307] and of local excited states.[229] For a review of these WFT-in-DFT embedding approaches and their applications, see ref. 7.

For the calculation of excitation energies, wavefunction based methods are often required because of the well-known limitations of TDDFT, but nevertheless a DFT calculation provides an adequate ground-state density. Therefore, a simplified WFT-in-DFT embedding scheme, in which the embedding potential is obtained from a DFT-in-DFT embedding calculation (either using a fixed approximate environment density or an environment density polarized in freeze-and-thaw iterations) has been proposed.[70] This simplified scheme has been applied to study electronic excitations of $\mathrm{NpO}_2^{2+}$ impurities embedded in ionic crystals using IHFSCC methods.

In applications of in WFT-in-DFT embedding, the response of the environment has not yet been accounted for. With the state-specific wavefunction based methods that were mainly employed (*i.e.*, CASSCF, CI, and IHFSCC), this would be possible by using state-specific embedding potentials.[148] However, this approach has not been attempted in practice so far, and would introduce additional problems in the calculation of transition moments since the different electronic states of the active subsystem will no longer be orthogonal. Therefore, an inclusion of the environment response should be easier within response theory, and the corresponding theory as well as working equations for linear-response coupled-cluster methods have been derived recently.[152]

## 4.6 Frozen-density embedding with optimized effective potentials

For calculating local excitations and other local molecular properties, FDE calculations employing approximate kinetic-energy functional can provide an accurate description of environment effects in certain cases. In particular, the available approximations are applicable if the interaction between the subsystem of interest and its environment is weak or dominated by electrostatic interactions. However, even in these cases the available approximations to the kinetic-energy component $v_T[\rho_{\mathrm{I}},\rho_{\mathrm{II}}]$ of the embedding potential have deficiencies. These inevitably introduce small, but sometimes not negligible errors into the calculated excitation energies. These can be reduced by increasing the size of the active subsystem, but especially in WFT-in-DFT embedding calculations this is not desirable and often not feasible. On the other hand, a description of covalent bonds between subsystems is not possible with the currently available approximations.

Therefore, variants of the FDE scheme that avoid such approximations for the kinetic-energy functional or its functional derivative have been developed in recent years by several groups. The evaluation of the kinetic-energy component $v_T[\rho_{\mathrm{I}},\rho_{\mathrm{II}}]$ of the embedding potential requires the evaluation of the functional derivative of the noninteracting kinetic-energy functional $T_s[\rho]$ for two different densities, the total density $\rho_{\text{tot}} = \rho_{\text{I}} + \rho_{\text{II}}$ and the density of the active subsystem $\rho_{\text{I}}$. By using the Euler–Lagrange equation for the KS system of noninteracting electron with a given, fixed density $\rho(\boldsymbol{r})$ this functional derivative can be related to the local potential $v_s[\rho](\boldsymbol{r})$ that has this density $\rho(\boldsymbol{r})$ as its ground state,[308]

$$\frac{\delta T_s[\rho]}{\delta \rho(\boldsymbol{r})} = -v_s[\rho](\boldsymbol{r}) + \mu, \tag{124}$$

where $\mu$ is a constant shift that is related to the chemical potential. Thus, the kinetic-energy component of the embedding potential can be evaluated from[279]

$$v_T[\rho_{\text{I}},\rho_{\text{II}}](\boldsymbol{r}) = v_s[\rho_{\text{I}}](\boldsymbol{r}) - v_s[\rho_{\text{tot}}](\boldsymbol{r}) + \Delta\mu \tag{125}$$

as the difference between the local potentials yielding the density of the active system and the total density, respectively. These local potentials yielding a certain density can be evaluated numerically. Different algorithms for such a potential reconstruction (often also referred to as optimization of effective potentials or OEP methods) have been developed. In the context of embedding calculations, the algorithms of van Leeuwen and Baerends [123] and of Zhao, Morrison, and Parr (ZMP)[309] as well as schemes based on the direct optimization algorithm of Wu and Yang (WY)[310] have been employed. While the van Leeuwen–Baerends and the ZMP schemes employ a numerical representation of the potential on a grid, the algorithm of Wu and Yang expands the potential in a suitable basis set. Even though the details differ, all embedding schemes avoiding approximations for $v_T[\rho_{\text{I}},\rho_{\text{II}}]$ are based on such an optimization of an effective potential.

Within DFT-in-DFT embedding schemes, approaches calculating an approximate embedding potential are usually computationally not advantageous. For determining the embedding potential, one or more calculations on the full system are required, which embedding schemes usually aim to avoid. Nevertheless, such calculations can be employed to demonstrate that schemes based on the embedding potential of eqn (82) do indeed reproduce the electron density of a full calculation. Moreover, the reconstruction of accurate embedding potentials can further guide the development of new approximations to the kinetic-energy component of the embedding potential $v_T[\rho_{\text{I}},\rho_{\text{II}}]$. The latter was the aim of a recent study of Fux *et al.*,[146] and a similar study was performed by Goodpaster *et al.*[311] However, such schemes are not suitable for practical calculations. Therefore, Goodpaster *et al.* extended their scheme[312] by introducing a pairwise approximation that relies on a further partitioning of the frozen environment density (see eqn (73). Instead of calculating the kinetic-energy component of the embedding potential as in eqn (125), it is approximated as

$$\tilde{v}_T^{(\text{pair})}[\rho_{\text{I}}, \rho_{\text{II}}^{(n)}] \approx \sum_n v_s[\rho_{\text{I}}] - v_s[\rho_{\text{I}} + \rho_{\text{II}}^{(n)}] \tag{126}$$

This approximation turns out to be very accurate for small water clusters, and might provide a way to the efficient simulation of condensed-phase systems.

Within WFT-in-DFT embedding schemes, a DFT calculation on the full system is often feasible, while the correlated WFT calculation on the small subsystem of interest becomes the bottleneck. Thus, the use of accurate embedding potentials becomes feasible in this case. This was realized by Roncero *et al.*, who were the first to propose the use of OEP methods in the context of WFT-in-DFT embedding.[10] Their scheme starts with a DFT or HF calculation on the full system, from which the total electron density $\rho_{\text{tot}}(\boldsymbol{r})$ is obtained. This density is then partitioned into an active subsystem and its environment, and an accurate embedding potential for the active subsystem is determined with the ZMP algorithm by requiring that the chosen density of the active subsystem is reproduced in a DFT or HF calculation. This potential is then included in the wavefunction based treatment of the active subsystem. Note that, even though no approximate kinetic-energy functional is used, such a scheme still introduces several approximations: First, the total electron density is calculated with approximate DFT or HF. Second, neither the total density nor the embedding potential are refined to account for the difference between the DFT or HF electron density and the one obtained from a correlated wavefunction based treatment (*i.e.*, an accurate DFT-in-DFT embedding potential is used as approximation to the WFT-in-DFT embedding potential). Finally, when constructing a suitable partitioning of the total density, it is difficult to ensure that the subsystem densities are $v_s$-representable. In particular when localized orbitals are employed, these densities usually contain nodes, which makes them difficult to reproduce with a local potential expanded in a finite basis set (see also the discussion in ref. 146, 313, 314). To address the latter problem, Roncero *et al.* extended their scheme to allow for an iterative refinement of the density partitioning.[315]

However, as for the DFT-in-DFT studies in ref. 146 and 311 discussed above, the resulting density partitioning—and thus also the embedding potential—are not unique. This shortcoming was addressed by Carter and co-workers, who defined a unique partitioning by using the idea of partition density-functional theory (P-DFT) of Wasserman and co-workers[138,316] to require that the active subsystems and its environment share a common embedding potential.[11] Subsequently, they presented a reformulation of the embedding theory in terms of an optimization of the embedding potential, that allows for a conceptually simple implementation of WFT-in-DFT embedding schemes that do not rely on approximate kinetic-energy functionals.[12] Even though results were only presented for DFT-in-DFT embedding calculations, this scheme can be easily extended to obtain accurate WFT-in-DFT embedding potentials, provided a correlated WFT method that allows for an efficient calculation of the electron density is used.

In such a complete WFT-in-DFT scheme (*i.e.*, one in which the density calculated with WFT is used to construct an accurate embedding potential), the only remaining approximations are those inherent to the (approximate) WFT treatment of the subsystem of interest and the (approximate) DFT treatment of the environment as well as the use of an approximate functional for the exchange–correlation component of the embedding potential. However, all these approximations are justified and controllable. The largest remaining obstacle for such complete WFT-in-DFT schemes is the need for OEP methods. In combination with a finite orbital basis set the reconstruction of the local potential corresponding to a given density is an ill-posed problem.[317,318] Therefore, the embedding potentials obtained with finite-basis set OEP methods are in general not unique. This will affect the energy and density from a correlated WFT calculation on the active subsystem as well as molecular properties. Thus, numerically stable OEP methods that provide unambiguous embedding potentials are required[319–321] and a new approach addressing these issues has been developed recently.[322]

The existing complete WFT-in-DFT methods using accurate embedding potentials[11,12] can also be applied directly to a state-specific WFT approaches for calculating excited states. This can either be done in an approximate fashion using a common frozen environment density or in a full treatment that determines a state-specific embedding potential. However, the extension to response theory is still an open issue, because this will also require the calculation of an accurate kinetic-energy contribution to the embedding kernel.

## 5 Case studies

### 5.1 Excited states of acetone in aqueous solution

The determination of solvatochromic shifts of acetone in water is one of the *de facto* standards for evaluating the performance of theoretical approaches for describing solvent effects on excitation energies. Numerous studies have employed a range of electronic structure methods and embedding approaches (see ref. 221 for a non-exaustive summary up to 2005). In Table 1, some of these results are summarized.

The simplest approach are supermolecular calculations, where acetone and a number of water molecules are considered explicitly. However, such a treatment is computationally costly and often only a small number of solvent molecules can be considered. For instance, Serrano-Andrés *et al.*[323] performed CASPT2 calculations in which the effect of the solvent was modeled by only two additional water molecules. For these small clusters, static structures with an optimized geometry were used. While this resulted in a good agreement with experiment, it cannot be expected that these results are converged with respect to the size of the solvent shell. Moreover, dynamical effects resulting from the many different possible solvent structures and the associated temperature effects such as peak broadening are not included.

Alternatively, a treatment with periodic boundary conditions avoids errors introduced by a truncation of the system, and in combination with molecular dynamics allows for an inclusion of temperature effects by averaging over a number of snapshots. Such a treatment was employed by Bernasconi *et al.*[324] using Car-Parrinello molecular dynamics (CPMD) in combination with TDDFT. However, with non-hybrid functionals spurious charge-transfer excitations can obscure the picture, which can be alleviated with hybrid functionals.[325]

Another possibility is the use of continuum solvation models for including the effect of the environment. As discussed above, such an approach implicitly accounts for the dynamics of the solvent, but cannot describe specific interactions, in particular hydrogen bonding. Therefore, the agreement with experiment can be rather poor.[224] The popular solution for this shortcoming is the inclusion of a few solvent molecules to the active subsystem.[323,326] However, it should be noted that this again requires a suitable averaging over different solvent configurations.

A QM/MM description can significantly improve results with respect to continuum methods, while being significantly cheaper than the full quantum-mechanical treatment including solvent dynamics. Nevertheless, an averaging over a large number of solvent configurations is still required. The relative importance of different parameters characterizing the force fields used to represent the environment have been investigated in the recent benchmark studies of Sneskov *et al.*[330] and of Schwabe *et al.*,[224] using DFT and LR-CCSD cluster for the active subsystem. In the M2P0 model, static partial charges, dipoles, and quadrupoles are used to represent the solvent, but the polarization of the environment is not included. As shown in Table 1, such models underestimate the solvent shift.

Including the polarization of the environment through induced dipoles in the M2P2 model improves the solvatochromic shifts significantly. Furthermore, the analysis of Sneskov *et al.*[330] shows that for acetone, the main effect of the solvent

**Table 1** Excitation energies and solvatochromic shifts (in eV) for the $n \rightarrow \pi^*$ transition of acetone in aqueous solution. The different electronic structure methods and models representing the solvent are indicated. For the solvent model, "S(n)" indicates that $n$ solvent molecules have been explicitly included in the active subsystem. Additional details are given in the text and in the original references

| Method | Basis | Solvent | E | Shift |
|---|---|---|---|---|
| Supermolecular calculations | | | | |
| CASPT2[323] | ANO | S(2) | 4.54 | 0.18 |
| TDDFT/BLYP[324] | plane wave | S(periodic) | 4.37 | 0.19 |
| TDDFT/PBE0[325] | plane wave | S(periodic) | 4.51 | 0.20 |
| Continuum solvation models | | | | |
| TDDFT/CAM-B3LYP[224] | aug-cc-pVDZ | PCM | 4.59 | 0.08 |
| CASSCF[326] | 6–31G* | S(1) + PCM | 4.49 | 0.21 |
| CASPT2[323] | ANO | S(2) + DC | 4.50 | 0.14 |
| QM/MM with non-polarizable force fields | | | | |
| TDDFT/CAM-B3LYP[224] | aug-cc-pVDZ | M2P0 | 4.63 | 0.12 |
| CCSD[224] | aug-cc-pVDZ | M2P0 | 4.69 | 0.11 |
| QM/MM with polarizable force fields | | | | |
| TDDFT/CAM-B3LYP[224] | aug-cc-pVDZ | M2P2 | 4.75 | 0.24 |
| | | S(1) + M2P2 | 4.70 | 0.19 |
| | | S(2) + M2P2 | 4.68 | 0.17 |
| CCSD[224] | aug-cc-pVDZ | M2P2 | 4.80 | 0.22 |
| TDDFT/B3LYP[234] | Dunning-Hay | EFP-1 | 4.59 | 0.21 |
| TDDFT/B3LYP[225] | aug-cc-pVTZ | MM-5 | 4.53 | 0.12 |
| | | MM-5 + PCM | 4.57 | 0.16 |
| Frozen Density Embedding (PW91k approximation) | | | | |
| TDDFT/SAOP[292] | TZP | LDA/DZ | 4.67 | 0.20 |
| TDDFT/SAOP[70] | TZ2P | LDA/DZP | 4.63 | 0.16 |
| CC2[70] | aug-cc-pVDZ | LDA/DZP | 4.55 | 0.20 |
| Exp.[327–329] | | | 4.68–4.69 | 0.19–0.21 |

polarization is captured already in the description of the ground-state, with only minor contributions to excited state. A curious finding is that for the better force field models (M2P2), the excitation energies are slightly overestimated for both DFT and coupled cluster. Furthermore, including two water molecules explicitly in the active subsystem results in an improvement of the excitation energies, while the shift remains accurate with respect to experiment. As the change in the shift is much less than for the excitation energies, this could indicate that there are electronic effects that are not captured by the QM/MM description. Moreover, the differences to the results obtained with effective fragment potentials[234] indicates that these results are still quite sensitive to the parametrization of the MM model.

In QM/MM calculations, another important question is the size of the MM environment. The studies discussed so far always employed rather large solvent shells because the electrostatic effects are of long range. As a large MM part will necessarily mean more expensive molecular dynamics calculations, Steindal *et al.*[225] have devised a three-level approach, where specific interactions are included with a polarizable QM/MM model (in the Table, MM-5 indicates that waters within a radius of 5 Å are treated explicitly), whereas the bulk contribution is treated with a continuum model. This leads to a faster convergence of the excitation energy with respect to the size of the explicit solvent environment.

The application of approaches based on FDE with approximations for the kinetic energy part of the embedding potential to study solvatochromic shifts has been pioneered by Neugebauer *et al.*[292] They employed snapshots from CPMD simulations of both the gas phase and the solution to obtain geometries of acetone surrounded by 88 water molecules. For those TDDFT calculations were carried out, in which the solvent environment was included *via* the FDE embedding potential. One important finding of ref. 292 was that nearly identical solvent shifts are obtained when the FDE embedding potential is constructed from an approximate density. Thus, they suggested to use a superposition of densities obtained for isolated water molecules. This approach was subsequently also used[70] in combination with CC2 calculations for the active subsystem. Both with TDDFT and with CC2 a very good agreement with experiment is found for the solvatochromic shifts. However, with CC2 the absolute excitation energies are systematically underestimated both in the gas-phase and for solvated acetone, which could be attributed to the approximate treatment of correlation in CC2 and possibly also the use of BLYP-generated structures that do not yield proper $C=O$ distances.

It should be noted that the FDE calculations of Neugebauer *et al.*[292] use a fixed embedding potential which does not include the polarization of the environment, neither for the ground nor for the excited state. In ref. 70, only the ground-state polarization was included *via* freeze-and-thaw iterations. Both studies include only the uncoupled embedding contributions in the response part, *i.e.*, the response of the environment is not included. Thus, polarizable QM/MM approaches guard an advantage over uncoupled FDE in this respect.[296] However, the recent developments for including this polarization at the response level also for FDE should make the two methods comparable for general response properties. On the other hand, FDE keeps the advantage of retaining a full electron density for the solvent and should, therefore, provide a more accurate embedding potential, in particular at shorter distances.[296]

### 5.2 Electronic spectra in solid oxides: MgO in bulk and in the presence of defects

Unlike the case of a molecule in solution, there is no single model system for evaluating new methodologies in solid-state applications. Here, we have chosen to discuss MgO because it is a relatively simple ionic material and well-characterized experimentally. Therefore, it has been the subject of several theoretical studies of electronic states arising from excitations in the bulk, surfaces, or of so-called $F^+$ or F-centers, which are due to vacant oxygen sites. The results of some of these studies are summarized in Table 2.

Excitations in the bulk have been studied by plane-wave DFT/PBE[229] as well as embedded clusters[44,229] and correlated solid-state approaches.[331–333] Unsurprisingly, one sees that the latter yield the best agreement with experiment, whereas DFT calculations severely underestimate the excitation energies. On the other hand, embedded cluster calculations employing wavefunction based methods perform rather well. Already CIS is significantly closer to experiment than the DFT/PBE calculations. The CISD calculation of Shluger *et al.*[44] using a polarizable force field to describe the environment yields results in excellent agreement with experiment. However, one cannot rule out a such a good agreement is not due to fortuitous error cancellation.

On the other hand, the results of Carter and coworkers[229] employing a better correlation method (CASPT2) in combination with a static point charge description of the environment are about 1 eV below experiment. Moreover, the change in excitation energies with increased cluster size in these calculations[229] does not show a clear convergence trend and the results are sensitive to the choice of the point charges for the environment. This could be due to an insufficient inclusion of Pauli repulsion *via* effective core pseudopotentials at of Mg$^{2+}$ atoms close to the embedded clusters.

**Table 2** Singlet (doublet) excitation energies (in eV) for bulk MgO and F (F$^{+}$) vacancy defects on oxygen centers calculated for different cluster models and representations of the environment. Here "Madelung" denote a point-charge embedding potential, "AIMP" is used to indicate the use of *ab initio* model potentials for the environment surrounded by point charges, and "FDE" is used if FDE-derived potentials. Further details can be found in the text and the original references

| Method | Cluster | Environment | | E |
|---|---|---|---|---|
| Bulk MgO | | | | |
| ΔDFT/PBE[229] | Periodic | | | 4.48 |
| GW/BSE[331–333] | Periodic | | | 7.2–7.7 |
| CIS[44] | $Mg_4O_4$ | $(MgO)_{108}$ | Force field[a] | 8.9 |
| CISD[44] | | | | 7.5 |
| CASPT2[229] | $Mg_4O_4$ | $(MgO)_{252}$ | Madelung[b] | 6.62 |
| | | | Madelung[c] | 6.87 |
| MRCISD[229] | $Mg_4O_4$ | $(MgO)_{252}$ | FDE | 5.63 |
| Exp.[334,335] | | | | 7.5–7.8 |
| F center (neutral O vacancy defect, 2 electrons trapped) | | | | |
| ΔSCF-HF[336] | $Mg_{14}O_{12}$ | $(MgO)_{1674}$ | Madelung | 2.62 |
| | | $(MgO)_{168}$ | AIMP | 7.45 |
| MRCI[337] | $Mg_{14}O_{12}$ | $Mg_{24}^{2+}$ | AIMP | 6.00 |
| CASPT2[338] | | | | 5.59 |
| CASSCF[339] | $Mg_{14}O_{12}$ | $Mg_{157}^{2+}\ O_{159}^{2-}$ | AIMP | 6.45 |
| CASPT2[339] | | | | 5.47 (5.01[d]) |
| Exp.[340] | | | | 5.03 |
| F$^{+}$ center (O$^{-}$ vacancy defect, one electron trapped) | | | | |
| MRCI[337] | $Mg_{14}O_{12}$ | $Mg_{24}^{2+}$ | AIMP | 5.75 |
| CASPT2[338] | | | | 5.95 |
| CASSCF[339] | $Mg_{14}O_{12}$ | $Mg_{157}^{2+}\ O_{159}^{2-}$ | AIMP | 6.73 |
| CASPT2[339] | | | | 5.96 (5.22[d]) |
| Exp.[340] | | | | 4.96 |

[a] Polarizable force field using a semiempirical shell-model for the ion polarizabilities. [b] Formal point charges (±2) on the site positions on the atoms in the environment, with effective core potentials at positions of Mg atoms close to the cluster. [c] Fractional point charges from a periodic calculation. [d] Calculated on a reoptimized geometry in the presence of the vacancy.

It is also interesting to see that an FDE description of the environment in combination with a MR-CISD treatment of the active subsystem also underestimates the excitation energies rather strongly. This is apparently in contrast to the good performance of FDE for other local excitations for impurities in ionic solids.[70,288–290] This could be due to an insufficient account of Pauli repulsion by the kinetic energy functionals in use, even though the authors argue from an analysis of the embedding potential that this is not the cause of the problem.[229] Nevertheless, it might merit further investigation, for instance with the recently developed FDE scheme employing accurate optimized embedding potentials.[11,12] In addition, it should be pointed out that the FDE calculations do not account for the response of the environment, since the fixed embedding potential obtained for the ground-state is also employed for the excited states.

Finally, we turn to local excitations of defect sites, which represent a situation also encountered when describing materials with impurities or doping agents. Comparing the results of Miyoski *et al.*[336] with point-charge embedding and AIMPs clearly shows the importance of the inclusion of non-classical, repulsive parts of the embedding potential. With a purely electrostatic embedding potential, a spurious delocalization of the embedded cluster wavefunction over the environment occurs. The use of AIMPs prevents this,[257,336] even though the ΔSCF-HF calculation overestimates the experimental excitation energy significantly. This can be improved if electron correlation is included in an appropriate fashion.[338,339] Moreover, comparing the two CASPT2 results shows that a sufficiently large environment and a more flexible description of the buffer region are still important.

For the defects another important aspect is the proper description of the geometry. Relaxation effects due to the creation of the vacancies need to be included. In the examples discussed here, these were found to be as important as electron correlation, as they lower the excitation energies of the F and $F^+$ centers by about 0.5 and 0.8 eV, respectively. If these are included, the CASPT2 results are in very good agreement with the experimental values. It should be noted here that the same accuracy is not achieved for both defects. This is due to the more delocalized nature of the excited states for the $F^+$ centers, which would likely require larger clusters for the active subsystem as well as extended basis sets.

## 6 Concluding remarks

In this review we have presented the ingredients needed for a quantum-chemical description of electronic excitations in complex chemical systems. This includes electronic structure methods capable of treating excited states as well as embedding methods for extending their applicability from relatively small molecules to larger systems. In this respect, we have attempted to outline the strengths and weaknesses of the different approaches in practical applications, with a particular focus on the treatment of local electronic excitations. From these it becomes evident that both a proper inclusion of electron correlation in the electronic structure calculation and an appropriate inclusion of non-classical contributions to the embedding potential at short range as well as of long-range electrostatic effects are all decisive. However, no single method or combination of methods can claim to be accurate, computationally affordable, and generally applicable at the same time.

Thus, when considering quantum-chemical embedding schemes it is more relevant to think of them as a framework in which different approximations can be made in practice, in order to arrive at a good balance between accuracy and computational cost.

We believe that the FDE theory can provide such a framework. First, for the ground-state it allows the seamless combination of density-functional and wavefunction theory-based electronic structure methods through their interaction *via* a formally exact DFT-based embedding potential. Second, in combination with response theory, the same can be achieved for electronically excited states. Going beyond local excited states, FDE-based approaches offer the additional advantage that they are able to describe the coupling of electronic excitations of different subsystems, since a quantum-mechanical description is retained for all parts.

Nevertheless, there are still several challenges FDE-based approaches should address in the future. The first one is the development of approximations to the kinetic-energy component of the embedding potential that are both computationally efficient and sufficiently accurate to describe, for instance, situations where the active subsystem and its environment are linked by strong interactions such as covalent bonds. Methods based on the use of accurate optimized embedding potentials might prove to be a valuable tool in this respect, but these will probably only be feasible within WFT-in-DFT embedding schemes. Second, with the recent emergence of WFT-in-DFT approaches for calculating excited states and other molecular properties with response theory, the proper inclusion of couplings between the subsystem remains a challenge and will require additional methodological developments as well as flexible computer implementations and applications of such schemes.

## Acknowledgements

C.R.J. gratefully acknowledges funding from the DFG-Center for Functional Nanostructures at KIT. A.S.P.G. acknowledges support from PhLAM (Laboratoire de Physique des Lasers, Atomes et Molécules, Unité Mixte de Recherche de l'Université de Lille 1 et du CNRS).

## References

1 G. D. Scholes, G. R. Fleming, A. Olaya-Castro and R. van Grondelle, *Nature Chem.*, 2011, **3**, 763–774.
2 A. Hagfeldt, G. Boschloo, L. Sun, L. Kloo and H. Pettersson, *Chem. Rev.*, 2010, **110**, 6595–6663.
3 B. M. van der Ende, L. Aarts and A. Meijerink, *Phys. Chem. Chem. Phys.*, 2009, **11**, 11081–11095.
4 I. Navizet, Y.-J. Liu, N. Ferré, D. Roca-Sanjuán and R. Lindh, *ChemPhysChem*, 2011, **12**, 3064–3076.
5 J.-L. Brédas, D. Beljonne, V. Coropceanu and J. Cornil, *Chem. Rev.*, 2004, **104**, 4971–5004.
6 C. König and J. Neugebauer, *ChemPhysChem*, 2012, **13**, 386–425.
7 P. Huang and E. A. Carter, *Annu. Rev. Phys. Chem.*, 2008, **59**, 261–290.
8 J. Neugebauer, *ChemPhysChem*, 2009, **10**, 3148–3173.
9 J. Neugebauer, *Phys. Rep.*, 2010, **489**, 1–87.
10 O. Roncero, M. P. de Lara-Castells, P. Villarreal, F. Flores, J. Ortega, M. Paniagua and A. Aguado, *J. Chem. Phys.*, 2008, **129**, 184104.
11 C. Huang, M. Pavone and E. A. Carter, *J. Chem. Phys.*, 2011, **134**, 154110.
12 C. Huang and E. A. Carter, *J. Chem. Phys.*, 2011, **135**, 194104.
13 S. Grimme, in *Reviews in Computational Chemistry*, ed. K. B. Lipkowitz, R. Larter and T. R. Cundari, Wiley, 2004, vol. 20, pp. 153–218.
14 P. H. P. Harbach and A. Dreuw, in *Modeling of Molecular Properties*, ed. P. Comba, Wiley, 2011, pp. 29–47.
15 L. González, D. Escudero and L. Serrano-Andrés, *ChemPhysChem*, 2012, **13**, 28–51.
16 C. Filippi, M. Zaccheddu and F. Buda, *J. Chem. Theory Comput.*, 2009, **5**, 2074–2087.
17 Ch. R. Jacob and M. Reiher, *J. Chem. Phys.*, 2009, **130**, 084106.
18 Ch. R. Jacob, S. Luber and M. Reiher, *Chem.-Eur. J.*, 2009, **15**, 13491–13508.

19 O. Christiansen, P. Jørgensen and C. Hättig, *Int. J. Quantum Chem.*, 1998, **68**, 1–52.
20 D. J. Tannor, *Introduction to Quantum Mechanics: A Time-Dependent Perspective*, University Science Books, 2006.
21 T. Helgaker, S. Coriani, P. Jorgensen, K. Kristensen, J. Olsen and K. Ruud, *Chem. Rev.*, 2012, **112**, 543–631.
22 P. Hohenberg and W. Kohn, *Phys. Rev.*, 1964, **136**, B864–B871.
23 W. Kohn and L. J. Sham, *Phys. Rev.*, 1965, **140**, A1133–A1138.
24 W. Koch and M. C. Holthausen, *A Chemist's Guide to Density Functional Theory*, Wiley-VCH, Weinheim, 2nd edn., 2001.
25 J. N. Harvey, *Annu. Rep. Prog. Chem., Sect. C*, 2006, **102**, 203–226.
26 D. Rappoport, N. R. M. Crawford, F. Furche and K. Burke, in *Computational Inorganic and Bioinorganic Chemistry*, ed. E. I. Solomon, R. A. Scott and R. B. King, Wiley, 2009, pp. 159–172.
27 A. J. Cohen, P. Mori-Sanchez and W. Yang, *Science*, 2008, **321**, 792–794.
28 A. J. Cohen, P. Mori-Sánchez and W. Yang, *Chem. Rev.*, 2012, **112**, 289–320.
29 O. Gunnarsson and B. I. Lundqvist, *Phys. Rev. B*, 1976, **13**, 4274–4298.
30 U. von Barth, *Phys. Rev. A*, 1979, **20**, 1693–1703.
31 J. P. Perdew, A. Ruzsinszky, L. A. Constantin, J. Sun and G. I. Csonka, *J. Chem. Theory Comput.*, 2009, **5**, 902–908.
32 R. Gaudoin and K. Burke, *Phys. Rev. Lett.*, 2004, **93**, 173001.
33 T. Ziegler, A. Rauk and E. J. Baerends, *Theor. Chim. Acta*, 1977, **43**, 261–271.
34 C. Daul, *Int. J. Quantum Chem.*, 1994, **52**, 867–877.
35 M. Levy and A. Nagy, *Phys. Rev. Lett.*, 1999, **83**, 4361–4364.
36 A. T. B. Gilbert, N. A. Besley and P. M. W. Gill, *J. Phys. Chem. A*, 2008, **112**, 13164–13171.
37 C.-L. Cheng, Q. Wu and T. Van Voorhis, *J. Chem. Phys.*, 2008, **129**, 124112.
38 T. Kowalczyk, S. R. Yost and T. V. Voorhis, *J. Chem. Phys.*, 2011, **134**, 054128.
39 T. Ziegler, M. Seth, M. Krykunov, J. Autschbach and F. Wang, *J. Chem. Phys.*, 2009, **130**, 154102.
40 J. Cullen, M. Krykunov and T. Ziegler, *Chem. Phys.*, 2011, **391**, 11–18.
41 T. Helgaker, P. Jørgensen and J. Olsen, *Molecular Electronic Structure Theory*, John Wiley & Sons, Chichester, 2000.
42 R. G. Szalay, T. M. an G. Gidofalvi, H. Lischka and R. Shepard, *Chem. Rev.*, 2012, **112**, 108–181.
43 A. Dreuw and M. Head-Gordon, *Chem. Rev.*, 2005, **105**, 4009–4037.
44 A. L. Shluger, P. V. Sushko and L. N. Kantorovich, *Phys. Rev. B*, 1999, **59**, 2417–2430.
45 P. V. Sushko and A. L. Shluger, *Surf. Sci.*, 1999, **421**, L157–L165.
46 L. Goerigk and S. Grimme, *J. Chem. Phys.*, 2010, **132**, 184103.
47 H. H. Falden, K. R. Falster-Hansen, K. L. Bak, S. Rettrup and S. A. Sauer, *J. Phys. Chem. A*, 2009, **113**, 11995–12012.
48 M. Head-Gordon, R. J. Rico, M. Oumi and T. J. Lee, *Chem. Phys. Lett.*, 1994, **219**, 21–29.
49 B. O. Roos, P. R. Taylor and P. E. M. Siegbahn, *Chem. Phys.*, 1980, **48**, 157–173.
50 G. Li Manni, A. L. Dzubak, A. Mulla, D. W. Brogden, J. F. Berry and L. Gagliardi, *Chem.-Eur. J.*, 2012, **18**, 1737–1749.
51 G. K.-L. Chan and S. Sharma, *Annu. Rev. Phys. Chem.*, 2011, **62**, 465–481.
52 K. H. Marti and M. Reiher, *Phys. Chem. Chem. Phys.*, 2011, **13**, 6750–6759.
53 J. Miralles, O. Castell, R. Caballol and J.-P. Malrieu, *Chem. Phys.*, 1993, **172**, 33–43.
54 V. M. Garcia, R. Caballol and J.-P. Malrieu, *J. Chem. Phys.*, 1998, **109**, 504–511.
55 F. Neese, *J. Chem. Phys.*, 2003, **119**, 9428–9443.
56 I. Negodaev, C. de Graaf and R. Caballol, *J. Phys. Chem. A*, 2010, **114**, 7553–7560.
57 C. de Graaf, X. López, J. L. Ramos and J. M. Poblet, *Phys. Chem. Chem. Phys.*, 2010, **12**, 2716–2721.
58 R. Maurice, A. M. Pradipto, N. Guihéry, R. Broer and C. de Graaf, *J. Chem. Theory Comput.*, 2010, **6**, 3092–3101.
59 F. Neese, *J. Inorg. Biochem.*, 2006, **100**, 716–726.
60 D. Ganyushin and F. Neese, *J. Chem. Phys.*, 2008, **128**, 114117.
61 A. Venkatnathan, A. B. Szilva, D. Walter, R. J. Gdanitz and E. A. Carter, *J. Chem. Phys.*, 2004, **120**, 1693–1704.
62 R. J. Bartlett and M. Musial, *Rev. Mod. Phys.*, 2007, **79**, 291–351.
63 H. Koch, H. J. A. Jensen, P. Jorgensen and T. Helgaker, *J. Chem. Phys.*, 1990, **93**, 3345–3350.
64 H. Koch, R. Kobayashi, A. S. de Meras and P. Jorgensen, *J. Chem. Phys.*, 1994, **100**, 4393–4400.

65 D. I. Lyakh, M. Musial, V. F. Lotrich and R. J. Bartlett, *Chem. Rev.*, 2012, **112**, 182–243.
66 V. V. Ivanov, D. I. Lyakh and L. Adamowicz, *Phys. Chem. Chem. Phys.*, 2009, **11**, 2355–2370.
67 I. Infante, E. Eliav, M. J. Vilkas, Y. Ishikawa, U. Kaldor and L. Visscher, *J. Chem. Phys.*, 2007, **127**, 124308.
68 I. Infante, A. S. P. Gomes and L. Visscher, *J. Chem. Phys.*, 2006, **125**, 074301.
69 C. Danilo, V. Vallet, J.-P. Flament and U. Wahlgren, *Phys. Chem. Chem. Phys.*, 2009, **12**, 1116–1130.
70 A. S. P. Gomes, Ch. R. Jacob and L. Visscher, *Phys. Chem. Chem. Phys.*, 2008, **10**, 5353–5362.
71 F. Real, A. S. P. Gomes, L. Visscher, V. Vallet and E. Eliav, *J. Phys. Chem. A*, 2009, **113**, 12504–12511.
72 F. Ruipérez, C. Danilo, F. Réal, J.-P. Flament, V. Vallet and U. Wahlgren, *J. Phys. Chem. A*, 2009, **113**, 1420–1428.
73 P. Tecmer, A. S. P. Gomes, U. Ekström and L. Visscher, *Phys. Chem. Chem. Phys.*, 2011, **13**, 6249–6259.
74 J.-B. Rota, S. Knecht, T. Fleig, D. Ganyushin, T. Saue, F. Neese and H. Bolvin, *J. Chem. Phys.*, 2011, **135**, 114106.
75 I. Lindgren and D. Mukherjee, *Phys. Rep.*, 1987, **151**, 93–127.
76 D. Mukhopadhyay, S. Mukhopadhyay, R. Chaudhuri and D. Mukherjee, *Theor. Chim. Acta*, 1991, **80**, 441–467.
77 U. Kaldor, *Theor. Chem. Acc*, 1991, **80**, 427–439.
78 L. Meissner, *J. Chem. Phys.*, 1998, **108**, 9227–9235.
79 L. Meissner and M. Musiał, in *Recent Progress in Coupled Cluster Methods*, ed. P. Ćársky, Springer, 2010, p. 395.
80 A. Landau, E. Eliav, Y. Ishikawa and U. Kaldor, *J. Chem. Phys.*, 2000, **113**, 9905–9910.
81 A. Landau, E. Eliav, Y. Ishikawa and U. Kaldor, *J. Chem. Phys.*, 2001, **115**, 6862–6865.
82 E. Eliav, A. Borschevsky, K. R. Shamasundar, S. Pal and U. Kaldor, *Int. J. Quantum Chem.*, 2009, **109**, 2909–2915.
83 N. Vaval, P. Manohar and S. Pal, *Collect. Czech. Chem. Commun.*, 2005, **70**, 851–863.
84 A. S. P. Gomes, L. Visscher, H. Bolvin, T. Saue, S. Knecht, T. Fleig and E. Eliav, *J. Chem. Phys.*, 2010, **133**, 064305.
85 M. Musial and R. J. Bartlett, *J. Chem. Phys.*, 2008, **129**, 044101.
86 M. Musial and R. J. Bartlett, *J. Chem. Phys.*, 2008, **129**, 134105.
87 M. Musial and R. J. Bartlett, *Chem. Phys. Lett.*, 2008, **457**, 267–270.
88 K. Andersson, P.-A. Malmqvist, B. O. Roos, A. J. Sadlej and K. Wolinski, *J. Phys. Chem.*, 1990, **94**, 5483–5488.
89 K. Andersson, P.-A. Malmqvist and B. O. Roos, *J. Chem. Phys.*, 1992, **96**, 1218–1226.
90 J. Finley, P.-A. Malmqvist, B. O. Roos and L. Serrano-Andrés, *Chem. Phys. Lett.*, 1998, **288**, 299–306.
91 J. P. Finley, *Chem. Phys. Lett.*, 1998, **283**, 277–282.
92 B. O. Roos and K. Andersson, *Chem. Phys. Lett.*, 1995, **245**, 215–223.
93 N. Forsberg and P.-A. Malmqvist, *Chem. Phys. Lett.*, 1997, **274**, 196–204.
94 G. Ghigo, B. O. Roos and P.-A. Malmqvist, *Chem. Phys. Lett.*, 2004, **396**, 142–149.
95 H. A. Witek, Y.-K. Choe, J. P. Finley and K. Hirao, *J. Comput. Chem.*, 1998, **108**, 1081–1088.
96 C. Angeli, R. Cimiraglia, S. Evangelisti, T. Leininger and J. P. Malrieu, *J. Chem. Phys.*, 2001, **114**, 10252–10264.
97 G. La Macchia, I. Infante, R. Juraj, J. K. Gibson and L. Gagliardi, *Phys. Chem. Chem. Phys.*, 2008, **10**, 7278–7283.
98 I. Infante, A. Kovacs, G. L. Macchia, A. R. M. Shahi, J. K. Gibson and L. Gagliardi, *J. Phys. Chem. A*, 2010, **114**, 6997–6015.
99 C. de Graaf, C. Sousa, I. de P. R. Moreira and F. Illas, *J. Phys. Chem. A*, 2001, **105**, 11371–11378.
100 A. Ghosh and P. R. Taylor, *Curr. Opin. Chem. Biol.*, 2003, **7**, 113–124.
101 K. Pierloot, *Mol. Phys.*, 2003, **101**, 2083–2094.
102 S. Villaume, A. Strich, C. Daniel, S. A. Perera and R. J. Bartlett, *Phys. Chem. Chem. Phys.*, 2007, **9**, 6115–6122.
103 S. Vancoillie, H. Zhao, M. Radon and K. Pierloot, *J. Chem. Theory Comput.*, 2010, **6**, 576–582.
104 K. Pierloot and E. van Besien, *J. Chem. Phys.*, 2005, **123**, 204309.
105 P. Wahlin, V. Vallet, U. Wahlgren and I. Grenthe, *Inorg. Chem.*, 2009, **48**, 11310–11313.

106 O. Christiansen, A. Halkier, H. Koch, P. Jorgensen and T. Helgaker, *J. Chem. Phys.*, 1998, **108**, 2801–2816.
107 E. K. U. Gross and W. Kohn, *Adv. Quantum Chem.*, 1990, **21**, 255–291.
108 M. E. Casida, in *Recent Advances in Density-Functional Methods*, ed. D. P. Chong, World Scientific, Singapore, 1995, pp. 155–192.
109 P. Sałek, O. Vahtras, T. Helgaker and H. Ågren, *J. Chem. Phys.*, 2002, **117**, 9630–9645.
110 P. Sałek, T. Helgaker and T. Saue, *Chem. Phys.*, 2005, **311**, 187–201.
111 A. Kovyrshin and J. Neugebauer, *J. Chem. Phys.*, 2010, **133**, 174114.
112 J. Autschbach and T. Ziegler, *Coord. Chem. Rev.*, 2003, **238–239**, 83–126.
113 F. Furche and D. Rappoport, *Computational Photochemistry*, in *Computational and Theoretical Chemistry*, ed. M. Olivucci, Elsevier, Amsterdam, 2005, vol. 16.
114 F. Neese, *Coord. Chem. Rev.*, 2009, **253**, 526–563.
115 D. Jacquemin, E. A. Perpéte, I. Ciofini and C. Adamo, *J. Chem. Theory Comput.*, 2010, **6**, 1532–1537.
116 J. Preat, D. Jacquemin, J.-M. A. V. Wathelet and E. A. Perpéte, *J. Phys. Chem. A*, 2006, **110**, 8144–8150.
117 D. Jacquemin, V. Wathelet, E. A. Perpéte, I. Ciofini and C. Adamo, *J. Chem. Theory Comput.*, 2009, **5**, 2420–2435.
118 Y. Zhao and D. Truhlar, *Theor. Chem. Acc.*, 2008, **120**, 215–241.
119 M. A. Rohrdanz, K. M. Martins and J. M. Herbert, *J. Phys. Chem.*, 2009, **130**, 054112.
120 M. R. Silva-Junior, M. Schreiber, S. P. A. Sauer and W. Thiel, *J. Chem. Phys.*, 2008, **129**, 104103.
121 M. R. Silva-Junior, M. Schreiber, S. P. A. Sauer and W. Thiel, *J. Chem. Phys.*, 2010, **133**, 174318.
122 D. J. Tozer and N. C. Handy, *Phys. Chem. Chem. Phys.*, 2000, **2**, 2117–2121.
123 R. van Leeuwen and E. J. Baerends, *Phys. Rev. A*, 1994, **49**, 2421–2431.
124 P. R. T. Schipper, O. V. Gritsenko, S. J. A. van Gisbergen and E. J. Baerends, *J. Chem. Phys.*, 2000, **112**, 1344–1352.
125 A. Dreuw, J. L. Weisman and M. Head-Gordon, *J. Chem. Phys.*, 2003, **119**, 2943–2946.
126 O. V. Gritsenko and E. J. Baerends, *J. Chem. Phys.*, 2004, **121**, 655–660.
127 J. Autschbach, *ChemPhysChem*, 2009, **10**, 1757–1760.
128 M. E. Casida, *J. Chem. Phys.*, 2005, **122**, 054111.
129 N. T. Maitra, F. Zhang, R. J. Cave and K. Burke, *J. Chem. Phys.*, 2004, **120**, 5932–5937.
130 O. Christiansen, A. Halkier, H. Koch, P. Jorgensen and T. Helgaker, *J. Chem. Phys.*, 1998, **108**, 2801–2815.
131 O. Christiansen, H. Koch and P. Jørgensen, *Chem. Phys. Lett.*, 1995, **243**, 409–418.
132 C. Hättig and F. Weigend, *J. Chem. Phys.*, 2000, **113**, 5154–5161.
133 D. Kats, T. Korona and M. Schütz, *J. Chem. Phys.*, 2006, **125**, 104106.
134 T. A. Wesolowski and A. Warshel, *J. Phys. Chem.*, 1993, **97**, 8050–8053.
135 G. Senatore and K. R. Subbaswamy, *Phys. Rev. B*, 1986, **34**, 5754–5757.
136 M. D. Johnson, K. R. Subbaswamy and G. Senatore, *Phys. Rev. B*, 1987, **36**, 9202–9211.
137 P. Cortona, *Phys. Rev. B*, 1991, **44**, 8454–8458.
138 P. Elliott, K. Burke, M. H. Cohen and A. Wasserman, *Phys. Rev. A*, 2010, **82**, 024501.
139 M. Iannuzzi, B. Kirchner and J. Hutter, *Chem. Phys. Lett.*, 2006, **421**, 16–20.
140 Ch. R. Jacob, J. Neugebauer and L. Visscher, *J. Comput. Chem.*, 2008, **29**, 1011–1018.
141 M. S. Gordon, D. G. Fedorov, S. R. Pruitt and L. V. Slipchenko, *Chem. Rev.*, 2012, **112**, 632–672.
142 N. Govind, Y. A. Wang and E. A. Carter, *J. Chem. Phys.*, 1999, **110**, 7677–7688.
143 T. A. Wesolowski, *Phys. Rev. A*, 2008, **77**, 012504.
144 F. Aquilante and T. A. Wesolowski, *J. Chem. Phys.*, 2011, **135**, 084120.
145 T. A. Wesolowski, in *Computational Chemistry: Reviews of Current Trends*, ed. J. Leszczynski, World Scientific, Singapore, 2006, vol. 10, pp. 1–82.
146 S. Fux, Ch. R. Jacob, J. Neugebauer, L. Visscher and M. Reiher, *J. Chem. Phys.*, 2010, **132**, 164101.
147 T. A. Wesolowski and J. Weber, *Chem. Phys. Lett.*, 1996, **248**, 71–76.
148 Y. G. Khait and M. R. Hoffmann, *J. Chem. Phys.*, 2010, **133**, 044107.
149 M. E. Casida and T. A. Wesolowski, *Int. J. Quantum Chem.*, 2004, **96**, 577–588.
150 J. Neugebauer, *J. Chem. Phys.*, 2007, **126**, 134116.
151 J. Neugebauer, *J. Chem. Phys.*, 2009, **131**, 084104.
152 S. Höfener, A. Severo Pereira Gomes and L. Visscher, *J. Chem. Phys.*, 2012, **136**, 044104.
153 D. Bakowies and W. Thiel, *J. Phys. Chem.*, 1996, **100**, 10580–10594.
154 J. Tomasi and M. Persico, *Chem. Rev.*, 1994, **94**, 2027–2094.
155 Ch. J. Cramer and D. G. Truhlar, *Chem. Rev.*, 1999, **99**, 2161–2200.

156 J. Tomasi, B. Mennucci and R. Cammi, *Chem. Rev.*, 2005, **105**, 2999–3094.
157 J. Tomasi, *Theor. Chem. Acc.*, 2004, **112**, 184–203.
158 B. Mennucci and R. Cammi, *Continuum Solvation Models in Chemical Physics: From Theory to Applications*, Wiley, 1st edn., 2008.
159 A. Pedone, M. Biczysko and V. Barone, *ChemPhysChem*, 2010, **11**, 1812–1832.
160 B. Mennucci, *J. Phys. Chem. Lett.*, 2010, **1**, 1666–1674.
161 A. Klamt and G. Schüürmann, *J. Chem. Soc., Perkin Trans.*, 1993, **2**, 799–805.
162 R. Cammi, B. Mennucci and J. Tomasi, *J. Phys. Chem. A*, 1999, **103**, 9100–9108.
163 O. Christiansen and K. V. Mikkelsen, *J. Chem. Phys.*, 1999, **110**, 1365–1375.
164 B. Mennucci, C. Cappelli, C. A. Guido, R. Cammi and J. Tomasi, *J. Phys. Chem. A*, 2009, **113**, 3009–3020.
165 M. Cossi, V. Barone and M. A. Robb, *J. Chem. Phys.*, 1999, **111**, 5295–5302.
166 R. Cammi, L. Frediani, B. Mennucci, J. Tomasi, K. Ruud and K. V. Mikkelsen, *J. Chem. Phys.*, 2002, **117**, 13–26.
167 O. Christiansen and K. V. Mikkelsen, *J. Chem. Phys.*, 1999, **110**, 8348–8360.
168 J. Kongsted, A. Osted, K. V. Mikkelsen and O. Christiansen, *J. Chem. Phys.*, 2003, **119**, 10519–10535.
169 C. B. Nielsen, S. P. A. Sauer and K. V. Mikkelsen, *J. Chem. Phys.*, 2003, **119**, 3849–3870.
170 J. Kongsted, T. B. Pedersen, A. Osted, A. E. Hansen, K. V. Mikkelsen and O. Christiansen, *J. Phys. Chem. A*, 2004, **108**, 3632–3641.
171 J. Kongsted, A. Osted, K. V. Mikkelsen and O. Christiansen, *J. Chem. Phys.*, 2003, **118**, 1620–1633.
172 G. Brancato, N. Rega and V. Barone, *J. Chem. Phys.*, 2006, **125**, 164515.
173 J. Kongsted and B. Mennucci, *J. Phys. Chem. A*, 2007, **111**, 9890–9900.
174 J. Thar, S. Zahn and B. Kirchner, *J. Phys. Chem. B*, 2008, **112**, 1456–1464.
175 A. Warshel and M. Levitt, *J. Mol. Biol.*, 1976, **103**, 227–249.
176 J. Gao, in *Reviews in Computational Chemistry*, ed. K. B. Lipkowitz and D. B. Boyd, VCH, New York, 1995, vol. 7, pp. 119–185.
177 P. Sherwood, in *Modern Methods and Algorithms of Quantum Chemistry, of NIC Series*, ed. J. Grotendorst, John von Neumann Institute for Computing, Jülich, 2000, vol. 1, pp. 257–277.
178 H. Lin and D. G. Truhlar, *Theor. Chem. Acc.*, 2006, **117**, 185–199.
179 H. M. Senn and W. Thiel, *Top. Curr. Chem.*, 2007, **268**, 173–290.
180 H. M. Senn and W. Thiel, *Angew. Chem., Int. Ed.*, 2009, **48**, 1198–1229.
181 M. Wanko, M. Hoffmann, P. Strodel, A. Koslowski, W. Thiel, F. Neese, T. Frauenheim and M. Elstner, *J. Phys. Chem. B*, 2005, **109**, 3606–3615.
182 M. Hoffmann, M. Wanko, P. Strodel, P. H. König, T. Frauenheim, K. Schulten, W. Thiel, E. Tajkhorshid and M. Elstner, *J. Am. Chem. Soc.*, 2006, **128**, 10808–10818.
183 K. Fujimoto, S. Hayashi, J.-y. Hasegawa and H. Nakatsuji, *J. Chem. Theory Comput.*, 2007, **3**, 605–618.
184 J. S. Frähmcke, M. Wanko, P. Phatak, M. A. Mroginski and M. Elstner, *J. Phys. Chem. B*, 2010, **114**, 11338–11352.
185 J.-y. Hasegawa, K. J. Fujimoto and H. Nakatsuji, *ChemPhysChem*, 2011, **12**, 3106–3115.
186 M. A. L. Marques, X. López, D. Varsano, A. Castro and A. Rubio, *Phys. Rev. Lett.*, 2003, **90**, 258101.
187 E. Epifanovsky, I. Polyakov, B. Grigorenko, A. Nemukhin and A. I. Krylov, *J. Chem. Theory Comput.*, 2009, **5**, 1895–1906.
188 C. Filippi, F. Buda, L. Guidoni and A. Sinicropi, *J. Chem. Theory Comput.*, 2011, **8**, 112–124.
189 K. B. Bravaya, M. G. Khrenova, B. L. Grigorenko, A. V. Nemukhin and A. I. Krylov, *J. Phys. Chem. B*, 2011, **115**, 8296–8303.
190 J. Sauer, *Chem. Rev.*, 1989, **89**, 199–255.
191 K. Jug and T. Bredow, *J. Comput. Chem.*, 2004, **25**, 1551–1567.
192 J. Weber and J. Schmedt auf der Günne, *Phys. Chem. Chem. Phys.*, 2010, **12**, 583–603.
193 E. V. Stefanovich and T. N. Truong, *J. Phys. Chem. B*, 1998, **102**, 3018–3022.
194 H. M. Evjen, *Phys. Rev.*, 1932, **39**, 675–687.
195 A. Gellé and M.-B. Lepetit, *J. Chem. Phys.*, 2008, **128**, 244716.
196 P. V. Sushko and I. V. Abarenkov, *J. Chem. Theory Comput.*, 2010, **6**, 1323–1333.
197 P. P. Ewald, *Ann. Phys.*, 1921, **369**, 253–287.
198 S. E. Derenzo, M. K. Klintenberg and M. J. Weber, *J. Chem. Phys.*, 2000, **112**, 2074–2081.
199 M. Klintenberg, S. E. Derenzo and M. J. Weber, *Comput. Phys. Commun.*, 2000, **131**, 120–128.

200 B. Herschend, M. Baudin and K. Hermansson, *J. Chem. Phys.*, 2004, **120**, 4939–4948.
201 A. M. Burow, M. Sierka, J. Döbler and J. Sauer, *J. Chem. Phys.*, 2009, **130**, 174710.
202 K. Fink, *Phys. Chem. Chem. Phys.*, 2005, **7**, 2999–3004.
203 J. A. Mejias, V. Staemmler and H. J. Freund, *J. Phys. Condens. Matter*, 1999, **11**, 7881–7891.
204 N. Govind, P. V. Sushko, W. P. Hess, M. Valiev and K. Kowalski, *Chem. Phys. Lett.*, 2009, **470**, 353–357.
205 D. Stueber, F. N. Guenneau and D. M. Grant, *J. Chem. Phys.*, 2001, **114**, 9236–9243.
206 J. Torras, S. Bromley, O. Bertran and F. Illas, *Chem. Phys. Lett.*, 2008, **457**, 154–158.
207 R. Bjornsson and M. Bühl, *J. Chem. Theory Comput.*, 2012, **8**, 498–508.
208 B. G. Dick and A. W. Overhauser, *Phys. Rev.*, 1958, **112**, 90–103.
209 J. M. Vail, *J. Phys. Chem. Solids*, 1990, **51**, 589–607.
210 V. E. Puchin, E. V. Stefanovich and T. N. Truong, *Chem. Phys. Lett.*, 1999, **304**, 258–264.
211 V. A. Nasluzov, E. A. Ivanova, A. M. Shor, G. N. Vayssilov, U. Birkenheuer and N. Rösch, *J. Phys. Chem. B*, 2003, **107**, 2228–2241.
212 B. T. Thole and P. T. van Duijnen, *Theor. Chim. Acta*, 1980, **55**, 307–318.
213 B. T. Thole, *Chem. Phys.*, 1981, **59**, 341–350.
214 L. Jensen, P. T. van Duijnen and J. G. Snijders, *J. Chem. Phys.*, 2003, **118**, 514–521.
215 L. Jensen, P. T. van Duijnen and J. G. Snijders, *J. Chem. Phys.*, 2003, **119**, 3800–3809.
216 C. B. Nielsen, O. Christiansen, K. V. Mikkelsen and J. Kongsted, *J. Chem. Phys.*, 2007, **126**, 154112.
217 J. Kongsted, A. Osted, K. V. Mikkelsen and O. Christiansen, *J. Phys. Chem. A*, 2003, **107**, 2578–2588.
218 A. Osted, J. Kongsted, K. V. Mikkelsen and O. Christiansen, *Mol. Phys.*, 2003, **101**, 2055–2071.
219 J. Kongsted, A. E. Hansen, T. B. Pedersen, A. Osted, K. V. Mikkelsen and O. Christiansen, *Chem. Phys. Lett.*, 2004, **391**, 259–266.
220 J. Kongsted, A. Osted, T. B. Pedersen, K. V. Mikkelsen and O. Christiansen, *J. Phys. Chem. A*, 2004, **108**, 8624–8632.
221 K. Aidas, J. Kongsted, A. Osted, K. V. Mikkelsen and O. Christiansen, *J. Phys. Chem. A*, 2005, **109**, 8001–8010.
222 J. M. Olsen, K. Aidas and J. Kongsted, *J. Chem. Theory Comput.*, 2010, **6**, 3721–3734.
223 K. Sneskov, T. Schwabe, J. Kongsted and O. Christiansen, *J. Chem. Phys.*, 2011, **134**, 104108.
224 T. Schwabe, J. M. H. Olsen, K. Sneskov, J. Kongsted and O. Christiansen, *J. Chem. Theory Comput.*, 2011, **7**, 2209–2217.
225 A. H. Steindal, K. Ruud, L. Frediani, K. Aidas and J. Kongsted, *J. Phys. Chem. B*, 2011, **115**, 3027–3037.
226 I. V. Yudanov, V. A. Nasluzov, K. M. Neyman and N. Rösch, *Int. J. Quantum Chem.*, 1997, **65**, 975–986.
227 N. W. Winter, R. M. Pitzer and D. K. Temple, *J. Chem. Phys.*, 1987, **86**, 3549–3556.
228 G. Rossmüller, V. Kleinschmidt, J. Kossmann and C. Hättig, *J. Phys. Chem. C*, 2009, **113**, 1418–1425.
229 D. K. Kanan, S. Sharifzadeh and E. A. Carter, *Chem. Phys. Lett.*, 2012, **519–520**, 18–24.
230 P. Schwerdtfeger, *ChemPhysChem*, 2011, **12**, 3143–3155.
231 P. N. Day, J. H. Jensen, M. S. Gordon, S. P. Webb, W. J. Stevens, M. Krauss, D. Garmer, H. Basch and D. Cohen, *J. Chem. Phys.*, 1996, **105**, 1968–1986.
232 M. S. Gordon, M. A. Freitag, P. Bandyopadhyay, J. H. Jensen, V. Kairys and W. J. Stevens, *J. Phys. Chem. A*, 2001, **105**, 293–307.
233 P. Arora, L. V. Slipchenko, S. P. Webb, A. DeFusco and M. S. Gordon, *J. Phys. Chem. A*, 2010, **114**, 6742–6750.
234 S. Yoo, F. Zahariev, S. Sok and M. S. Gordon, *J. Chem. Phys.*, 2008, **129**, 144112.
235 M. S. Gordon, J. M. Mullin, S. R. Pruitt, L. B. Roskop, L. V. Slipchenko and J. A. Boatz, *J. Phys. Chem. B*, 2009, **113**, 9646–9663.
236 D. Ghosh, D. Kosenkov, V. Vanovschi, Ch. F. Williams, J. M. Herbert, M. S. Gordon, M. W. Schmidt, L. V. Slipchenko and A. I. Krylov, *J. Phys. Chem. A*, 2010, **114**, 12739–12754.
237 D. D. Kemp, J. M. Rintelman, M. S. Gordon and J. H. Jensen, *Theor. Chem. Acc.*, 2010, **125**, 481–491.
238 S. Humbel, S. Sieber and K. Morokuma, *J. Chem. Phys.*, 1996, **105**, 1959–1967.
239 M. Svensson, S. Humbel, R. D. J. Froese, T. Matsubara, S. Sieber and K. Morokuma, *J. Phys. Chem.*, 1996, **100**, 19357–19363.
240 T. Vreven and K. Morokuma, *J. Comput. Chem.*, 2000, **21**, 1419–1432.

241 H. P. Hratchian, P. V. Parandekar, K. Raghavachari, M. J. Frisch and T. Vreven, *J. Chem. Phys.*, 2008, **128**, 034107.
242 N. J. Mayhall, K. Raghavachari and H. P. Hratchian, *J. Chem. Phys.*, 2010, **132**, 114107.
243 H. P. Hratchian, A. V. Krukau, P. V. Parandekar, M. J. Frisch and K. Raghavachari, *J. Chem. Phys.*, 2011, **135**, 014105.
244 D. G. Fedorov and K. Kitaura, *J. Phys. Chem. A*, 2007, **111**, 6904–6914.
245 E. E. Dahlke and D. G. Truhlar, *J. Chem. Theory Comput.*, 2006, **3**, 46–53.
246 J. L. Pascual, J. Schamps, Z. Barandiarán and L. Seijo, *Phys. Rev. B*, 2006, **74**, 104105.
247 G. Fradelos and T. A. Wesolowski, *J. Phys. Chem. A*, 2011, **115**, 10018–10026.
248 G. Fradelos and T. A. Wesolowski, *J. Chem. Theory Comput.*, 2011, **7**, 213–222.
249 L. Seijo and Z. Barandiarán, in *Computational Chemistry: Reviews of Current Trends*, ed. J. Leszczynski, World Scientific, Singapore, 1999, vol. 4, p. 55.
250 B. Swerts, L. F. Chibotaru, R. Lindh, L. Seijo, Z. Barandiaran, S. Clima, K. Pierloot and M. F. A. Hendrickx, *J. Chem. Theory Comput.*, 2008, **4**, 586–594.
251 J. L. Pascual, N. Barros, Z. Barandiarán and L. Seijo, *J. Phys. Chem. A*, 2009, **113**, 12454–12460.
252 L. Seijo and Z. Barandiarán, *Int. J. Quantum Chem.*, 1996, **60**, 617–634.
253 R. Llusar, M. Casarrubios, Z. Barandiarán and L. Seijo, *J. Chem. Phys.*, 1996, **105**, 5321–5330.
254 J. L. Pascual, Z. Barandiarán and L. Seijo, *Phys. Rev. B*, 2007, **76**, 104109.
255 B. Ordejón, L. Seijo and Z. Barandiarán, *J. Chem. Phys.*, 2007, **126**, 194712.
256 F. Real, B. Ordejon, V. Vallet, J.-P. Flament and J. Schamps, *J. Chem. Phys.*, 2009, **131**, 194501.
257 J. L. Pascual and L. G. M. Pettersson, *Chem. Phys. Lett.*, 1997, **270**, 351–356.
258 J. L. Pascual and L. Seijo, *J. Chem. Phys.*, 1995, **102**, 5368–5376.
259 J. L. Whitten and H. Yang, *Int. J. Quantum Chem.*, 1995, **56**, 41–47.
260 U. Gutdeutsch, U. Birkenheuer, S. Krüger and N. Rösch, *J. Chem. Phys.*, 1997, **106**, 6020–6030.
261 T. M. Henderson, *J. Chem. Phys.*, 2006, **125**, 014105.
262 R. J. Buenker, H. P. Liebermann, D. B. Kokh, E. I. Izgorodina and J. L. Whitten, *Chem. Phys.*, 2003, **291**, 115–124.
263 B. Paulus, *Phys. Rep.*, 2006, **428**, 1–52.
264 R. G. Gordon and Y. S. Kim, *J. Chem. Phys.*, 1972, **56**, 3122–3133.
265 Y. S. Kim and R. G. Gordon, *J. Chem. Phys.*, 1974, **60**, 1842–1850.
266 Ch. R. Jacob, T. A. Wesolowski and L. Visscher, *J. Chem. Phys.*, 2005, **123**, 174104.
267 S. Laricchia, E. Fabiano and F. Della Sala, *J. Chem. Phys.*, 2010, **133**, 164111.
268 T. A. Wesolowski and J. Weber, *Int. J. Quantum Chem.*, 1997, **61**, 303–311.
269 Y. A. Wang and E. A. Carter, in *Theoretical Methods in Condensed Phase Chemistry*, ed. S. D. Schwartz, Kluwer, Dordrecht, 2000, pp. 117–184.
270 F. Tran and T. A. Wesolowski, *Int. J. Quantum Chem.*, 2002, **89**, 441–446.
271 J. M. Garcia Lastra, J. W. Kaminski and T. A. Wesolowski, *J. Chem. Phys.*, 2008, **129**, 074107.
272 A. W. Götz, S. M. Beyhan and L. Visscher, *J. Chem. Theory Comput.*, 2009, **5**, 3161–3174.
273 S. Laricchia, E. Fabiano, L. A. Constantin and F. Della Sala, *J. Chem. Theory Comput.*, 2011, **7**, 2439–2451.
274 T. A. Wesolowski, H. Chermette and J. Weber, *J. Chem. Phys.*, 1996, **105**, 9182–9190.
275 T. A. Wesolowski, *J. Chem. Phys.*, 1997, **106**, 8516–8526.
276 A. Lembarki and H. Chermette, *Phys. Rev. A*, 1994, **50**, 5328–5331.
277 K. Kiewisch, G. Eickerling, M. Reiher and J. Neugebauer, *J. Chem. Phys.*, 2008, **128**, 044114.
278 S. Fux, K. Kiewisch, Ch. R. Jacob, J. Neugebauer and M. Reiher, *Chem. Phys. Lett.*, 2008, **461**, 353–359.
279 Ch. R. Jacob, S. M. Beyhan and L. Visscher, *J. Chem. Phys.*, 2007, **126**, 234116.
280 S. M. Beyhan, A. W. Götz, Ch. R. Jacob and L. Visscher, *J. Chem. Phys.*, 2010, **132**, 044114.
281 Ch. R. Jacob and L. Visscher, *J. Chem. Phys.*, 2008, **128**, 155102.
282 P. Cortona and A. Villafiorita Monteleone, *Int. J. Quantum Chem.*, 1994, **52**, 987–992.
283 P. Cortona, A. Villafiorita Monteleone and P. Becker, *Int. J. Quantum Chem.*, 1995, **56**, 831–837.
284 J.-M. Gillet and P. Cortona, *Phys. Rev. B*, 1999, **60**, 8569–8574.
285 L. L. Boyer and M. J. Mehl, *Ferroelectrics*, 1993, **150**, 13–24.

286 W. N. Mei, L. L. Boyer, M. J. Mehl, M. M. Ossowski and H. T. Stokes, *Phys. Rev. B*, 2000, **61**, 11425–11431.
287 M. M. Ossowski, L. L. Boyer, M. J. Mehl and H. T. Stokes, *Phys. Rev. B*, 2002, **66**, 224302.
288 J. M. García-Lastra, T. Wesolowski, M. T. Barriuso, J. A. Aramburu and M. Moreno, *J. Phys.: Condens. Matter*, 2006, **18**, 1519–1534.
289 M. Zbiri, M. Atanasov, C. Daul, J. M. Garcia-Lastra and T. A. Wesolowski, *Chem. Phys. Lett.*, 2004, **397**, 441–446.
290 M. Zbiri, C. A. Daul and T. A. Wesolowski, *J. Chem. Theory Comput.*, 2006, **2**, 1106–1111.
291 T. A. Wesolowski, *J. Am. Chem. Soc.*, 2004, **126**, 11444–11445.
292 J. Neugebauer, M. J. Louwerse, E. J. Baerends and T. A. Wesolowski, *J. Chem. Phys.*, 2005, **122**, 094115.
293 J. Neugebauer, Ch. R. Jacob, T. A. Wesolowski and E. J. Baerends, *J. Phys. Chem. A*, 2005, **109**, 7805–7814.
294 J. Neugebauer, *J. Phys. Chem. B*, 2008, **112**, 2207–2217.
295 J. Neugebauer, J. Veldstra and F. Buda, *J. Phys. Chem. B*, 2011, **115**, 3216–3225.
296 Ch. R. Jacob, J. Neugebauer, L. Jensen and L. Visscher, *Phys. Chem. Chem. Phys.*, 2006, **8**, 2349–2359.
297 J. Neugebauer, C. Curutchet, A. Muñoz Losa and B. Mennucci, *J. Chem. Theory Comput.*, 2010, **6**, 1843–1851.
298 C. König and J. Neugebauer, *Phys. Chem. Chem. Phys.*, 2011, **13**, 10475–10490.
299 N. Govind, Y. A. Wang, A. J. R. da Silva and E. A. Carter, *Chem. Phys. Lett.*, 1998, **295**, 129–134.
300 T. Klüner, N. Govind, Y. A. Wang and E. A. Carter, *Phys. Rev. Lett.*, 2001, **86**, 5954–5957.
301 T. Klüner, N. Govind, Y. A. Wang and E. A. Carter, *J. Chem. Phys.*, 2002, **116**, 42–54.
302 P. Huang and E. A. Carter, *J. Chem. Phys.*, 2006, **125**, 084102.
303 D. Lahav and T. Klüner, *J. Phys. Condens. Matter*, 2007, **19**, 226001.
304 P. Huang and E. A. Carter, *Nano Lett.*, 2006, **6**, 1146–1150.
305 S. Sharifzadeh, P. Huang and E. Carter, *J. Phys. Chem. C*, 2008, **112**, 4649–4657.
306 P. Huang and E. A. Carter, *Nano Lett.*, 2008, **8**, 1265–1269.
307 S. Sharifzadeh, P. Huang and E. A. Carter, *Chem. Phys. Lett.*, 2009, **470**, 347–352.
308 S. Liu and P. W. Ayers, *Phys. Rev. A*, 2004, **70**, 022501.
309 Q. Zhao, R. C. Morrison and R. G. Parr, *Phys. Rev. A*, 1994, **50**, 2138–2142.
310 Q. Wu and W. Yang, *J. Chem. Phys.*, 2003, **118**, 2498–2509.
311 J. D. Goodpaster, N. Ananth, F. R. Manby and T. F. Miller, *J. Chem. Phys.*, 2010, **133**, 084103.
312 J. D. Goodpaster, T. A. Barnes and T. F. Miller, *J. Chem. Phys.*, 2011, **134**, 164108.
313 T. A. Wesolowski, *J. Chem. Phys.*, 2011, **135**, 027101.
314 S. Fux, Ch. R. Jacob, J. Neugebauer, L. Visscher and M. Reiher, *J. Chem. Phys.*, 2011, **135**, 027102.
315 O. Roncero, A. Zanchet, P. Villarreal and A. Aguado, *J. Chem. Phys.*, 2009, **131**, 234110.
316 J. Nafziger, Q. Wu and A. Wasserman, *J. Chem. Phys.*, 2011, **135**, 234101.
317 S. Hirata, S. Ivanov, I. Grabowski, R. J. Bartlett, K. Burke and J. D. Talman, *J. Chem. Phys.*, 2001, **115**, 1635–1649.
318 V. N. Staroverov, G. E. Scuseria and E. R. Davidson, *J. Chem. Phys.*, 2006, **124**, 141103.
319 A. Heßelmann, A. W. Götz, F. Della Sala and A. Görling, *J. Chem. Phys.*, 2007, **127**, 054102.
320 T. Heaton-Burgess, F. A. Bulat and W. Yang, *Phys. Rev. Lett.*, 2007, **98**, 256401.
321 T. Heaton-Burgess and W. Yang, *J. Chem. Phys.*, 2008, **129**, 194102.
322 Ch. R. Jacob, *J. Chem. Phys.*, 2011, **135**, 244102.
323 L. Serrano-Andrés and M. P. Fülscher, and G. Kallström, *Int. J. Quantum Chem.*, 1997, **65**, 167–181.
324 L. Bernasconi, M. Sprik and J. Hutter, *J. Chem. Phys.*, 2003, **119**, 12417–12431.
325 L. Bernasconi, M. Sprik and J. Hutter, *Chem. Phys. Lett.*, 2004, **394**, 141–146.
326 M. Cossi and V. Barone, *J. Chem. Phys.*, 2000, **112**, 2427–2435.
327 C. W. Portern and C. Iddings, *J. Am. Chem. Soc.*, 1926, **48**, 40–44.
328 N. S. Bayliss and R. G. McRae, *J. Phys. Chem.*, 1954, **58**, 1006–1011.
329 N. S. Bayliss and G. Wills-Johnson, *Spectrochim. Acta, Part A*, 1968, **24**, 551–561.
330 K. Sneskov, T. Schwabe, O. Christiansen and J. Kongsted, *Phys. Chem. Chem. Phys.*, 2011, **13**, 18551–18560.

331 A. Schleife, C. Rödl, F. Fuchs, J. Furthmüller and F. Bechstedt, *Phys. Rev. B*, 2009, **80**, 035112.
332 L. X. Benedict, E. L. Shirley and R. B. Bohn, *Phys. Rev. Lett.*, 1998, **80**, 4514–4517.
333 N. P. Wang, M. Rohfling, P. Kruger and J. Pollman, *Appl. Phys. A*, 2004, **78**, 213–221.
334 M. L. Bortz, R. H. French, D. J. Jones, R. V. Kasowski and F. S. Ohuchi, *Phys. Scr.*, 1990, **41**, 537–541.
335 D. M. Roessler and W. C. Walter, *Phys. Rev.*, 1967, **159**, 733–738.
336 E. Miyoshi, Y. Miyake, S. Katsuki and Y. Sakai, *J. Mol. Struct.*, 1998, **451**, 81–88.
337 C. Sousa, G. Pacchioni and F. Illas, *Surf. Sci.*, 1999, **429**, 217–228.
338 C. Sousa and F. Illas, *J. Chem. Phys.*, 2001, **115**, 1435–1439.
339 D. Dominguez-Ariza, C. Sousa, F. Illas, D. Ricci and G. Pacchioni, *Phys. Rev. B*, 2003, **68**, 054101.
340 Y. Chen, R. T. Williams and W. A. Sibley, *Phys. Rev.*, 1969, **182**, 960–964.